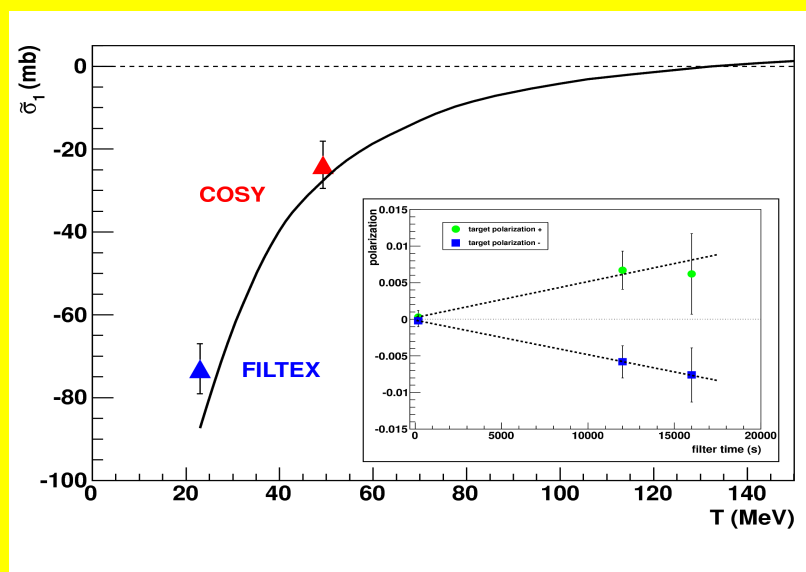


Jülich Center for Hadron Physics (JCHP)
 Institut für Kernphysik (IKP)
 COSY

Spin-filtering with PAX



Annual Report 2012

Annual Report 2012

Jülich Center for Hadron Physics / Institut für Kernphysik / COSY

DIRECTORS AT THE IKP:

Experimental Hadron Structure (IKP-1):

Experimental Hadron Dynamics (IKP-2):

Theory of the Strong Interactions (IKP-3/IAS-4):

Large-Scale Nuclear Physics Equipment (IKP-4):

Prof. James Ritman

Prof. Hans Ströher (managing director)

Prof. Ulf-G. Meißner

Prof. Rudolf Maier

EDITORIAL BOARD:

Priv. Doz. Dr. Markus Büscher

Dr. Dieter Grzonka

Priv. Doz. Dr. Christoph Hanhart

Prof. Siegfried Krewald

Prof. Rudolf Maier

Prof. Ulf-G. Meißner

Prof. James Ritman

Dr. Hans Stockhorst

Prof. Hans Ströher

Cover picture:

Polarization induced in the COSY beam after filtering for different times and different signs of the target polarization (insert). Measured spin-dependent polarizing cross section for the interaction (only statistical errors are shown). The solid line represents the prediction from the SAID database. See Sect. 1.2.9 for details.

Preface

Halfway through the second period of the Programme oriented Funding (PoF-2), the Institute for Nuclear Physics (IKP) is focusing on tasks along the lines outlined in the corresponding documents for the Helmholtz Association (HGF): foremost this comprises the design of and preparations for the High Energy Storage Ring (HESR) of FAIR (Facility for Antiproton and Ion Research) as well as for the PANDA experiment. It also includes hadron physics experiments at the Cooler Synchrotron COSY, exploiting the internal experiments ANKE, PAX and WASA and TOF with the extracted COSY beam. In addition, the institute is involved in the future projects JEDI (Jülich Electric Dipole Moment Investigations) and JuSPARC (Short-Pulsed Particle and Radiation Center at Forschungszentrum Jülich). Furthermore, the institute became member of two new projects of the Helmholtz Society: ARD (Accelerator Research and Development) and the Detector Technology and System Platform. Since the head of the accelerator division (IKP-4), Rudolf Maier, will retire in early 2014, the institute — with the help of colleagues from other institutes of Forschungszentrum Jülich (FZJ) — has prepared a strategy paper, which outlines the possible future developments of IKP and other institutes of FZJ and emphasizes the need for a replacement of the position. Finally the institute has started preparations for the next period of program-oriented funding (PoF-3), which starts in 2015.

Physics highlights of the past year comprise:

Ab initio calculation of the Hoyle state The Hoyle state is one of the most interesting and important challenges in nuclear physics. This excited state of the ^{12}C nucleus plays a key role in the fusion of three alpha particles to form carbon in red giant stars. *Ab initio* lattice calculations have been performed which unravel the structure of this state and find evidence for a low-lying spin-2 rotational excitation. For the structure of the ^{12}C ground state and first spin-2 state, a compact triangular configuration of alpha clusters is found, while for the Hoyle state and second spin-2 state a bent-arm or obtuse triangular configuration of alpha clusters is obtained.

Nature of the $D_{s0}^*(2317)$ from Lattice QCD The scattering of light pseudoscalar mesons off charmed mesons in full lattice QCD has been studied. The *S*-wave scattering lengths are calculated for all channels without disconnected diagrams and a chiral unitary approach was used for the chiral extrapolation and predictions for other channels and observables. The results support the interpretation of the $D_{s0}^*(2317)$ as a *DK* molecule. Especially, the decay width $\Gamma(D_{s0}^*(2317) \rightarrow D_s \pi)$ to (133 ± 19) keV is 6σ larger than the values predicted for a non-molecular state.

WASA ABC-resonance The isospin dependence of two-pion production in proton-nucleon fusion reactions to a deuteron has been investigated in a series of experiments with WASA at COSY. A clear difference between the isoscalar and the isovector production part is obtained: while the latter shows a smooth behavior consistent with $\Delta\Delta$ production and decay, the former exhibits a narrow resonance-like structure at a center-of-mass energy of 2.37 GeV.

ANKE double polarized measurements Experiments with a polarized deuteron COSY beam, incident on polarized hydrogen of the ANKE ABS, have been successfully conducted. The spin-correlation parameters obtained for *np* charge-exchange scattering will add valuable information to the *NN* data base, while those for the $np \rightarrow pp_s \pi^-$ reaction provide important constraints for ChPT calculations.

PAX spin filtering experiment A test measurement to study the feasibility of polarizing a stored beam by means of spin filtering, which had been conducted with protons at COSY in 2011, has been analyzed and published. It was demonstrated that the method works and — for protons — is well understood. The next step is to perform a similar experiment with anti-protons.

TOF experimental program Experiments with a polarized proton beam on a proton and deuteron target have been performed. These results on strangeness production in pp and pn reactions address resonance contributions and cusp effects. COSY-TOF has now successfully completed its long running measurement program.

EDM spin coherence time One essential issue for investigations of electric dipole moments of charged particles in storage rings is the optimization of the so-called spin coherence time (SCT), which determines the maximum time span, during which the effect of a particle EDM can be observed. In a set of measurements the horizontal polarization as a function of time has been studied for different emittances and sextupole corrections, resulting in a SCT of more than about 200 seconds.

Laser-induced particle acceleration A first experiment to determine the degree of polarization of Laser-accelerated proton beams has been carried out at the 100-TW Arcturus Laser facility at the University of Düsseldorf. Based on simulation studies with the Juropa supercomputer the data reveal that the proton spins are not affected by the strong magnetic fields in the plasma. This is a promising finding for the realization of Laser-based polarized ion sources using pre-polarized targets, like ^3He .

Noteworthy further items are:

PANDA spokesperson Jim Ritman has been elected as the new spokesperson of the international PANDA collaboration for a period of two years, starting at the beginning of 2013.

COSY High Energy Electron Cooler The 2.5 MV electron cooler, which has been planned with and produced at the Budker Institute in Novosibirsk, arrived at FZJ; after further preparations it will be installed and commissioned in COSY during the upcoming year.

JARA|Fame A new section of the Jülich-Aachen Research Alliance (JARA), called JARA|Fame (Forces and Matter Experiments), has been founded, joining scientists from RWTH Aachen (Physics, Engineering) and from Forschungszentrum Jülich (IKP, JSC). It is based questions concerning the fate of antimatter with two experimental pillars (AMS, EDM) as well as theory and technical issues (data handling, detector development).

PANDA Preassembly In order to significantly accelerate the construction, assembly and commissioning of the PANDA experiment at FAIR, in beam tests of individual detector components under realistic conditions are in progress at COSY and major components of the detector will be pre-assembled at FZ-Jülich. With this approach PANDA will be able to start doing physics measurements as early as possible once the antiproton beam is available at the High Energy Storage Ring HESR at FAIR in Darmstadt.

IKP conferences and meetings The 12th International Workshop on Meson Production, Properties and Interaction (MESON 2012) in Cracow, Poland, was co-organized by the IKP, the Jagiellonian University and Institute of Nuclear Physics PAN Cracow, and INFN Frascati. The Hadron Physics Summer School was jointly organized by scientists from the Institute for Nuclear Physics, Forschungszentrum Jülich, and by the DFG Transregio TR 16 (Subnuclear Structure of Matter) of the Universities Bonn, Bochum and Giessen. The 5th Georgian German School and Workshop was organized in Tbilisi and Batumi (Georgia) during August 2012. It was also used to elect master and PhD students from Georgian universities to perform their studies at Forschungszentrum Jülich within an exchange program between Jülich and the national Georgian science foundation (SRNSF). In October, an ECT* Workshop on “EDM Searches at Storage Rings”, co-organized with Brookhaven National Lab scientists, was held in Trento (Italy).

Finally I would like to express my sincere gratitude to all our colleagues and co-workers, since without their help and support, we would not have been able to achieve our milestones. We also acknowledge the continuous support by the board of management of the FZJ and HGF.

Jülich, April 2013

Hans Ströher

Contents

1	Physics at COSY.....	1
2	COSY Operation and Developments ..	15
3	Theoretical Investigations	17
4	HESR Project Progress Report	25
5	Day-one Experiment at HESR.....	27
6	The PANDA Experiment	29
7	Further Experimental Activities	37
 Appendix		
A	Councils	43
B	Publications	44
C	Talks and Colloquia.....	50
D	Diploma and Ph.D. Theses.....	57
E	Awards & Offers for Professorships...	59
F	Funded Projects	60
G	JCHP-FFE Projects.....	61
H	Conferences (co-)organized by the IKP	63
I	Teaching Positions	66
J	Personnel.....	67
K	Further Contributions	70

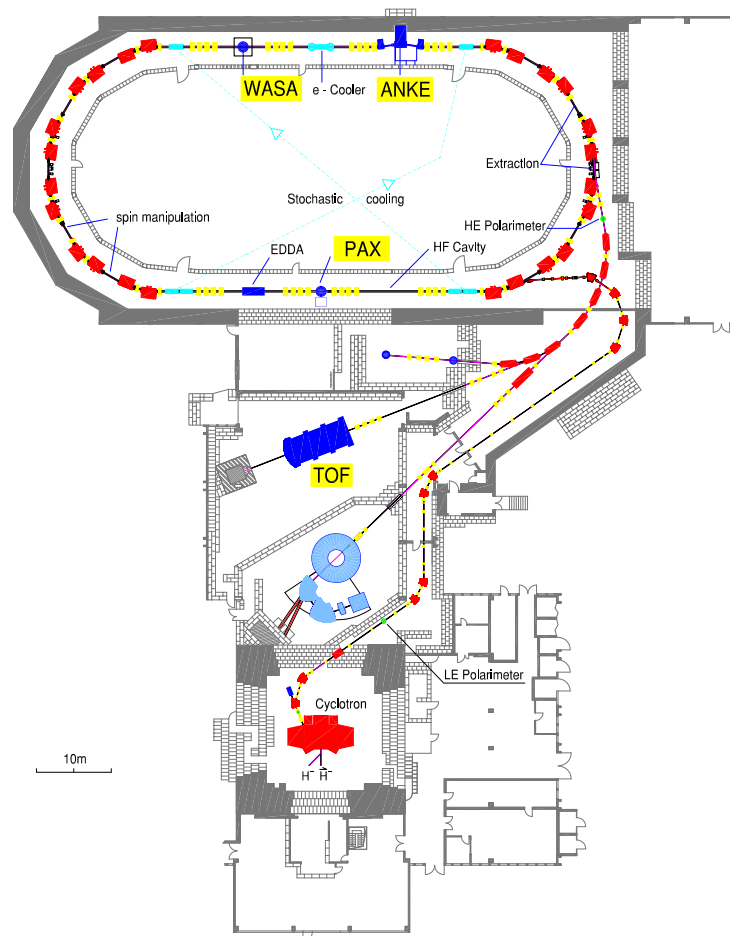
1 Physics at COSY

1.1 Overview

The cooler synchrotron and storage ring COSY delivers unpolarized and polarized beams of protons and deuterons with momenta up to 3.7 GeV/c for three internal experiments — ANKE, PAX and WASA — and one experiment — TOF — at an external target position. All detection systems are operated by large international collaborations.

- **ANKE** (Apparatus for Studies of Nucleon and Kaon Ejectiles) is a large acceptance forward magnetic spectrometer at an internal target station in the COSY ring. The central dipole is movable to adjust the momenta of the detected particles independent of the beam momentum. Using deuterium cluster targets, reactions on the neutron are tagged by detecting the low-energy recoil proton in silicon strip detectors in vacuum next to the target. In addition, a polarized internal target with a storage cell can be used.
- **PAX** (Polarized Antiproton EXperiment) is the test set-up to investigate spin filtering as a method to produce polarized beams. It uses an atomic beam source, an openable storage cell and a Breit-Rabi polarimeter in a low- β section of COSY.
- **TOF** (Time Of Flight) is a non-magnetic spectrometer combining excellent tracking capabilities with large acceptance and full azimuthal symmetry allowing to measure complete Dalitz plots. TOF is optimized for final states with strangeness. With the new straw tube tracking system (STT), TOF has a significantly improved mass resolution and reconstruction efficiency.
- **WASA** (Wide Angle Shower Apparatus), an internal 4π spectrometer for neutral and charged particles, is operated at the internal COSY beam. WASA comprises an electro-magnetic calorimeter, a very thin superconducting solenoid, inner and forward trigger and tracking detectors, and a frozen-pellet target.

The unique COSY capabilities are also used by the Storage-Ring EDM (srEDM) and JEDI (Jülich Electric Dipole Moment Investigations) collaborations to investigate spin-manipulations as preparation to build (a) dedicated storage ring(s) to search for electric dipole moments of light ions (p , d , ^3He).



1.2 Major Physics Results at COSY

1.2.1 Charge Symmetry Breaking in $dd \rightarrow {}^4\text{He}\pi^0$

Charge symmetry is a special case of isospin symmetry, and thus broken by the different masses of the up and down quarks and by electromagnetic interaction. It has the advantage, that the π -mass term, which is dominating general isospin symmetry breaking, is invariant under charge symmetry. Therefore, in order to access quark mass ratios it is advised to look at charge symmetry breaking observables.

Triggered by high-precision experiments at IUCF ($dd \rightarrow {}^4\text{He}\pi^0$, Stephenson *et al.*) and TRIUMF ($pn \rightarrow d\pi^0$, Opper *et al.*) an international collaboration has been formed aiming at a consistent description of the data within chiral perturbation theory. In course of the ongoing analysis a set of essential observables has been identified, which are now being addressed by the experimental program of WASA-at-COSY. The final goal of this program is to quantify the contribution of higher partial waves in the charge symmetry breaking reaction $dd \rightarrow {}^4\text{He}\pi^0$.

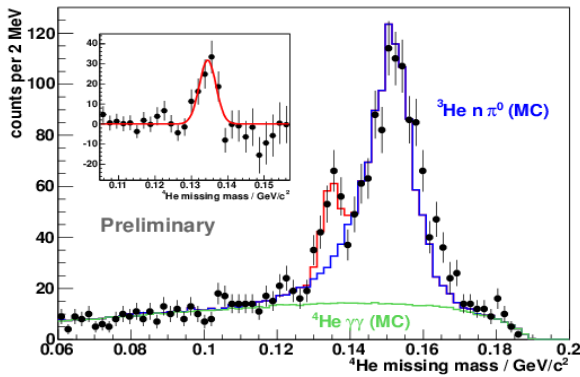


Fig. 1: ${}^4\text{He}$ missing-mass distribution. The plot contains misidentified events from $dd \rightarrow {}^3\text{He}n\pi^0$ (blue), background from $dd \rightarrow {}^4\text{He}\gamma\gamma$ (green) and the signal from $dd \rightarrow {}^4\text{He}\pi^0$ (red). The inset shows a fit to the background subtracted data.

In a first step the focus was on an exclusive measurement of the reaction $dd \rightarrow {}^3\text{He}n\pi^0$ at $p_d = 1.2\text{ GeV}/c$. The data have been compared to a quasi-free reaction model based on existing data for the two-body reaction $dp \rightarrow {}^3\text{He}\pi^0$ and a partial-wave expansion for the three-body reaction limited to at most one p -wave in the system, both added incoherently. The ${}^3\text{He}n\pi^0$ final state is described by the two Jacobi momenta \vec{q} and \vec{p} , where \vec{q} is the π^0 momentum in the overall c.m. frame and \vec{p} the relative momentum in the ${}^3\text{He}n$ subsystem. A corresponding publication is in preparation.

In a subsequent run first data for the charge-symmetry breaking reaction $dd \rightarrow {}^4\text{He}\pi^0$ at $p_d = 1.2\text{ GeV}/c$ have been taken. The basic analysis conditions for selecting event candidates for Helium and two photons in final state were the same as for $dd \rightarrow {}^3\text{He}n\pi^0$. In addition, for the final event selection kinematic fitting was introduced for

two purposes: (i) a combined χ^2 -cut after testing the hypotheses $dd \rightarrow {}^3\text{He}n\gamma\gamma$ and $dd \rightarrow {}^4\text{He}\gamma\gamma$ was used to suppress background from ${}^3\text{He}$ isotopes, and, (ii) the fit to $dd \rightarrow {}^4\text{He}\gamma\gamma$ was used to refine the data and to ensure energy and momentum conservation. No constraint on the pion mass was added.

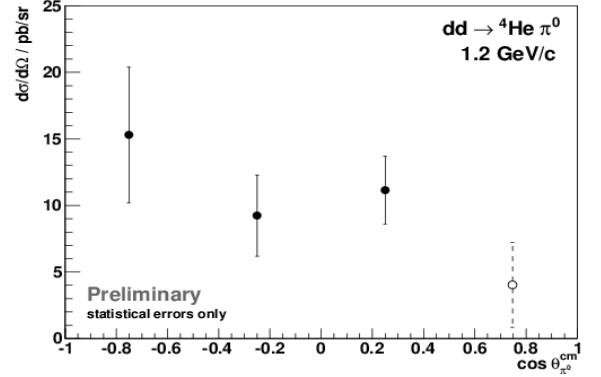


Fig. 2: Angular distribution as a function of $\theta_{\pi^0}^{\text{cm}}$ (statistical errors only). The data are consistent with s -wave pion production.

Figure 1 shows the final ${}^4\text{He}$ missing mass distribution. On top of a flat background two peaks emerge, one from $dd \rightarrow {}^4\text{He}\pi^0$ at $m_{\pi} = 135\text{ MeV}/c^2$ and one from $dd \rightarrow {}^3\text{He}n\pi^0$ shifted to higher masses by the ${}^4\text{He}$ -(${}^3\text{He}$ - n) binding energy difference. The background has been fitted by Monte-Carlo filtered distributions for $dd \rightarrow {}^3\text{He}n\pi^0$ and $dd \rightarrow {}^4\text{He}\gamma\gamma$. For the first channel the model discussed earlier was used, for the latter a homogeneous 3-body phase-space distribution was assumed. The background subtracted data contain about 120 signal events (see inset), which were fitted with a Gaussian. The following preliminary total cross sections (statistical errors only) have been extracted:

$$\begin{aligned}\sigma_{\text{tot,prelim.}}^{4\text{He}\pi^0} &= (120 \pm 20_{\text{stat}}) \text{ pb} \\ \sigma_{\text{tot,prelim.}}^{4\text{He}\gamma\gamma} &= (960 \pm 45_{\text{stat}}) \text{ pb}\end{aligned}$$

The fit procedure was repeated for four bins in $\theta_{\pi^0}^{\text{cm}}$. Figure 2 shows the extracted preliminary angular distribution. The errors shown are statistical only. At this stage of the analysis, especially the most forward angular bin — corresponding to low energetic ${}^4\text{He}$ ejectiles — is expected to have large systematic uncertainties as it is most sensitive to variations in the detector acceptance. Within the limited statistics the angular distribution is consistent with s -wave pion production.

Based on these results a new measurement using a modified detector setup has been proposed: removing the Forward Range Hodoscope and other detector components will introduce a 1.5 m time-of-flight path in order to improve ${}^3\text{He}$ - ${}^4\text{He}$ separation and kinetic energy reconstruction. The goals of the measurement are to increase statistics and to minimize systematic errors for data taken at $p_d = 1.2\text{ GeV}/c$ as well as to add a higher energy data point to study the influence of the Δ resonance on charge symmetry breaking.

1.2.2 Search of the recently observed ABC resonance structure in the $pn \rightarrow pp\pi^0\pi^-$ reaction

Recent data on the basic double-pionic fusion reactions $pn \rightarrow d\pi^0\pi^0$ and $pn \rightarrow d\pi^+\pi^-$ obtained with the WASA detector setup at COSY (see Annual Reports 2010 and 2011) demonstrate that the so-called ABC effect is tightly correlated with a narrow resonance structure in the total cross section of these reactions. The ABC effect denotes an extraordinary low-mass enhancement in the $\pi\pi$ invariant mass spectrum and is observed to happen, if the initial nucleons or light nuclei fuse to a bound final nuclear system and if the produced pion pair is isoscalar. Since there has been no real understanding of this phenomenon so far, it just has been named after the initials of Abashian, Booth and Crowe, who first observed it in the inclusive measurement of the $pd \rightarrow {}^3\text{He}X$ reaction more than fifty years ago.

In exclusive high-statistics measurements of the isoscalar $pn \rightarrow d\pi^0\pi^0$ reaction and of the isospin mixed $pn \rightarrow d\pi^+\pi^-$ reaction we could demonstrate that this ABC effect is correlated with a pronounced resonance structure in the total cross section at $\sqrt{s} = 2.37$ GeV with a width of only 70 MeV and quantum numbers $I(J^P) = 0(3^+)$. This structure is situated about 90 MeV below $\sqrt{s} = 2m_\Delta$, the peak position of the conventional t -channel $\Delta\Delta$ process, and has a width, which is about three times narrower than this process. From the $pn \rightarrow d\pi^0\pi^0$ Dalitz plot we conclude that this resonance decays nevertheless via the intermediate $\Delta^+\Delta^0$ system into its final $d\pi^0\pi^0$ state.

If this scenario is correct, then also the $pn \rightarrow pp\pi^0\pi^-$ reaction should be affected by this resonance, since this channel may proceed via the same intermediate $\Delta^+\Delta^0$ system. We have investigated this question experimentally by using a pd run taken at $T_p = 1.2$ GeV with the WASA detector facility at COSY. From this data sample we have analyzed the reaction $pd \rightarrow pp\pi^0\pi^- + p_{\text{spectator}}$ using quasifree kinematics. Utilizing that way the Fermi motion of the nucleons bound within the target deuteron the selected data span an energy region $2.35 \text{ GeV} \leq \sqrt{s} \leq 2.45 \text{ GeV}$ and thus cover the full region of the ABC effect and its associated resonance structure.

Preliminary results for the total cross section are shown in Fig. 3 together with previous data from bubble chamber measurements. They exhibit a monotonically rising total cross section with some pronounced shoulder in the energy region of the ABC effect. As already observed in other two-pion production channels the Gatchina bubble-chamber data (open squares in Fig. 3) exhibit much higher cross sections than all other data do — pointing to a systematic problem of the Gatchina data. Hence we do not consider them further.

Original Valencia model calculations based on resonant and non-resonant t -channel processes for the two-pion production are depicted by the dash-dotted line with their largest contributions originating from Roper excitation and its decay route $N^* \rightarrow \Delta\pi$ (dotted) as well as from the t -channel $\Delta\Delta$ process, the mutual excitation of two nucleons into the $\Delta(1232)$ state by t -channel meson ex-

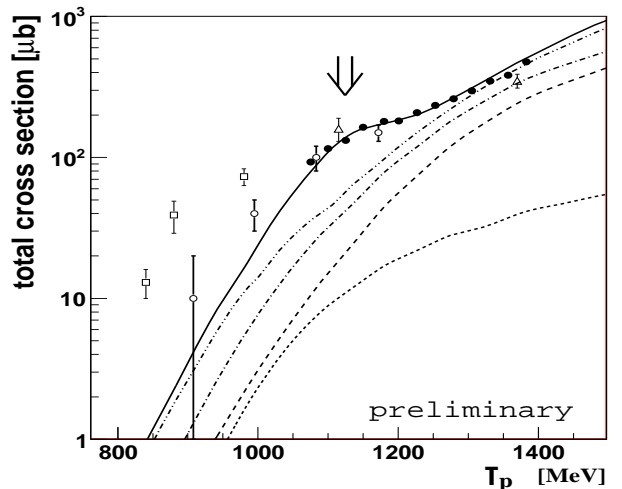


Fig. 3: Energy dependence of the total $pn \rightarrow pp\pi^0\pi^-$ cross section. Preliminary results of this work are shown by the full circles, previous bubble-chamber measurements from KEK by open circles, from NIMROD at RAL by open triangles and from Gatchina by open squares. The original Valencia model calculations are shown by the dash-dotted line. Contributions from Roper excitation and its decay into $N^* \rightarrow \Delta\pi$ are given by the dotted line and those from the t -channel $\Delta\Delta$ process by the dashed line. The modified Valencia model calculation (see text) is shown by the dot-dot-dashed line. The solid line shows the result, if the s -channel ABC resonance amplitude is added. The vertical arrow indicates the position of the ABC resonance. From EPJ Web of Conferences 37, 09033 (2012).

change (dashed). Modified calculations of the Valencia model tuned to describe the isovector pp -induced channels quantitatively by modifications of the Roper decay, the $\Delta\Delta$ excitation process as well as inclusion of the $\Delta(1600)$ resonance provide slightly larger cross sections and lead to agreement with the data at high energies. However, at low energies they still under-predict the observed cross section severely. This failure points to an isoscalar reaction component, not included in the t -channel treatment of two-pion production.

It is intriguing that this failure appears to be largest in the energy region, where the ABC effect has been observed in the other isoscalar channel, the $d\pi^0\pi^0$ channel. Indeed, adding an amplitude for the ABC resonance at $m = 2.37$ GeV with $\Gamma = 70$ MeV, $I(J^P) = 0(3^+)$ and fitting the strength of its contribution to the data leads to a reasonable description of the total cross section also at low energies (solid line in Fig. 3).

The observed differential cross sections are reasonably well described by conventional t -channel resonance processes. In particular the $\pi^0\pi^-$ invariant mass spectra show no ABC effect — in agreement with the fact that the isovector pion pair must be in relative p -wave and hence strongly suppresses any low-mass enhancement.

1.2.3 The neutron-proton elastic amplitude studies in the $\bar{n}p \rightarrow \bar{p}n$ reaction at ANKE

Any nucleon-nucleon amplitude analysis, such as that offered by the SAID collaboration, can only be as good as the input data. The situation is quite serious for neutron-proton scattering where there are major holes in the experimental database above about 1 GeV.

Extra information in the np sector can be found by performing experiments with a deuteron beam or a deuterium target. Quasi-free (p, n) or (n, p) reactions on the deuteron can act, in suitable kinematic regions, as a spin filter that selects the spin-dependent contributions to the np elastic cross section. Much information on the np charge-exchange amplitudes can be extracted by studying the deuteron charge-exchange break-up reaction, $\vec{d}p \rightarrow \{pp\}_s X$, where the final $\{pp\}_s$ diproton system is at very low excitation energy and hence in the 1S_0 state. Two channels here of interest are $X = n$ and $X = \Delta^0$ [see IKP annual reports 2010, 2011]. In impulse approximation these reactions can be interpreted in terms of $np \rightarrow pn$ or $np \rightarrow p\Delta^0$ charge exchanges with a spectator proton. In the 1S_0 limit, the $\vec{d}\vec{p} \rightarrow \{pp\}_s n$ reaction observables are directly related to the np spin-dependent amplitudes and, even away from this limit, theory can predict analysing powers, spin-correlation coefficients, and cross sections.

In order to constrain further the np amplitudes, the ANKE collaboration has embarked on a systematic programme to measure the $\vec{d}\vec{p} \rightarrow \{pp\}_s n$ observables up to the maximum COSY deuteron energy of $T_d \approx 2.3$ GeV. The proof of principle of the method was the experiment carried out at a deuteron energy of 1.17 GeV where, because of the wealth of neutron-proton data, the SAID amplitudes used as input in the calculations should be quite reliable. The measured values of the unpolarised cross section and the two deuteron Cartesian tensor analysing powers A_{xx} and A_{yy} were then quantitatively reproduced in impulse approximation. Dilutions of the signals due to higher partial waves in the final pp system were taken into account in the calculations.

The results of similar measurements are now available at deuteron beam energies of 1.2, 1.6, 1.8, and 2.27 GeV. The cross sections were integrated over $E_{pp} < 3$ MeV to provide the differential distributions in momentum transfer q presented in Fig. 4. In addition to the statistical errors that are shown, there are also overall systematic uncertainties arising from the luminosity determinations. Within these uncertainties, the agreement with the theoretical impulse approximation predictions at $T_d = 1.2$, 1.6, and 1.8 GeV is very encouraging and is in line with the 1.17 GeV data. In contrast, the unpolarised differential cross section at $T_d = 2.27$ GeV falls about 15% below the predictions based upon the current $np \rightarrow np$ partial wave analysis.

The results for the tensor analysing powers are shown in Fig. 5 at three beam energies as functions of the momentum transfer. The agreement between the experimental data and the impulse approximation predictions is very good at $T_n = 800$ and 900 MeV. At these energies the

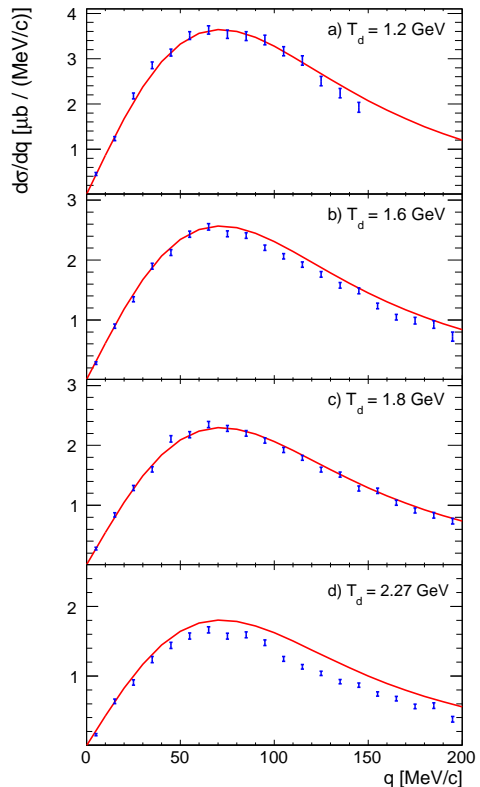


Fig. 4: Differential cross sections for the $dp \rightarrow \{pp\}_s n$ reaction at four different energies compared with impulse approximation predictions based upon the current SAID $np \rightarrow np$ amplitude analysis. The data are integrated over the $E_{pp} < 3$ MeV interval. Only statistical errors are shown.

SAID np amplitudes used as input in the calculations are considered to be reliable but at 1135 MeV, corresponding to the maximum deuteron energy available at COSY, the agreement is much worse. Since there are also severe discrepancies in the unpolarised cross section at this energy, it is natural to question whether there might be deficiencies in the SAID np analysis at this energy.

To check this possibility, the predictions were recomputed with the longitudinal spin-spin amplitude $\varepsilon(q)$ being reduced uniformly by 25%. This gives the much better overall agreement with the data that is demonstrated by the dashed curves in the lower panel of Fig. 5. This therefore suggests that the current SAID amplitudes might overestimate the relative strength of the $\varepsilon(q)$ at small q . Further proof of this hypothesis is furnished by the spin-correlations data that are compared with theory in Fig. 6. Although there is good agreement at $T_d = 1.2$ GeV, this is only achieved at 2.27 GeV when the SAID $\varepsilon(q)$ amplitude is scaled by the same 0.75 factor.

By analysing also the polarised target yields for an unpolarised deuteron beam, we could obtain the dependence of the target analysing power A_y^t on q that is presented in Fig. 7 at 1.2 and 2.27 GeV. This is predicted very well in impulse approximation at the lower energy but at 2.27 GeV the corresponding prediction can hardly be

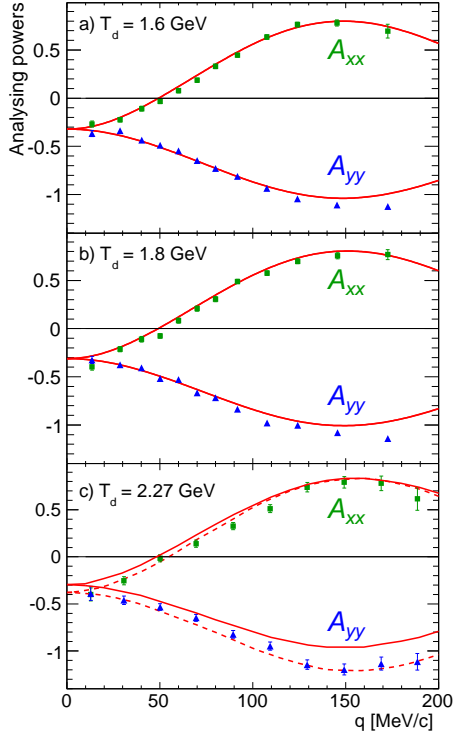


Fig. 5: Tensor analysing powers A_{xx} (squares) and A_{yy} (triangles) of the $\bar{d}p \rightarrow \{pp\}_s n$ reaction at three beam energies for $E_{pp} < 3$ MeV, compared to predictions based upon the current SAID $np \rightarrow np$ amplitudes. The dashed curves at 2.27 GeV correspond to a reduction of $\varepsilon(q)$ by 25%.

distinguished from the x -axis. There must therefore be a serious problem also with the SAID determination of the spin-orbit amplitude at 1.135 GeV.

The fact that the impulse approximation with the current SAID input reproduces well all the data below 1 GeV per nucleon shows that the theory works well there and this should get even better as the energy is raised. The discrepancies seen at the higher energy can only be resolved by reducing the strength of the spin-spin amplitudes, especially in the longitudinal direction, while increasing the spin-orbit contribution. The charge exchange on the deuteron therefore contains valuable information on the neutron-proton amplitudes.

To go higher in energy at COSY, an experiment will have to be undertaken in inverse kinematics with a polarised proton incident on a polarised deuterium gas cell, with the two slow protons being detected in the ANKE Silicon Tracking Telescopes. Such an experiment is scheduled at COSY in 2013 and this will allow the studies [D. Mchedlishvili et al., arXiv:nucl-ex/1212.2365] to be continued up to 2.8 GeV per nucleon.

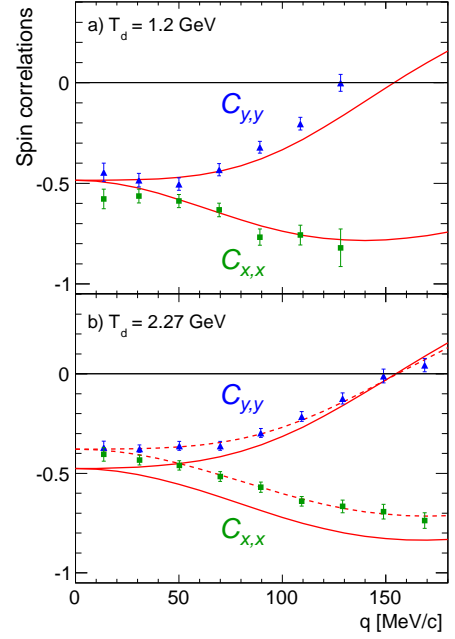


Fig. 6: The spin-correlation coefficients $C_{x,x}$ and $C_{y,y}$ for the $\bar{d}p \rightarrow \{pp\}_s n$ reaction at $T_d = 1.2$ and 2.27 GeV for $E_{pp} < 3$ MeV. The error bars include the uncertainties from the beam and target polarisations. The curves are impulse approximation predictions; dashed curves at 2.27 GeV correspond to $\varepsilon(q)$ being reduced by 25%.

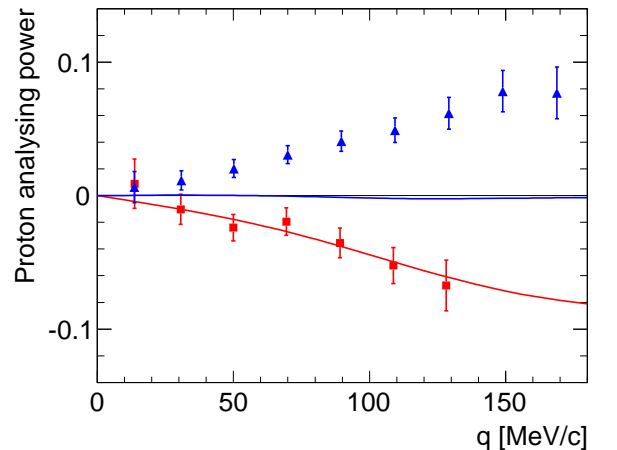


Fig. 7: Proton analysing powers A_y^p for the $\bar{d}p \rightarrow \{pp\}_s n$ reaction at $T_d = 1.2$ (red squares) and 2.27 GeV (blue triangles) for $E_{pp} < 3$ MeV compared to theory.

1.2.4 Search for a new boson in $\pi^0 \rightarrow \gamma e^+ e^-$ decays

Astrophysical observations like the excess of 511 keV photons from the galactic bulge and the unexplained amount of cosmic ray positrons motivate a new boson in the MeV scale. Such a particle could also explain the failure to reproduce the muon anomalous magnetic moment in the Standard Model (SM). If the new boson is vector like it could couple to a normal photon with a strength ε . A part of the ε vs. M_U parameter space, where M_U denotes the mass of the hypothetical U boson, could account also for the discrepancy in the muon $g-2$. This region is covered by results of other experiments except for U boson masses below 100 MeV.

In 2010 WASA-at-COSY recorded a data sample of π^0 decays in a four day pp test run. The π^0 are produced with a cross section of 1.1 mbarn at the chosen kinetic beam energy of 550 MeV. With a branching ratio of 1.2% $\pi^0 \rightarrow e^+ e^- \gamma$ decays can be produced abundantly. Since the decay is well understood within the SM, it is an ideal tool to search/look for a new boson with a mass below 100 MeV which decays to $e^+ e^-$.

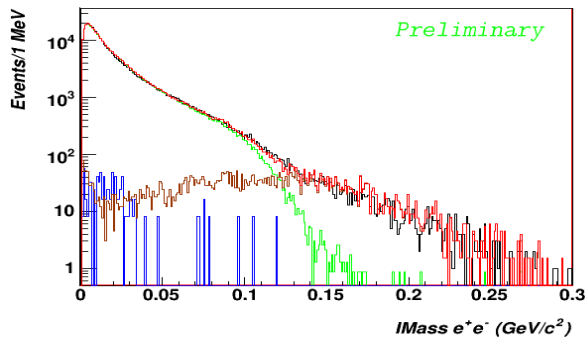


Fig. 8: Invariant Mass of e^+e^- after conversion reduction cuts. Black: data, Green: MC simulation of $\pi^0 \rightarrow e^+e^- \gamma$, Blue: pair production from $\pi^0 \rightarrow \gamma\gamma$ (MC), Brown: accidental coincidence of $\pi^0 \rightarrow e^+e^- \gamma$ and π^+ decays when π^+ is misidentified as a positron (MC), Red: MC sum.

The invariant e^+e^- mass spectrum is shown in Fig. 8. To maximize statistics no constraints on the γ and the final-state pp were set except for the requirement of one detected proton in the forward detector for timing reasons. The leptons are selected in the θ range of $45^\circ - 120^\circ$. They are identified using $E-\Delta E$ and $p-E$ techniques. Two sources of background are still present in data sample, random coincidence from π^+ mistaken for a positron and external $\pi^0 \rightarrow 2\gamma$ conversion. The former background is of the order of 1% up to 100 MeV and hence not significant below this energy. e^+e^- pair production from $\pi^0 \rightarrow 2\gamma$, however, contributes almost half the data in this region. While the use of a pellet target effectively eliminates external conversion in the target, most conversion happens at the beryllium beam pipe. Reduction to 2% of the original background contribution is accomplished via reconstructing the e^+e^- intersection point and the invariant mass at the beam tube that should equal zero for

external conversion. The corresponding cut reduces the $\pi^0 \rightarrow \gamma e^+ e^-$ signal by one half.

Based on the e^+e^- invariant mass spectrum, no evidence for a new boson has been found. The result for the new upper limit is shown in Fig. 9 together with the result by the SINDRUM collaboration based on the so far largest data set for the decay $\pi^0 \rightarrow \gamma e^+ e^-$. The figure also shows the expected upper limit from a new data set recorded by WASA 2012 based only on the statistical improvement. The limit on the branching ratio for $\pi^0 \rightarrow \gamma U$ can be used to set a new upper limit on the coupling ε . In Fig. 10 the ε upper limit is shown with the region in the U boson parameter space which corresponds to two standard deviations around the present discrepancy between the experimental and theoretical values of the anomalous magnetic moment of the muon. If the hypothetical U boson was to solely explain the muon $g-2$ discrepancy, its coupling to the SM photon and its mass would be expected in this region. In this region further limits are set by the experimental values of the muon and electron $g-2$ and by a search via $\phi \rightarrow \eta e^+ e^-$ from the KLOE experiment.

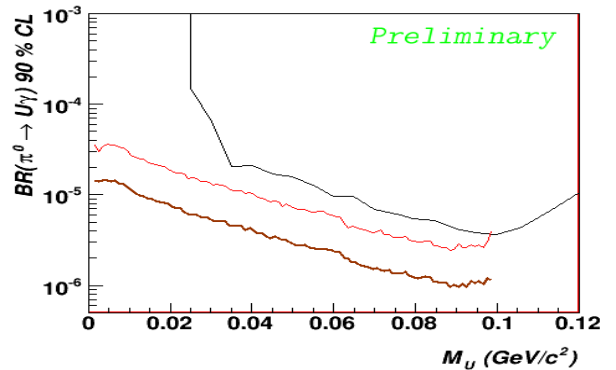


Fig. 9: Upper limits for the decay $\pi^0 \rightarrow U\gamma \rightarrow e^+e^- \gamma$. Black: SINDRUM, Red: WASA 2010 (this work), Brown: WASA 2012 (expected).

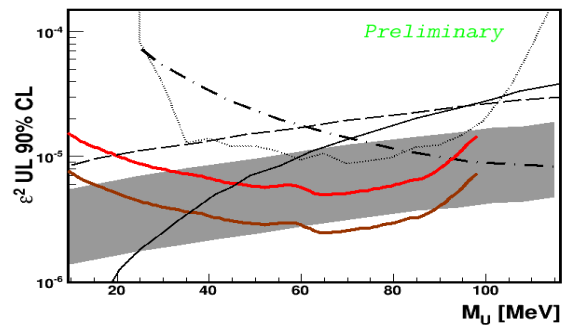


Fig. 10: Upper limits in the parameter space ε^2 vs. mass M_U . Dotted: Sindrums, Red: WASA 2010 (this work), Brown: WASA 2012 (expected), Dashed: muon $g-2$ experimental value, Solid black: electron $g-2$ experimental value, Dotted dashed: KLOE ($\phi \rightarrow \eta e^+ e^-$), Grey region: Region motivated by the discrepancy between experiment and the SM prediction of the muon $g-2$.

1.2.5 Pion production in pN collisions with the formation of a 1S_0 diproton in the final state

A wide programme of pion production studies in NN interactions has been realized by the ANKE collaboration. It includes measurements at the close-to-threshold energy of 353 MeV, which are relevant for chiral perturbation theory, and experiments at higher energies, where new information on NN dynamics could be obtained. Selecting the final pp -pairs in the 1S_0 state allows a more clear theoretical interpretation because few reaction channels are then allowed by the spin and parity constraints. In such kinematics, these processes involve large momentum transfers and are therefore sensitive to the short-range part of the NN interaction. A pair is predominantly in the 1S_0 state, denoted here by $\{pp\}_s$, if the relative energy E_{pp} of the two protons does not exceed ≈ 3 MeV. The S -wave dominance is checked in the experiments by the observed E_{pp} spectra (which have to follow the Migdal-Watson distribution) and by the flat distribution of the proton emission angle in the final pp rest frame. Results on the differential cross section and vector analyzing power for the $\bar{p}p \rightarrow \{pp\}_s\pi^0$ reaction, obtained with a polarized proton beam at 353 MeV, have been published recently [D.Tsirkov et al., Phys. Lett. B **712** (2012) 370]. After making plausible assumptions regarding the phases based on the Watson theorem, the measured observables allowed the complex s - and d - wave pion-production amplitudes to be determined. These partial wave amplitudes are also required in the analysis of the $\bar{p}n \rightarrow \{pp\}_s\pi^-$ reaction in order to isolate the p -wave amplitude, which can be linked to low energy three-nucleon scattering.

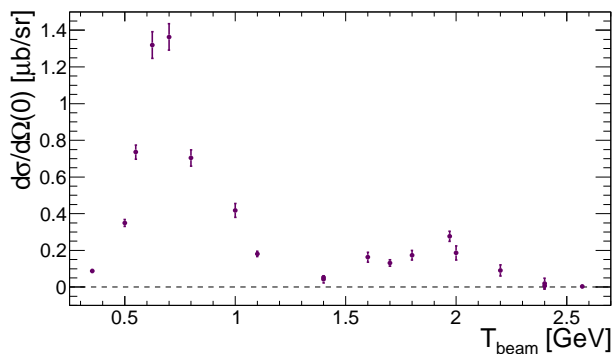


Fig. 11: Differential cross section of the $pp \rightarrow \{pp\}_s\pi^0$ reaction for zero emission angle of the diproton $\{pp\}_s$. All points represent ANKE results.

We can now present the differential cross section of the $pp \rightarrow \{pp\}_s\pi^0$ reaction measured at small diproton angles over almost the whole energy range of COSY. In recent experiments, together with our older ones, values of the forward differential cross section were determined at seventeen energies from 0.353 to 2.56 GeV; see Fig. 11. The peak at low energy (~ 0.7 GeV) obviously results from the excitation of the $\Delta(1232)$ isobar in the intermediate state. The second broader peak around 2 GeV,

which seemed to be not very convincing in the initial data, is now reliably observed. It is likely to have its origin in the excitation of isobars heavier than the $\Delta(1232)$ but more theoretical analysis is clearly required.

At the energies of 353, 500, 550 and 700 MeV the measurements were done with a polarized beam. This allowed us to measure the analyzing powers A_y of the reaction that are shown in Fig. 12. Though at the three higher energies the angular range is rather limited, the available data at these energies show strong disagreement with predictions based on the excitation of a $N\Delta$ intermediate state in the framework of a coupled-channel theory.

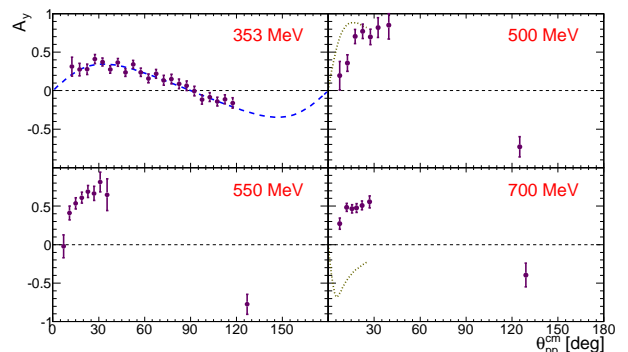


Fig. 12: Analyzing power of the $\bar{p}p \rightarrow \{pp\}_s\pi^0$ reaction at 353, 500, 550 and 700 MeV. The 353 MeV curve is the fit resulting from the partial wave analysis; those at 500 and 700 MeV are model predictions.

The π^- production in the diproton channel was investigated in quasi-free kinematics in the effective energy range $T_{\text{free}} = (353 \pm 20)$ MeV. As a first step, the proton analyzing power A_y and the differential cross section were measured with a polarized proton beam incident on a deuterium cluster-jet target [S. Dymov et al., Phys. Lett. B **712** (2012) 375]. These results, combined with the ANKE π^0 production data at 353 MeV, allowed a partial wave analysis to be carried out in both isospin channels.

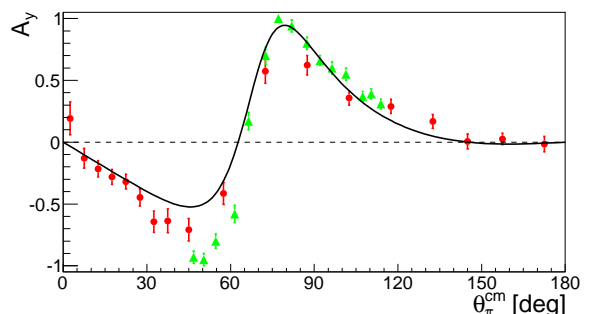


Fig. 13: Measured values of A_y for the $\bar{p}n \rightarrow \{pp\}_s\pi^-$ reaction showing both the reanalyzed ANKE (circles) and TRIUMF data [H. Hahn et al Phys. Rev. Lett. **82** (1999) 2258] (triangles). The line represents the PWA fit to the published ANKE results.

To reconstruct the complete kinematics of the $pd \rightarrow \{pp\}_s \pi^- p_{\text{spec}}$ reaction one has to detect the spectator proton p_{spec} in coincidence with the diproton. The accidental coincidence background was a major source of systematic uncertainty in this experiment. In Fig. 13 the results of a refined analysis are presented that now uses the timing data from the Silicon Tracking Telescope. This information reduced dramatically the accidental background level and increased the useful statistics. However, the updated results are in a good agreement with the published ones.

In the next step, the transverse spin correlations A_{xx} and A_{yy} were measured in the $\vec{d}\vec{p} \rightarrow p_{\text{sp}}\{pp\}_s\pi^-$ reaction at 353 MeV using a polarized hydrogen gas cell. The preliminary results of the measurement are shown in Fig. 14 in comparison with the predictions of the PWA. The value of $(1 - A_{xx}) \times d\sigma/d\Omega$ is proportional to the square of one of the pion p -wave production amplitudes that is important for the $4N\pi$ contact interaction. Independent of any assumptions made in the subsequent data analysis, the value of the spin-correlation A_{xx} in the $np \rightarrow \{pp\}_s\pi^-$ reaction at 90° is fixed completely by the unpolarised $pp \rightarrow \{pp\}_s\pi^0$ and $np \rightarrow \{pp\}_s\pi^-$ differential cross sections. However, the quasi-free nature of the π^- production experiment, as well as the mass differences among the pions and nucleons, means that there is uncertainty in the relative normalizations of the two unpolarised measurements and so the direct study of A_{xx} is definitely preferable. The value of A_{yy} in the diproton channel should be equal to unity, which provides an excellent test of the systematic uncertainties.

The theoretical uncertainties inherent in the assumptions made in the PWA are hard to estimate. These assumptions can be tested by studying additional observables and the only non-trivial one that is yet to be investigated is the spin-correlation coefficient $A_{z,x}$. Its measurement in the $pn \rightarrow \{pp\}_s\pi^-$ and $pp \rightarrow \{pp\}_s\pi^0$ reactions is proposed as the next step in the pion production programme at ANKE. The results will provide new constraints on the PWA and make the analysis more robust. The experiment will require a longitudinally polarised proton beam at COSY, which can be accomplished with the use of a Siberian snake. The installation of the snake at the PAX interaction point is foreseen for the Spring of 2013.

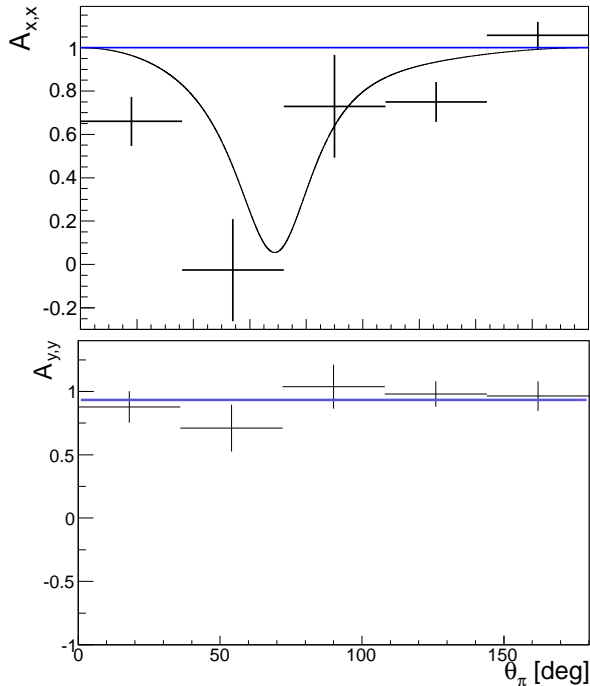


Fig. 14: Spin correlation coefficients A_{xx} and A_{yy} for the $\vec{n}\vec{p} \rightarrow \{pp\}_s\pi^-$ reaction at 353 MeV. The curves represent the ANKE PWA results.

1.2.6 The $\bar{p}p \rightarrow pK^+\Lambda$ reaction measured at different beam momenta

The $\bar{p}p \rightarrow pK^+\Lambda \rightarrow pK^+p\pi^-$ reaction has been recently measured with the COSY-TOF detector at beam momenta 2.7 and 2.95 GeV/c. The reconstruction of the charged tracks from the primary particles and the secondary particles of the Λ decay was done with the Straw-Tube-Tracker (STT). After a kinematic fit the data samples consist of about 150 000 reconstructed $pK\Lambda$ events for the measurement at 2.7 GeV/c and about 42 000 events for the measurement at 2.95 GeV/c. An $m_{p\Lambda}$ invariant mass resolution of $\sigma = 1.1 \text{ MeV}/c^2$ was achieved which is a factor 5 improvement compared to the TOF measurements without STT.

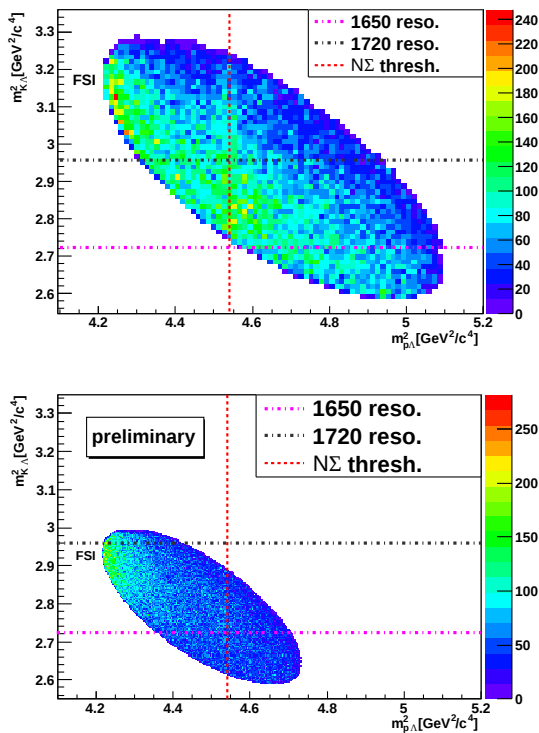


Fig. 15: Acceptance corrected Dalitz plot for the 2.95 GeV/c data (top) and for the 2.7 GeV/c data (bottom). The red line indicates the $N\Sigma$ threshold. The purple and black lines show the position of the $N(1650)$ and $N(1720)$ resonances, respectively.

In Fig. 15 the acceptance corrected Dalitz plots for the 2.95 GeV/c data (top) and 2.7 GeV/c (bottom) are shown. The black and purple lines show the position of the $N(1650)$ and $N(1720)$ resonances, respectively. The red line marks the position of the $N\Sigma$ threshold. In the 2.95 GeV/c data (Fig. 15, top) an enhancement can be seen at this threshold position. This could be related to a $p\Lambda - N\Sigma$ coupled channel effect, which produces a cusp at the $N\Sigma$ threshold. The density underneath is not homogenous but increases along the $m_{K^+p}^2$ diagonal axis to-

wards low $m_{K^+p}^2$ masses. This density distribution can be explained by the interference of $p\Lambda$ final state interaction (FSI) with the broad N^* resonances. Furthermore, the FSI enhancement at low $p\Lambda$ masses is tilted compared to the expectation of an exponentially decreasing density for increasing $m_{p\Lambda}^2$ because of this interference.

In the 2.7 GeV/c data (Fig. 15, bottom) no enhancement at the $N\Sigma$ threshold is seen which could be due to the energy dependent phase space overlap of $p\Lambda K$ and $N\Sigma K$ reactions. However, calculations show that this difference would be much smaller than the observed discrepancy. The FSI enhancement in the 2.7 GeV/c Dalitz plot is also distorted by an interference with the N^* resonances but the effect seems to be weaker compared with the Dalitz plot for the 2.95 GeV/c data.

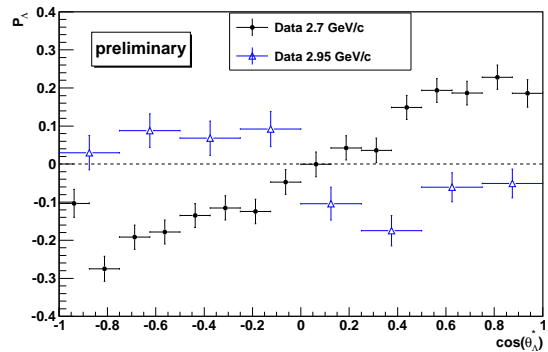


Fig. 16: The Λ polarisation as a function of $\cos \theta_{\Lambda}^*$ for the data at 2.7 GeV/c (black, preliminary) and 2.95 GeV/c (blue, from M. Roeder, PhD Thesis, University Bochum 2011).

The Λ polarization (P_{Λ}) can be determined from the self analyzing Λ decay. P_{Λ} as a function of the Λ scattering angle is shown in Fig. 16 for the data at 2.7 GeV/c (black) and 2.95 GeV/c (blue). As expected the polarization vanishes for $\cos \theta_{\Lambda}^* = \pm 1$, because the quantization axis is not defined there. In both cases there is a zero crossing at $\cos \theta_{\Lambda}^* = 0$. Comparing the shapes the position of the maximum is shifted and the sign is flipped.

The large difference in the Λ polarization can not be explained by the events in the $N\Sigma$ threshold enhancement since their relative contribution to all events is less than 5%. The influence of other effects such as resonances on the Λ polarization are not known yet.

Only a theoretical description of the associated strangeness production including resonance contributions, final state interaction and coupled channel effect may explain the strong variation of the observables at the different beam momenta.

1.2.7 The $\bar{p}p \rightarrow pK^0\Sigma^+$ reaction measured at 2.95 GeV/c beam momentum

The reaction $\bar{p}p \rightarrow pK^0\Sigma^+$ was studied with the COSY-TOF detector. A polarized proton beam with momentum of 2.95 GeV/c was focused on a liquid hydrogen target. The $pK^0\Sigma^+$ final state was identified based on the analysis of the delayed decays of the strange hadrons $K_s \rightarrow \pi^+\pi^-$ and $\Sigma^+ \rightarrow p\pi^0, n\pi^+$. The azimuthal symmetry and large angular acceptance of the detector as well as the excellent tracking capability provided by the silicon quirl and straw tube tracking subdetectors allows to measure the complete $pK^0\Sigma^+$ final state distribution. 905 $pK^0\Sigma^+$ events were reconstructed. The fraction of background events in this data sample is estimated to be at most 5.9%. Based on these numbers, the total cross section of the reaction $\bar{p}p \rightarrow pK^0\Sigma^+$ was determined to be $\sigma = (2.95 \pm 0.11_{stat} \pm 0.22_{syst}) \mu b$. This result is consistent with the energy dependence of the total cross section for this reaction measured by previous experiments.

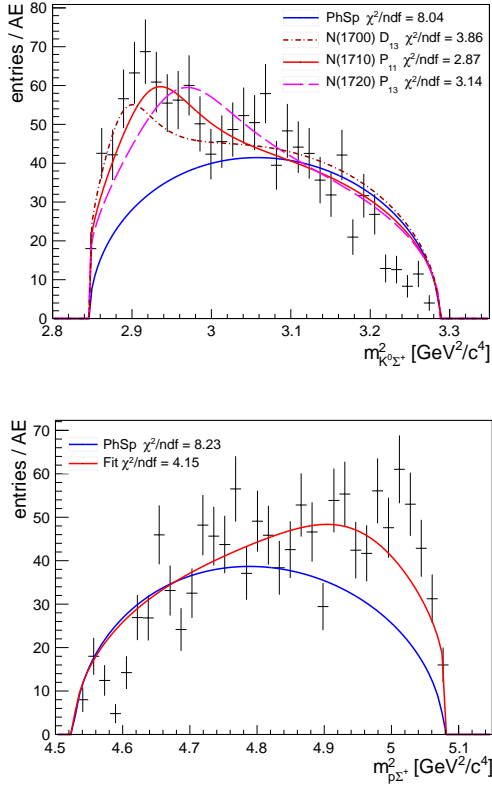


Fig. 17: Projections of the Dalitz plot on the $K^0\Sigma^+$ (top) and the $p\Sigma^+$ (bottom) squared mass. The blue line denotes the phase space distribution. The other lines correspond to fits using the coherent sum of phase space and nucleon resonances parameterized by Breit-Wigner functions. See text for details.

Projections of the acceptance corrected Dalitz plot are shown in Fig. 17. The $K^0\Sigma^+$ invariant mass spectrum shows a clear enhancement at low masses. This can be interpreted as a significant contribution of nucleon reso-

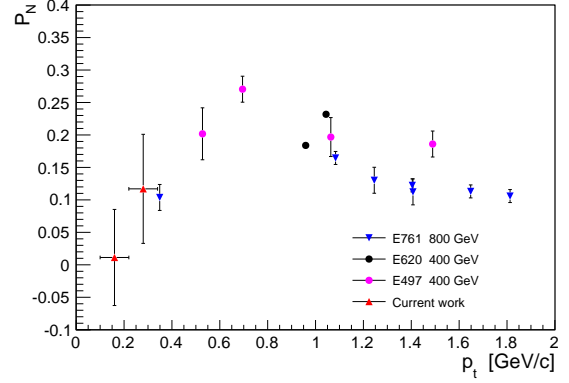


Fig. 18: Σ^+ polarization as a function of the Σ^+ transverse momentum p_t . The red triangles indicate the result of this work. The other data points represent the inclusive measurements at Fermilab.

nances to the production mechanism. Under the assumption that only a single resonance contributes, the best fit result is obtained for a contribution of the $N(1710) P_{11}$ resonance (solid red line), but neighboring resonances $N(1700) D_{13}$ (dot-dashed grey line) and $N(1720) P_{13}$ (dashed magenta line) can also contribute. The enhancement at high $p\Sigma^+$ masses can be explained as a kinematical reflection of the resonance contribution. The red line represents such contribution for the $N(1710) P_{11}$ resonance. In contrast to the $p\Lambda$ case in the reaction $pp \rightarrow pK^+\Lambda$, a strong $p\Sigma^+$ final state interaction seems to be absent.

For the first time, the polarization P_N of the Σ^+ hyperon in the reaction $\bar{p}p \rightarrow pK^0\Sigma^+$ was determined.

Within the statistical uncertainty the obtained Σ^+ polarization as a function of the transverse momentum p_t is in agreement with the only available data from high energy inclusive measurements (see Fig. 18).

The polarization of the Σ^+ as a function of its polar angle in the center-of-mass system (CMS) is shown in Fig. 19 by the red triangles together with the polarization of the Λ hyperon measured by COSY-TOF at 2.95 GeV/c beam momentum. In forward and backward direction corresponding to $\cos\theta_{hyperon}^* = \pm 1$ the polarization has to be zero. At $\cos\theta_{hyperon}^* = 0$ the polarization changes sign which is a consequence of the forward-backward symmetry of the entrance channel.

The Σ^+ and Λ polarization distributions appear to have the similar shape but with opposite sign. This is illustrated in Fig. 19 by a fit to the data with a sine function: the red solid line for P_{Σ^+} ($\chi_{ndf}^2 = 0.67$) and the blue dashed line for P_{Λ} ($\chi_{ndf}^2 = 1.12$). The amplitude of the sine function determines the maximum value of the polarization, which is $(10 \pm 7)\%$ for Σ^+ and $(-11 \pm 2)\%$ for Λ .

The obtained Σ^+ analyzing power A_N is shown in Fig. 20 by the red triangles together with the A_N of the Λ measured by COSY-TOF and DISTO [M. Maggiora, Nucl.Phys., A691:329–335]. The Σ^+ analyzing power

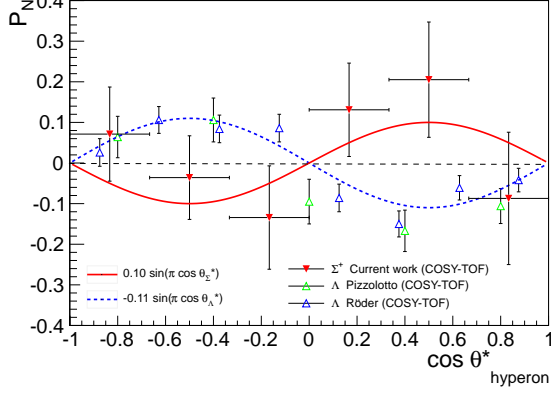


Fig. 19: The hyperon polarization as a function of the hyperon polar angle in the CMS. The red triangles indicate the Σ^+ polarization as the result of the current work, while the green [C. Pizzolotto, PhD Thesis, Erlangen] and blue [M. Röder, PhD Thesis, Bochum] triangles correspond to the Λ hyperon polarization measured by COSY-TOF at 2.95 GeV/c beam momentum.

appears to be a factor of two larger than that of Λ . The sine function fits the A_N of the Σ^+ distribution well ($\chi^2_{ndf} = 0.7$) in the whole range, as illustrated by the red line in Fig. 20, and has a maximum value of $(33 \pm 12)\%$. The depolarization D_{NN} as given in Fig. 21, quantifies the influence of a polarized initial state on the Σ^+ polarization. In the backward direction ($\cos \theta^*_{hyperon} \simeq -1$) the determined depolarization is consistent with zero. This could be explained by the fact that in this case the hyperon is more connected with the unpolarized target proton. In the forward direction ($\cos \theta^*_{hyperon} \simeq +1$) D_{NN} is large and positive ($D_{NN} \simeq +1$) for Σ^+ . According to the Laget model [J. Laget, Phys. Lett. B 259 24] this clearly indicates a dominant pion exchange in the production mechanism. The theoretical interpretation on the basis of the Laget model should be taken with a caveat since it misses an important ingredient of the production mechanism, namely the resonance contribution. As was shown from the analysis of the Dalitz plot, N^* resonances play a significant role in associated strangeness production and should, therefore, be included in the theoretical models.

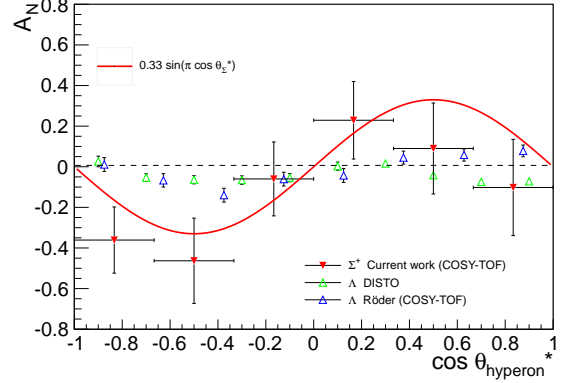


Fig. 20: Hyperon analyzing power A_N as a function of hyperon polar angle in CMS. The red triangles indicate the A_N of Σ^+ as the result of the current work; the green and blue triangles are the A_N of Λ from the DISTO and the COSY-TOF measurements, respectively.

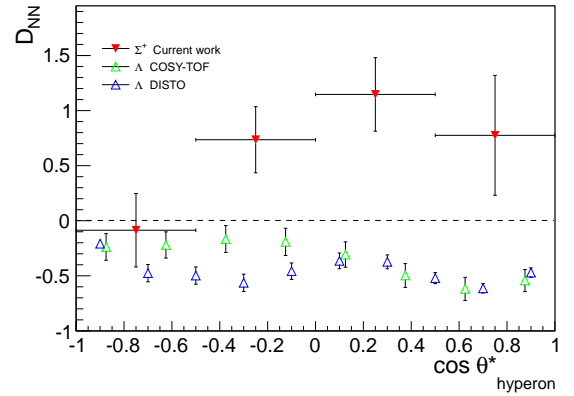


Fig. 21: Depolarization as a function of hyperon polar angle in the CMS. The red triangles indicate the D_{NN} of Σ^+ obtained in the current work; the green and blue triangles are the D_{NN} of Λ from the DISTO and the COSY-TOF measurements, respectively.

1.2.8 The production of K^+K^- pairs

The $pp \rightarrow ppK^+K^-$ reaction was measured at ANKE at three energies above the threshold for ϕ -meson production [Y. Maeda *et al.*, Phys. Rev. C **77** (2008) 015204; Q. J. Ye *et al.*, Phys. Rev. C **85** (2012) 035211]. In addition to the pp final state interaction (FSI), the non- ϕ data showed effects arising from the K^+K^- and K^-p interactions. The latter is seen most clearly in the ratio of the differential cross sections in terms of the K^-p and K^+p invariant masses. The first step in any analysis of these data is the separation of the contribution of the ϕ -meson from the rest and this is obviated when data are taken below the ϕ threshold. A second advantage of working in this region is that the data populate preferentially the *interesting* range of K^+K^- invariant masses. Data are already available at low energies from COSY-11 [M. Silarski *et al.*, Phys. Rev. C **80** (2009) 045202] but the limited statistics were not sufficient to yield detailed differential distributions. The previous ANKE experiments were therefore extended by carrying out measurements in an identical manner at an excess energy $\varepsilon_{KK} = 23.9$ MeV, which is well below the central ϕ -meson threshold at 32.1 MeV. Although ANKE covers a larger fraction of phase space at the lower ε_{KK} , assumptions have to be made to evaluate the cross sections from the counting rates. As in the earlier work, our *ansatz* is to weight the four-body phase space with the product of factors corresponding to pp , K^-p , and KK FSI. Great sensitivity to the K^-p FSI is found in the ratio of the cross sections in terms of the K^-p and K^+p invariant masses shown in Fig. 22. The distribution is even steeper than in our earlier data and the best fit requires an *effective* K^-p scattering length $a_{K^-p} \approx (0 + 2.45i)$ fm, which is larger than the 1.5 fm found from the above-threshold data. With this value of a_{K^-p} , the individual $d\sigma/dM(K^\pm p)$ and $d\sigma/dM(K^\pm pp)$ distributions, as well as their ratios, are all well described.

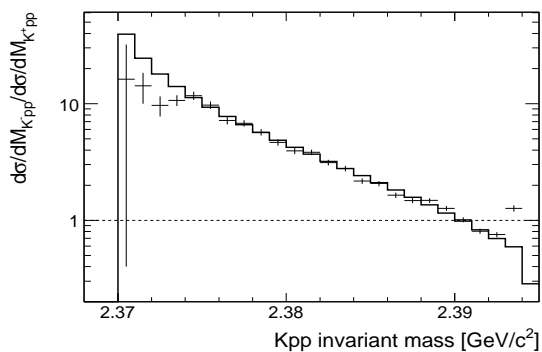


Fig. 22: Ratio of the $pp \rightarrow ppK^+K^-$ cross sections in terms of the K^-p and K^+p invariant masses. The histogram is the fit within the product FSI *ansatz*.

The change in a_{K^-p} with energy is not unexpected because this is an effective parameter within the product *ansatz*, which is a very simplistic approximation to the four-body final state interaction.

Further information on the dynamics is provided by the

distribution in K^+K^- invariant masses shown in Fig. 23. The behaviour at high $M_{K^+K^-}$ depends on the circulating beam energy, which decreases steadily through the cycle. The most striking effects though are the strength near the K^+K^- threshold and the dip at $M_{K^+K^-} \approx 0.995$ GeV/ c^2 , which corresponds exactly to the $K^0\bar{K}^0$ threshold. This is compelling evidence for a cusp effect arising from the $K^0\bar{K}^0 \rightleftharpoons K^+K^-$ transitions. Preliminary analysis within our coupled-channel description [A. Dzyuba *et al.*, Phys. Lett. B **668** (2008) 315] suggests that the $K\bar{K}$ enhancement is mainly in the isospin-zero channel.

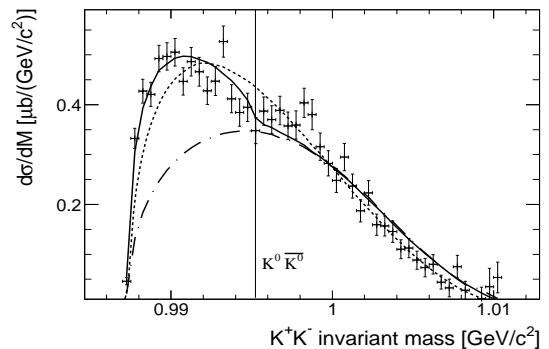


Fig. 23: The K^+K^- invariant mass distribution for the $pp \rightarrow ppK^+K^-$ reaction at $\varepsilon = 23.9$ MeV. The solid curve shows the calculation taking into account of the pp , K^-p and KK final state interaction (dash-dotted - strength without KK FSI). The dotted curve represents the four-body phase space simulation normalized to all data points.

Our preliminary total cross section for kaon pair production is plotted in Fig. 24 along with COSY-11, DISTO, and ANKE data. The four-body phase space distribution normalized to the highest ANKE point (dotted line) fails to describe the data. The inclusion of the pp , KK and K^-p (with $a_{K^-p} = (0 + 1.5i)$ fm) FSI (solid line) improves the situation. However, to describe simultaneously the old and new ANKE data would require a_{K^-p} to increase significantly at low ε_{KK} .

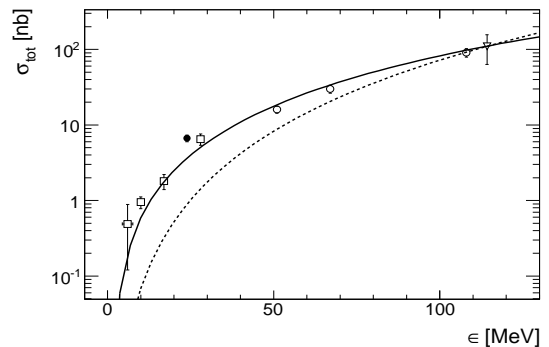


Fig. 24: Excess energy dependence of the $pp \rightarrow ppK^+K^-$ total cross section. Data are from ANKE (closed circle), previous ANKE (open), DISTO (open triangle), and COSY-11 (open squares). The curves are described in the text.

1.2.9 PAX polarizes a stored beam at COSY by spin-filtering

An intense beam of polarized antiprotons will open new experimental opportunities to investigate the still unknown structure of the nucleon. We remind, for instance, the first direct measurement of the transversity distribution of the valence quarks in the proton, a test of the predicted opposite sign of the Sivers-function, related to the quark distribution inside a transversely polarized nucleon in Drell-Yan as compared to semi-inclusive deep-inelastic scattering, and a first measurement of the moduli and the relative phase of the time-like electric and magnetic form factors $G_{E,M}$ of the proton [see PAX Collaboration Technical Proposal at <http://www.fz-juelich.de/ikp/pax>].

Although a number of methods to provide polarized antiproton beams have been proposed, no polarized antiproton beams have been produced so far. To provide the community with this still missing tool, the PAX Collaboration is, since years, pursuing a dedicated experimental program at the COSY storage ring. An initially unpolarized beam of spin-1/2 particles in a storage ring can, in principle, be polarized by two methods: either by selectively reversing the spin of particles in one spin state (“*spin-flipping*”) or by selectively discarding particles in one spin state (“*spin-filtering*”). Spin-flipping would be preferable over spin-filtering as it would offer the advantage of polarizing the beam while its intensity remains unaffected.

For this reason, the proposal of a group from Mainz of using co-moving electrons or positrons at slightly different velocities from the orbiting protons or antiprotons as a means to polarize the stored beam, attracted great attention in the community a few years ago. To provide an experimental test of this idea, the PAX Collaboration, in 2008, mounted an experiment that used the electrons in the electron cooler as a target and measured the effect of the electrons on the polarization of a 49.3 MeV proton beam orbiting in COSY. Instead of studying the build-up of polarization in an unpolarized beam, the team studied the inverse process by observing the depolarization of an initially (vertically) polarized beam. No depolarization effect on the proton beam could be detected within the statistical precision of the measurement. This translated into an upper limit for the e - p transverse and longitudinal spin-flip cross-sections of 1.5×10^7 b at a relative velocity of $v = 0.002$, six orders of magnitude below the numerical predictions [D. Oellers et al. Phys. Lett. B 674 , 269 (2009)].

The result ruled out the practical use of polarized leptons to polarize a beam of antiprotons and left spin-filtering as the only proven method to polarize a stored beam in situ. Spin-filtering exploits the spin-dependence of the strong interaction using a polarized internal target. Since the total cross section is different for parallel and antiparallel orientations of the spins of beam and target protons, one spin orientation of the beam particles is depleted at a higher rate than the other one and the circulating beam

becomes increasingly polarized, while the intensity decreases with time. The first spin-filtering experiment was performed by the FILTEX group at the TSR ring in Heidelberg in 1992 and exploited a 23-MeV stored proton beam. To provide an additional measurement confirming the validity of the filtering-method to polarize a stored beam and to test the present theoretical understanding of the mechanism under different experimental conditions, the PAX Collaboration implemented a new experiment at the COSY-ring. The two main components of the experimental apparatus used for the measurement are the polarized hydrogen gas target, installed at the PAX interaction point, and the beam polarimeter, realized by using the analyzing power of proton-deuteron elastic scattering on a deuterium cluster jet target, installed at the ANKE interaction point. The electron cooler achieves phase-space cooling of the stored beam.

The sequence of operations in the spin-filtering experiment is described below:

- An unpolarized proton beam is injected in the COSY ring at a beam energy of 45 MeV. The beam is cooled and subsequently accelerated to 49.3 MeV. This energy has been chosen for the spin-filtering experiments, because of existing data of the analyzing power in proton-deuteron elastic scattering.
- At this point the spin-filtering starts. Polarized hydrogen is injected in to the storage cell at the PAX interaction point. The holding field coils are powered in either up or down orientation for the duration of the spin-filtering period. Two different durations for the spin-filtering periods have been adopted: one lasting for 12000 s, and a longer one of 16000 s, corresponding to about 1.5 and 2 times the measured beam-lifetime (8000 s).
- At the end of the spin-filtering period, the PAX polarized target is switched off, the ANKE deuterium-cluster target is switched on and the data acquisition of the beam polarimeter starts.

Spin-filtering cycles were repeated for different directions of the target holding fields: up or down. The beam polarization obtained from spin-filtering cycles of different length for the two target spin-orientations is presented in Fig. 25.

By making use of the measured polarization buildup and additional information on the target polarization and density, and the beam revolution frequency, the effective polarizing cross section has been derived [W. Augustyniak et al. Phys. Lett. B 718 , 64 (2012)]:

$$\bar{\sigma}_1^{meas} = -23.4_{\pm 1.9}^{+3.9(stat.)} \text{ mb.} \quad (1)$$

The spin-dependent cross-section measured at COSY is presented in Fig. 26 together with the other existing measurement performed by the FILTEX collaboration. The

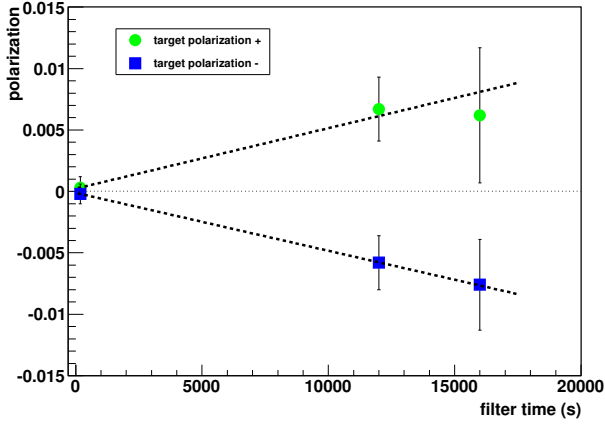


Fig. 25: Polarization induced in the beam after filtering for different times and different signs of the target polarization. The induced polarization in the beam has the same sign as the target polarization, reflecting the negative sign of the polarizing cross section.

solid line represents the theoretical prediction from the nucleon-nucleon interaction. The good agreement between experiment and theory confirms that spin-filtering of a stored proton beam is well-described taking into account only the contributions from proton-proton scattering.

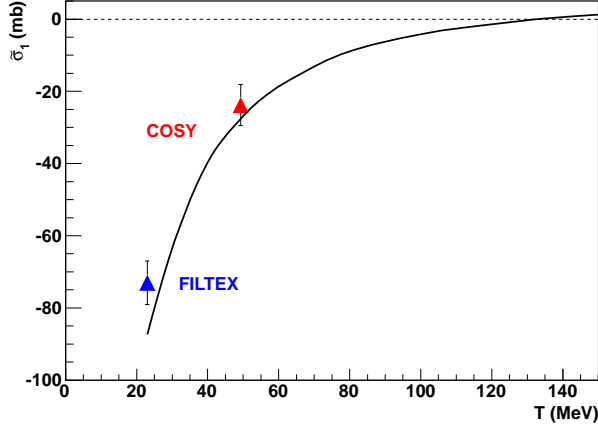


Fig. 26: Measured spin-dependent polarizing cross section for the interaction (only statistical errors are shown). The solid line represents the prediction from the SAID database

The achievement represents a milestone in the field and it is of fundamental importance in view of the possible application of the method to polarize a beam of stored antiprotons. It definitively proves that spin-filtering can be used to polarize a stored beam in situ and that the theoretical understanding of the spin-filtering mechanism is in excellent agreement with the experimental results. In this respect, the existing theoretical predictions for the polarization buildup with antiprotons are affected by the lack of knowledge of the proton-antiproton interactions and

differ by more than a factor 2. For this reason, a direct measurement of the polarizing cross sections in proton-antiproton interactions constitutes an inevitable step towards the design of a dedicated polarizer ring. To this purpose, the PAX Collaboration has submitted a proposal to the CERN-SPSC to measure the spin-dependence of the proton-antiproton interaction at the AD-ring.

The present work is supported by the EU grants of the Projects I3HP2 and I3HP3 (Grant Agreements 227431 and 283286) and of the ERC Advanced Grant POLPBAR (Grant Agreement 246980).

2 COSY Operation and Developments

2.1 Beam Time at COSY

For 2012 in total 6552 hours of operation were scheduled. 4144 hours (47.2%) were scheduled for user beam time, 1512 hours (17.2%) were scheduled for dedicated beam dynamic studies, equipment tests for HESR and FAIR related activities, 896 hours (10.2%) were used for COSY machine development and experimental set-up, see Fig. 27. Maintenance/shutdown duration was 2232 hours (25.4%). The distribution of user weeks is listed in Table 1.

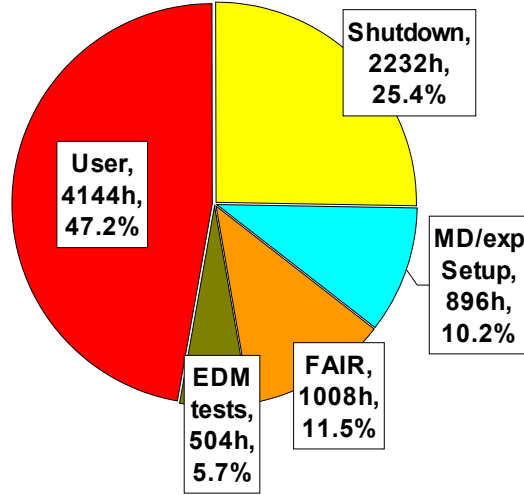


Fig. 27: COSY beam-time statistics in 2012.

Table 1: Overview COSY user beam time and EDM/FAIR weeks in 2012.

Date	Experiment	Duration	Reaction, experiment #
16.01.12.–22.01.12	FAIR (CBM)	1 week	FAIR week for CBM-group
28.01.–18.03.	WASA	7 weeks	Fundamental symmetries in $pp \rightarrow pp\eta$, 182.2
19.03.–25.03.	FAIR	1 weeks	Stochastic cooling tests and PANDA STT
26.03.–01.04.	EDM	1 week	EDM tests
07.04.–15.04.	WASA	1 week	Quasifree reaction $\bar{p}d \rightarrow d\pi^0\pi^0 + p_s, \bar{p}d \rightarrow pn + p_s$, 210
05.05.–13.05.	EDM	1 weeks	EDM, 176.6
14.05.–27.05.	EDM	2 weeks	EDM tests
02.06.–17.06.	ANKE	2 weeks	Polarized internal d gas target, 201.1
30.07.–11.08.	FAIR	2 weeks	PANDA STT and CBM
12.08.–09.09.	WASA	4 weeks	Test of the Standard Model in pi^0 decays, 196.2
17.09.–23.09.	FAIR	1 weeks	Beam dynamics and PANDA STT
24.09.–07.10.	TRIC	1 week	Time-Reversal invariance in pd scattering, 215
27.10.–09.12.	TOF	6 weeks	Strangeness physics at COSY-TOF, 193.2
10.12.–22.12.	FAIR	2 weeks	PANDA MVD and PANDA TOF walls prototype tests
Total 2012		32 weeks	
	user weeks	22 weeks	
	EDM weeks	3 weeks	
	FAIR weeks	7 weeks	

One of the highlights of the COSY machine operation in 2012 was the deceleration of a proton beam from injection down to 35 MeV kinetic energy. At this energy the PAX collaboration envisages to investigate the doubly polarized proton deuteron breakup by measuring 22 polarization observables. Since at COSY a beam was never before decelerated and the lowering of all magnetic fields may cause severe beam losses due to the hysteresis behavior of the magnets a feasibility test was carried out in December 2012. The final experiment will use the PAX low beta target point with a storage cell target and also requires an electron cooled beam. Therefore the tests have been carried out with PAX optics, electron cooling at injection, deceleration from the 45 MeV injection energy down to 35 MeV and cooling at 35 MeV.

First the usual magnet cycle setup was applied which, however, quickly showed that after one deceleration cycle the beam was lost at injection. The reason is that different hysteresis curves of all the magnets are passed through so that the correct injection fields were not recovered from cycle to cycle. To solve this problem a super-cycle was established consisting of one cycle with deceleration and a second cycle without beam with a standard acceleration ramp for all the magnets to 600 MeV/c to compensate hysteresis effects.

With the regular ramping scheme it was still not possible to decelerate sufficient beam because of the unsatisfactory margin to adjust the tune during the deceleration. To circumvent this, a rather sophisticated cycle setup was applied. It was already developed for the PAX experiments in the past. The starting fields for the main COSY magnets (dipoles, quadrupoles) were set below injection energy and a regular ramp to injection energy was adopted. Only then the beam could be successfully injected from the cyclotron. This procedure offered the possibility to define ramps independently for all elements down to 35 MeV. As a result sufficient beam down to the desired energy could be decelerated. Strong electron cooling at injection turned out to be an important issue. A sufficient long cooling time was unavoidable for a good transmission through the down-ramp process. At 20 sec cooling time the transmission reached roughly 50%. An increase of the cooling time to 30 s could improve the transmission to 80% corresponding to 7×10^9 un-polarized protons. The electron cooling at the low energy caused no severe problem. A readjustment of the electron high voltage and a slight adjustment of the electron beam position and angle led to a good cooling efficiency.

In conclusion this study has proven that with an appropriate magnet cycling program the proposed PAX experiment at this low energy can be carried out at COSY.

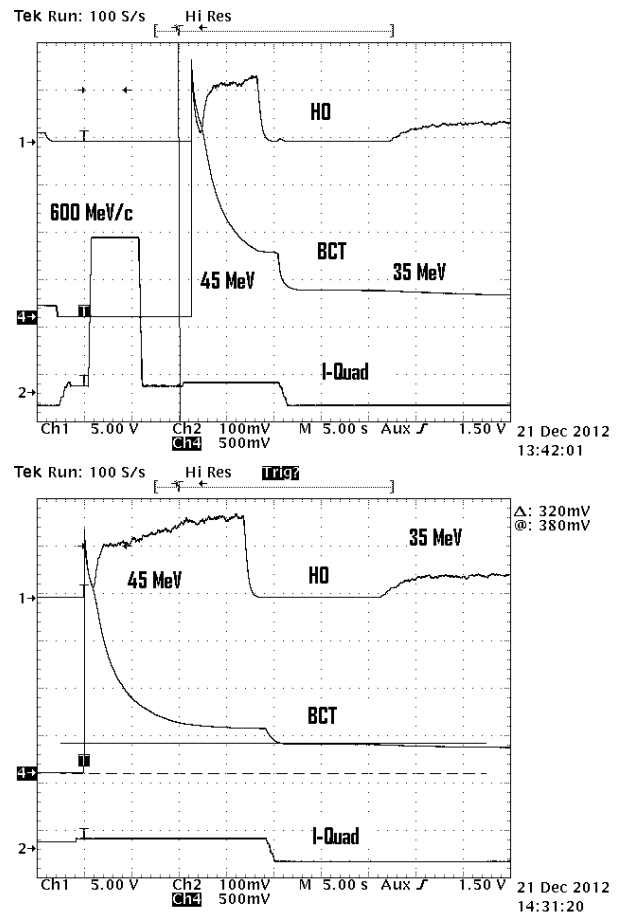


Fig. 28: Oscilloscope picture from the control room: H0: the rate of recombined protons of the beam with electrons from the cooler, as measure of electron cooling, BCT: beam current, I-Quad: current in one of the COSY quadrupoles. The upper panel shows a complete supercycle, first acceleration to 600 MeV/c without beam, and then the deceleration cycle. The lower panel is just the deceleration with prolonged cooling time and improved deceleration efficiency. In the H0 rate the cooling at injection and to the right the cooling at 35 MeV is visible.

3 Theoretical Investigations

3.1 Introduction

The IKP/IAS theory group studies the strong interactions in their various settings — spanning topics in hadron structure and dynamics with light and heavy quarks to lattice simulations of light nuclei and collective phenomena in heavy nuclei. The main focus is on the formulation and application of effective field theories for precision hadron and nuclear physics based on the symmetries of QCD. A shift of focus with more emphasis on high performance computing is presently taking place, spearheaded by the work on nuclear lattice simulations. Since July 2012, the group is heavily involved in the activities of the collaborative research center “Symmetries and the emergence of structure in QCD” (CRC 110) together with researchers from Bonn University, Technical University München, the Institute of High-Energy Physics (Beijing, China) and Peking University (China). Some of the highlights of these and other activities are discussed in the following.

3.2 Structure and rotations of the Hoyle state

The carbon nucleus ^{12}C is produced by fusion of three alpha particles inside red giant stars. Without any resonant enhancement, however, the triple-alpha reaction rate is too low to explain the abundance of carbon in our universe. In the early 1950’s, Öpik and Salpeter noted independently that the first step of merging two alpha particles is enhanced by the formation of ^8Be . The ground state of ^8Be is a resonance with energy 92 keV above the ^4He - ^4He threshold with a width of 2.5 eV. A year later, however, Hoyle realized that this enhancement is still not enough to explain the observed carbon abundance. To resolve the discrepancy, Hoyle predicted a new positive-parity resonance of ^{12}C just above the combined masses of ^8Be and ^4He . The Hoyle state was confirmed experimentally at Caltech in 1957 and has been an enigma to nuclear structure theory ever since. Around the time of the experimental confirmation of the Hoyle state, Morinaga conjectured that the structure of excited alpha-nuclei such as the Hoyle state maybe be non-spherical. This would imply low-lying even-parity rotational excitations. Last year, we have presented a lattice calculation of the Hoyle state, which was the first *ab initio* calculation of this elusive state. In that work the low-lying spectrum of ^{12}C was calculated using the framework of chiral effective field theory and Monte Carlo lattice simulations, also called nuclear lattice simulations. To investigate in more detail the structure of the Hoyle state (and also the ground and other excited states in ^{12}C), we had to improve our simulation methods. In our new projection Monte Carlo calculations we use a larger class of initial and final states than considered in previous work. For the calculation of ^4He we use an initial state with four nucleons, each at zero momentum. For the calculation of ^8Be we use the

same initial state as ^4He , but then apply creation operators after the first time step to inject four more nucleons at zero momentum. The analogous process is done to extract four nucleons before the last step. This injection and extraction process of nucleons at zero momentum helps to eliminate directional biases caused by initial and final state momenta. We make use of many different initial and final states to probe the structure of the ^{12}C states, such as 12 independent nucleons or cluster type wave functions. In all of the ^{12}C states investigated in our work we measure four-nucleon correlations by calculating the expectation value of ρ^4 , where ρ is the total nucleon density. We find strong four-nucleon correlations consistent with the formation of alpha clusters. We also find that the ground and the first excited 2_1^+ -state are dominated by a compact triangle configuration. The fact that it is an isosceles right triangle rather than an equilateral triangle is just an artifact of the lattice spacing. For another type of initial states, we use a set of three alpha clusters formed by Gaussian packets centered on the vertices of a bent-arm or obtuse triangular configuration as shown in Fig. 29. There are a total of 24 equivalent orientations of this configuration. This type of initial states produces a plateau at intermediate Euclidean times about 7.5 MeV above the ground state. We do not find the same plateau starting from other configurations of alpha clusters. We conclude that the configurations in Fig. 29 have the strongest overlap with the 0_2^+ Hoyle state of ^{12}C . This bent-arm or obtuse triangular configuration of alpha clusters therefore represents the Hoyle state and the 2_2^+ excitation just 3 MeV above it, consistent with very recent experiments at TUNL. We have also calculated at leading order the root-mean-square charge radius and quadrupole moment of the even-parity states of ^{12}C . The agreement with available experimental values is reasonable. The lattice results at leading order have a tendency to be somewhat smaller than experimental values. This presumably reflects the greater binding energies and smaller radii of the nuclei at leading order. We also predict electromagnetic decays involving the 2_2^+ state that may be measured experimentally in the near future.

3.3 Baryon electric dipole moments from the θ -term

Electric dipole moments (EDMs) of hadrons are sensitive probes of CP violation in the Standard Model and beyond. There is world-wide experimental activity to further reduce the upper limit on the neutron EDM and there are also proposals to measure charged particle (proton, light nuclei) EDMs in storage rings. Besides these challenging experimental activities, first full lattice QCD calculations of the neutron and the proton electric dipole moment are becoming available. Such simulation studies require the knowledge of the quark mass and finite volume dependence of the pertinent observables, as lattice QCD usually operates at quark mass values above the physical values and always in a finite volume. We have

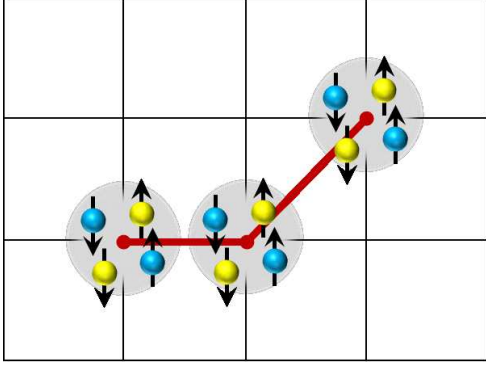


Fig. 29: Shown is the initial state of a wave function consisting of three alpha clusters formed by Gaussian packets centered on the vertices of a bent-arm or obtuse triangular configuration, the dominant configuration in the wave function of the Hoyle state. There are a total of 24 equivalent orientations of this configuration.

therefore revisited the theory of the baryon EDMs related to the θ -term in QCD, extending our earlier calculations of the nucleon electric dipole form factors (EDFFs) and EDMs to the ground state baryon octet up to NLO in the framework of $U(3)_L \times U(3)_R$ chiral perturbation theory. Our main findings can be summarized as follows: (1) We have shown that the complete one-loop expressions (i.e. accounting for all terms of $\mathcal{O}(p^3)$ and $\mathcal{O}(p^4)$, with p a genuine small parameter) for the baryon EDFFs and EDMs depend on two combinations of unknown LECs only, called w_a and w_b . In case of the charged baryons, the combination $w_b(\mu)$ combines two LECs from the tree graphs and one LEC that appears only in loops. (2) We have shown that the NLO corrections are large for the neutral hyperons Λ and Σ^0 . This is due to a suppression of the LO contributions based on exact cancellations between loops of positively and negatively charged pions. For the charged baryons, we find a strong sensitivity to the LEC combination w_b .

(3) We have derived a set of relations between various EDMs that are free of unknown LECs. These can be useful for future lattice simulations of baryon EDMs. (4) Based on recent lattice results for the neutron and proton EDMs at $M_\pi = 530 \text{ MeV}$ from the RBC/UKQCD collaboration (see Fig. 30), we could pin down the two LEC combinations w_a and w_b . Based on this, we can predict the baryon EDMs at the physical pion mass. In particular, we find $d_n = -2.9 \pm 0.9$ and $d_p = 1.1 \pm 1.1$ in units of $10^{-16} \theta_0 e \text{ cm}$. (5) The finite volume corrections to the baryon EDMs in the p -regime are also studied. Because the loops contribute already at LO, it is found that the finite volume corrections are huge for all the baryon EDMs except for the Λ and Σ^0 for the pion mass close to its physical value. For the neutron, the finite volume correction is about 10% at $M_\pi L = 4$. Clearly, lattice simulations at smaller quark masses are called for to get a better handle at these interesting quantities.

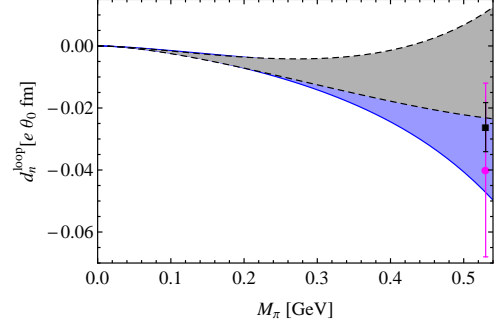


Fig. 30: Loop contributions to the neutron EDM as a function of the pion mass. The bands, reflecting the uncertainties by varying the renormalization scale between $\mu = M_\rho$ and m_Σ , between the solid and dashed boundaries are the NLO and the LO results, respectively. The filled circle and square with error bars are the lattice data from Shintani et al (2008) and from RBC/UKQCD (2012), respectively.

3.4 Scalar mesons in a finite volume and the role of partial wave mixing

One of the present issues in QCD lattice calculations is the determination of the excited hadron spectrum. The traces of the resonances are encoded in the volume dependence of the energy spectrum measured on the lattice. However, the extraction of resonance parameters is not simple - most resonances are wide and decay in more than one channel. Over the years, we have developed methods to deal with such situations, mostly restricted to the case of total momentum zero. It has been realized by various groups that working in moving frames can be equivalent to a variation of the volume. Our recent work provides a formulation for the scattering of two particles confined in a finite box with total nonzero momentum, adapted to the chiral unitary framework. The idea is based on extending previously known techniques for zero momentum, discretizing the energy levels by imposing the boundary conditions in the moving frame. Unitarized chiral perturbation theory can be used to stabilize the fits to the measured energy levels as shown earlier.

Given a hadronic interaction, levels for the first five boosts $\vec{P} = (2\pi/L)(0,0,0)$ to $(0,0,2)$ can be predicted and attributed to the subgroups of cubic symmetry. Employing coupled-channel unitarized chiral perturbation theory including the next-to-leading order terms, one can derive the levels for the mixed partial wave system with $I = 1/2$, $S = -1$ and $L = 0, 1$ [$\kappa(800)$ and $K^*(892)$, respectively] as well as for the scalar sector with $I = 0$, $S = 0$ and $L = 0, 2$ where the $\sigma(600)$ resides.

We have demonstrated for the $\kappa(800)/K^*(892)$ system that partial wave mixing is a very large effect for realistic box sizes and needs to be taken into account. In Fig. 31, we show the size of this effect for the S-wave, isospin-1/2 partial wave in elastic πK scattering. To disentangle the S-wave from P- or D-wave, we have derived a set of

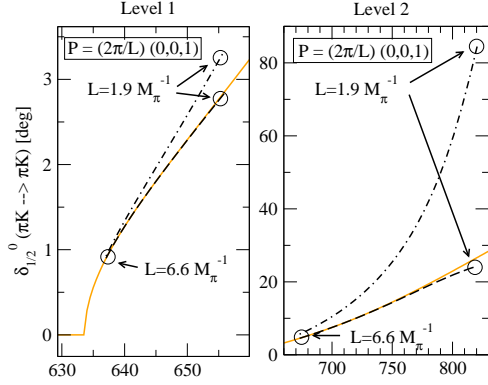


Fig. 31: Phase shifts [solid (orange) lines] for elastic πK scattering. The dashed lines give the reconstructed phase shifts using the methods developed here and including partial wave mixing. If partial wave mixing is neglected one obtains the dash-dotted lines. Results are shown for the boost $\sim (0,0,1)$. In the figure, also the corresponding values of the box size L are indicated.

equations in the one-channel formalism that are shown to be very precise as long as one stays below the inelastic thresholds.

Furthermore, a scheme was developed in which the hadronic interaction is expanded in energy to allow for the extraction of the infinite volume limit, simultaneously fitting levels for different boosts and at different energies. The model-independent information from the lowest order in the chiral expansion is kept explicitly in this expansion, greatly stabilizing the fit to lattice data. Such statistical analyses can be used for actual lattice data, or, as done in the present work, serve to determine promising lattice setups and the accuracy of lattice data to allow for reliable resonance extraction.

The method was tested for the example of the $\sigma(600)$. First, it was shown that for $L > 2.5 M_\pi^{-1}$ the effects from SD -wave mixing can be neglected. Second, synthetic lattice-data were produced and analyzed. We find that with only two different box sizes one can expect a similar precision on the $\sigma(600)$ pole position as by varying as much as 6 different box sizes at zero total momentum.

Using information from moving frames is, thus, indeed very useful since, with only a few different box sizes, phase shifts and resonance parameters of excited mesons can be determined.

3.5 Lattice study of pion and kaon scattering off D -mesons

In 2003, BaBar discovered a positive-parity scalar charm-strange meson $D_{s0}^*(2317)$ with a very narrow width. The state was confirmed later by CLEO. This discovery has inspired heated discussions in the past decade. The key point is to understand the low mass of this state, which is more than 100 MeV lower than the prediction for the lowest scalar $c\bar{s}$ meson in the quark model. There are

several interpretations of its structure, such as being a DK molecule, the chiral partner of the pseudoscalar D_s , a conventional $c\bar{s}$ state, coupled-channel effects between the $c\bar{s}$ state and DK continuum etc. In order to distinguish them, one has to explore the consequences of each interpretation, and identify quantities which have different values in different interpretations. Arguably the most promising quantity is the isospin breaking width $\Gamma(D_{s0}^*(2317) \rightarrow D_s \pi)$. It is of order 10 keV, if the $D_{s0}^*(2317)$ is a $c\bar{s}$ meson, while it is of order 100 keV in the DK molecular picture due to its large coupling to DK and the proximity of the DK threshold: the mass difference of charged and neutral intermediate mesons leads to large, non-analytical contributions that are absent in the quark model. Thus, the study of the DK interaction is very important in order to understand the structure of $D_{s0}^*(2317)$. Since direct DK scattering experiments are not possible, we here employ lattice calculations for scattering lengths for the scattering of the (pseudo)-Goldstone-Bosons off D mesons. A direct simulation of the $DK(I=0)$ channel, which is the channel of the $D_{s0}^*(2317)$, suffers from disconnected diagrams and is presently not possible. Still, one may obtain useful information on the DK interaction by calculating the scattering lengths of the disconnected-diagram-free channels which can be related to $DK(I=0)$ through $SU(3)$ flavor symmetry.

In this work we employ the “coarse” ($a \simeq 0.125$ fm) gauge configurations generated by the MILC collaboration using the one-loop tadpole-improved gauge action, where both $\mathcal{O}(a^2)$ and $\mathcal{O}(g^2 a^2)$ errors are removed. For the fermions in the vacuum, the Naik action with smeared links for the one-link terms was used, resulting in a reduction of the flavor symmetry violations. For the valence light quarks (up, down and strange) we use the five-dimensional Shamir domain-wall fermion action. The light quark propagators were provided to us by the NPLQCD and LHP collaborations. For the charm quark we use a relativistic heavy quark action motivated by the Fermilab approach. This action controls discretization errors of $\mathcal{O}((am_Q)^n)$, with m_Q the heavy quark mass. An effective continuum action is constructed using operators that are invariant under discrete rotations, parity-reversal and charge-conjugation transformations, representing the long-distance limit of our lattice theory.

Because the simulations are performed at unphysical quark masses, chiral extrapolation is necessary in order to obtain the values of scattering lengths at the physical quark masses. The basic observation is because of the coupled-channel effect and the large kaon mass, the interaction of some of the channels is so strong that a nonperturbative treatment is necessary, and in one channel even a bound state is produced. Here we use unitarized chiral perturbation theory to calculate the scattering lengths in all channels accessible for the scattering of the nonet of (pseudo)-Goldstone-Bosons off the triplet of D -mesons. From a fit to the lattice data the low energy constants that appear to next-to-leading order can be fixed.

Once all parameters are determined, the formalism can

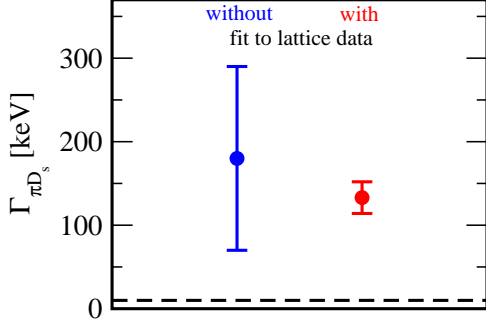


Fig. 32: Hadronic width of $D_{s0}^*(2317)$ as calculated within our approach. The right (left) value and uncertainty was determined by including (omitting) a fit to the lattice data. The dashed line indicates the width predicted for the $D_{s0}^*(2317)$, if it is assumed to be a $c\bar{s}$ state.

be used to calculate additional observables, in particular the isospin violating decay $D_{s0}^*(2317) \rightarrow D_s\pi$. In a previous calculation, where no reliable lattice data were available, we had to estimate the low energy constants using dimensional analysis. This calculation gave $\Gamma(D_{s0}^*(2317) \rightarrow D_s\pi) = (180 \pm 110)$ keV, which includes the width prediction of the quark model value of 10 keV within 2σ . The calculation that uses the lattice data to fix the low energy constants gives $\Gamma(D_{s0}^*(2317) \rightarrow D_s\pi) = (133 \pm 19)$ keV — thus now the prediction derived from a molecular structure of the $D_{s0}^*(2317)$ deviates by 6 standard deviations from the quark model value. The significant improvement in the accuracy of the width calculation is illustrated in Fig. 32. A measurement of a width down to 100 keV is an experimental challenge, however, given the importance to unambiguously establish the nature of the $D_{s0}^*(2317)$ it is worth the effort.

3.6 Determination of the $\Lambda\Lambda$ scattering length

The baryon-baryon interaction in the strangeness $S = -2$ sector and, specifically, the $\Lambda\Lambda$ system, has been a topic of interest for quite some time. The fascination was generated not least by the possible existence of the so-called H -dibaryon, a deeply bound 6-quark state with spin $J = 0$, isospin $I = 0$, and strangeness $S = -2$, predicted by Jaffe in 1977 based on a bag-model calculation. But, of course, the strength of the $\Lambda\Lambda$ interaction is also of more general interest, for example in the context of a better understanding of the role played by the SU(3) flavor symmetry.

Furthermore, studies of doubly strange hypernuclei will be possible at the future facility FAIR and pertinent experiments are planned by the PANDA collaboration. A more reliable knowledge of the $\Lambda\Lambda$ interaction would be rather useful for the preparation of such experiments. Finally, the $\Lambda\Lambda$ interaction, or the hyperon-hyperon interaction in general, plays an important role in investigations

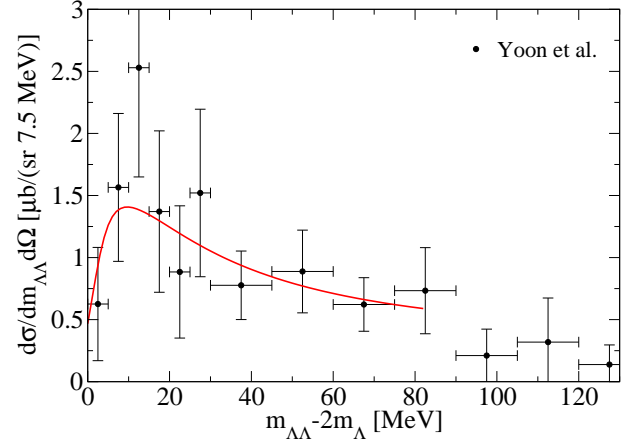


Fig. 33: Data for the $\Lambda\Lambda$ invariant mass spectrum from the reaction $^{12}\text{C}(K^-, K^+\Lambda\Lambda X)$ and our fit to it (solid line).

of the global properties of compact astrophysical objects like neutron stars. Their stability and size as well as the cooling process depend sensitively on the strength of the hyperon-hyperon interaction.

The scattering length is a quantity that provides a sensible measure for the strength of the interaction in a particular two-body system. In the past, we proposed a method based on dispersion integrals for extracting hadronic scattering lengths from production reactions. It consists in studying the final-state interaction of reactions where pairs of baryons are produced and, thus, can be applied to the $\Lambda\Lambda$ system, too.

Indeed, recently we explored the possibility of applying our dispersion method to the $\Lambda\Lambda$ interaction. Our study was encouraged by the available data on the $\Lambda\Lambda$ invariant mass distribution determined in the reaction $^{12}\text{C}(K^-, K^+\Lambda\Lambda X)$. These data are afflicted by sizeable uncertainties, but still they allow us to demonstrate the practicability of our method and to extract an actual value for the $\Lambda\Lambda$ 1S_0 scattering length.

The fit to the data in question is presented in Fig. 33. It forms the basis for the extraction of the scattering length from the dispersion integral. The result for the scattering length obtained from this invariant mass spectrum is

$$a_{\Lambda\Lambda} = -1.2 \pm 0.6 \text{ fm},$$

where the given error is due to the uncertainties in the data. The estimated theoretical error due to the dispersion method itself is about 0.4 fm.

The only other constraints on the $\Lambda\Lambda$ scattering length available so far come from analyses of the separation energy of the so-called Nagara event, i.e. the only unambiguously identified double hypernucleus, namely $^6_{\Lambda\Lambda}\text{He}$. Calculations that obtain separation energies in agreement with the experimental value suggest $\Lambda\Lambda$ scattering lengths in the order of -0.7 to -1.3 fm.

3.7 η and η' decays into four pions

Very little is known about the four-pion decays of the η and η' . From the experimental side, only upper limits on branching ratios exist; this, however, may change in the near future with the advent of high-statistics η' experiments such as BES-III, CB/TAPS at ELSA, CB-at-MAMI-C, CLAS at Jefferson Lab, etc.

Note that the decays $\eta' \rightarrow 4\pi$, in contradistinction to many other η' decay channels, seem not terribly forbidden by approximate symmetries: they are neither isospin-forbidden, nor required to proceed via electromagnetic interactions. The reaction $\eta \rightarrow 4\pi$, in contrast, is essentially suppressed by tiny phase space: $M_\eta - 4M_{\pi^0} = 7.9 \text{ MeV}$, $M_\eta - 2(M_{\pi^\pm} + M_{\pi^0}) = -1.2 \text{ MeV}$, such that only the decay into $4\pi^0$ is kinematically allowed.

As an odd number of pseudoscalars is involved in these strong-interaction decays, they are of odd intrinsic parity and belong to the greater class of anomalous decays. In low-energy QCD these anomalous decays are governed — in the chiral limit — by the Wess–Zumino–Witten (WZW) term via chiral anomalies which are of $\mathcal{O}(p^4)$ in the chiral counting. Since anomalous amplitudes always involve the totally antisymmetric tensor $\epsilon_{\mu\nu\alpha\beta}$, it can be shown that no two pseudoscalars are allowed to be in a relative S-wave. Thus any decay with five pseudoscalars can be expected to be P-wave dominated. This also holds for decays $\eta' \rightarrow 2(\pi^+\pi^-)$ and $\eta' \rightarrow \pi^+\pi^-2\pi^0$. However, since the antisymmetric product of four SU(2) (flavor) states vanishes, the leading contributions to the η' decay amplitudes with charged pions in the final state are of $\mathcal{O}(p^6)$ according to chiral power-counting rules because of the necessarily involved kaon loop and the pertinent counter terms of the $\mathcal{O}(p^6)$ anomalous Lagrangians. In the framework of hidden local symmetry for vector mesons, the vector-meson exchange saturates the $\mathcal{O}(p^6)$ low-energy constants of the kaon-loop, such that the (P-wave) decay amplitude, for all practical purposes, is entirely governed by ρ intermediate states. Hence the dominant contribution is given by the triangle anomaly via $\eta' \rightarrow \rho\rho$ (while the box term correction is numerically small), not by the pentagon anomaly. In this manner, the branching fractions for the (yet unmeasured) $\eta' \rightarrow 2(\pi^+\pi^-)$ and $\eta' \rightarrow \pi^+\pi^-2\pi^0$ decays are predicted to be

$$\begin{aligned}\mathcal{B}(\eta' \rightarrow 2(\pi^+\pi^-)) &= (1.0 \pm 0.3) \times 10^{-4}, \\ \mathcal{B}(\eta' \rightarrow \pi^+\pi^-2\pi^0) &= (2.4 \pm 0.7) \times 10^{-4},\end{aligned}$$

respectively, where the uncertainty estimates are based on the typical $1/N_c$ correction of about 30%. The branching ratio for the first decay is only a factor of two smaller than the current experimental upper limit. Thus it should be testable in the near future with the modern high-statistics facilities.

Predictions for the η' and η decays into four neutral pions are much more difficult, as Bose symmetry forbids two neutral pions to be in an odd partial wave. Therefore the decays $\eta' \rightarrow 4\pi^0$ and $\eta \rightarrow 4\pi^0$ require all π^0 to be at least in relative D-waves. This, combined with the

tiny phase space available, leads to the notion of $\eta \rightarrow 4\pi^0$ being CP-forbidden, although strictly speaking it is only S-wave CP-forbidden. An estimate of this decay via charged-pion-loop contribution with D-wave pion–pion charge-exchange rescattering predicts the following CP-conserving branching ratios: $\mathcal{B}(\eta' \rightarrow 4\pi^0) \sim 4 \times 10^{-8}$ and $\mathcal{B}(\eta \rightarrow 4\pi^0) \sim 3 \times 10^{-30}$.

Note that the D-wave mechanism for the $\eta' \rightarrow 4\pi^0$ decay is suppressed by 3–4 orders of magnitude compared to the decays with charged-pion final states which, as mentioned above, are of P-wave nature. It is also 4 orders of magnitude smaller than the current experimental bound. The CP-conserving decay width of $\eta \rightarrow 4\pi^0$ on the other hand is so small that any signal to be observed would indicate CP-violating physics (the current bound is 6.9×10^{-7}).

3.8 The pion vector form factor revisited

Nowadays, hadron physics has reached a high level of precision for a variety of observables. This is not only because there is now data available with unprecedented accuracy but also because the theoretical tools are very advanced. This is also necessary, as, e.g., the main uncertainty in the evaluation of the anomalous magnetic moment of the muon at present comes from the hadron physics that contributes to the vertex corrections. In the evaluation of this quantity the pion vector form factor in the neutral channel is a key ingredient. In order to also include the pion vector form factor in the charged channel in the analysis, it is necessary to control quantitatively all isospin violating effects, as will be discussed below.

In addition the pion vector form factor is also interesting on its own right, for here the excited vector mesons in the rho channel are clearly visible as interference phenomena. At present not even their number is known — one may hope from a combined analysis of various channels not only to determine their number but also to extract the resonance parameters reliably. In the work presented here we included, in addition to the $\rho(770)$ two resonances, ρ' and ρ'' .

In recent years a lot of high quality data has been accumulated for the pion vector form factor both in the neutral channel, from $e^+e^- \rightarrow \pi^+\pi^-$, and in the charged channel, from $\tau^- \rightarrow \nu_\tau\pi^-\pi^0$. Traditionally they were analyzed using the isobar model or variants thereof. However, there is a one-to-one correspondence between form factors and dispersion theory, at least in the elastic regime via the Omnès representation. Especially since nowadays phase shifts are available with very high accuracy, it appears natural to employ these instead of using a particular model.

At higher energies ($s > 1 \text{ GeV}^2$) the phase shift information gets worse, inelasticities become potentially important and resonance contributions are observed. Thus, here an isobar prescription appears more appropriate. In our recent study we developed a parameterization of the pion vector form factor that combines the Omnès repre-

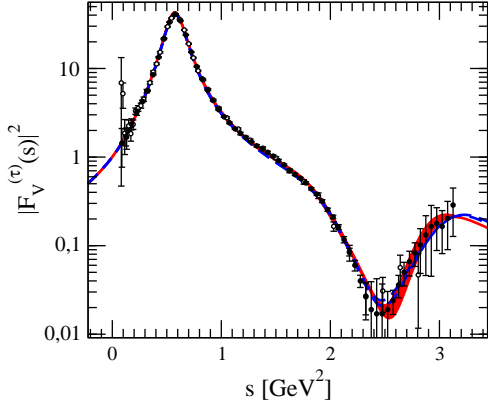


Fig. 34: Results for the pion vector form factor from $\tau^- \rightarrow \nu_\tau \pi^- \pi^0$ data.

resentation at low energies with a resonance prescription at higher energies.

The approach is based on the two potential formalism, that allows one to write the scattering T-matrix as a sum of the elastic $\pi\pi$ T-matrix that up to 1 GeV can be calculated directly from the $\pi\pi$ p-wave phase shifts δ_1^1 , and a resonance T-matrix that contains all resonances heavier than $\rho(770)$ as well as all inelasticities. For the form factor it then follows an expression that contains the resonances times the vertex functions — in the $\pi\pi$ channel again calculated from δ_1^1 , this time through the Omnès function.

In Fit 1 of the present model besides the $\pi\pi$ channel as inelastic channel a structureless 4π channel was included. This was sufficient to describe all two- π data. However, in order to also describe inelastic channels, in Fit 2 the $\pi\omega$ channel was considered in addition. In the $\pi^+\pi^-$ channel various sources of isospin violation are included, namely the higher order coupling to the photon, and $\pi\pi - \omega$ -, and $\pi\pi - \phi$ -mixing. We fitted the $\pi\pi$ p-wave phase shifts, the neutral pion vector form factor as well as a compilation of $e^+e^- \rightarrow (\text{non})\text{-}2\pi$ in the isovector channel. The results for the charged form factor then come as a prediction.

The parameters of the model are the resonance parameters for ρ' and ρ'' and a regulator, λ , introduced to prevent the self-energies from growing at high energies. The latter parameter is not fitted, but fits were performed for different values of λ , namely 4 GeV (fit A) and 6 GeV (fit B). The results of the fits are shown as the red band (blue curves) for Fit 2 (1) in the Fig. 34. As one can see an excellent description of the data is achieved. In a next step we plan to fit not to a compilation of inelastic data but to the various inelastic channels directly.

3.9 Electric dipole resonance in light and heavy nuclei

The electric giant dipole resonance (GDR) is a nuclear excitation mode which is related to bulk nuclear properties, such as the nuclear symmetry energy and the

Thomas-Reiche-Kuhn sum rule enhancement factor. One might assume that theories which describe bulk properties of nuclei rather well should have no problem in systematically reproducing the centroid energies of the GDR both for light and heavy nuclei. This is not the case, however. Note that the centroid energy of the GDR obtained in the state-of-the-art mean-field approach, see Fig. 35 (blue lines), agrees with the experimental data for ^{16}O , but is above the experimental data in ^{208}Pb . Recent reviews point out that this fact is one of the major shortcomings of effective nuclear interactions, which is embarrassing as the physics of the giant dipole resonance is related to the neutron skin thickness, currently under experimental observation by the PREX collaboration, and the pygmy dipole strength which is of astrophysical interest. Recent attempts to produce new interactions especially designed to solve the GDR problem failed. This fact suggests that the currently employed standard approach to the structure of heavy nuclei, mean field theory, is causing this problem. While mean field theory includes two major energy scales of nuclear physics, the pairing gap (1 MeV) and the nucleon separation energy at the Fermi surface (8 MeV), it ignores vibrations of the nuclear surface (3-6 MeV), called phonons in solid state physics. The coupling of the phonons to the nucleons induces an energy dependence of the nuclear self-energy that the mean field approximation can not reproduce. The so-called Quasi-Particle Time Blocking Approximation includes phonons explicitly and has been applied to both a light nucleus (^{16}O) and a heavy one (^{208}Pb) for calculations of the photoabsorption cross section, see Fig. 35. The excitation of energetically low-lying surface vibrations absorbs energy that in the mean field approximation would feed the GDR, and simultaneously shifts the centroid of the dipole resonance to lower energies. The magnitude of the shift depends on the mass number of the nucleus because there are many more relevant phonons in a heavy nucleus than in a light one.

Figure 35 shows that a shift of 1.6 MeV is produced in ^{208}Pb , while in ^{16}O , a small shift of only 0.4 MeV is observed. The present calculations are based on an effective interaction of the Skyrme family which reproduce the ground state properties of nuclei very well. While extrapolations to short-lived nuclear isotopes based on Skyrme interactions are possible, a further gain in predictive power is expected from interactions derived from effective field theory. The present results show that further research in this field is required.

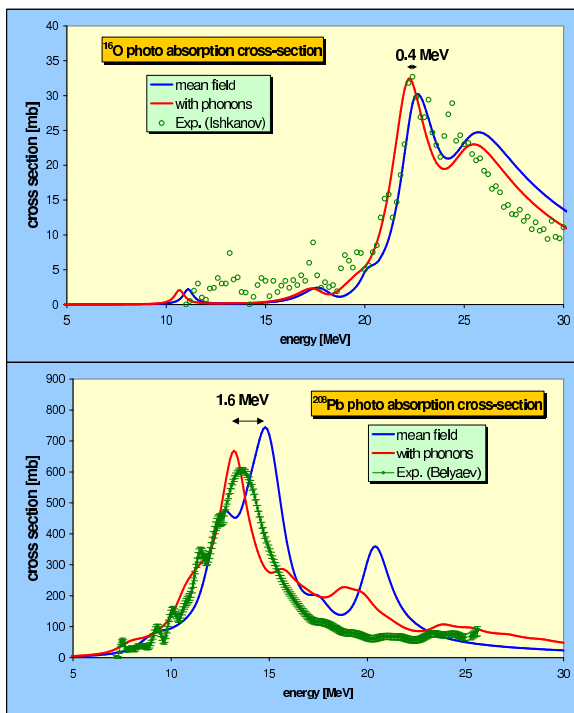


Fig. 35: Photoabsorption cross sections in ^{16}O (top) and ^{208}Pb (bottom) in mean field theory (blue) and with inclusion of phonons (red) compared with experimental data (green).

4 HESR Project Progress Report

Most important result of 2012's HESR activities is the start of the acquisition process on Sep 26th, 2012. This is the date of the publication of the first tender for HESR. On the administrative side, the time until then was filled with various efforts to fulfill the legal requirements to launch an order. Before, it was finally decided that FZJ will be hired by FAIR for technical follow-up of all HESR equipment and delivery of most items for HESR. Dipole and quadrupole magnets for HESR will be bought under the responsibility of FAIR. Throughout 2012 the technical work progressed continuously. By the end of 2012 orders covering approx. 30% of the project budget could be launched, and several items already arrived at Jülich. Meanwhile the contract concerning the main dipole and main quadrupole magnets for HESR has been signed and a first down payment has been made. The same applies to the quadrupole magnet power converters. For RF first amplifiers and other components have been ordered. For the stochastic cooling work package, combiner boards have been developed. First samples to qualify the possible vendor can be ordered in the beginning of 2013. In-house mechanical design of the associated vacuum vessels is well advanced, and in-house production is expected for 2013. The vacuum test bench was upgraded with state-of-the-art vacuum pumps combining different pumping techniques. These pumps later will be used in HESR. Technical preparations for ordering the stainless steel for vacuum chambers are finished. Flexible beam pipe elements had to be revised as the heating temperature now has to allow NEG activation. This will trigger a revision of the floor space management data especially in the arcs between two dipole magnets. Afterwards, most of the vacuum chambers and their supports can be designed mechanically. Design work for the injection equipment is nearly finished. Tendering is expected for Q1/2013. For the beam diagnostics work package the detailed specifications are still being edited. For the PANDA integration work package the specification of the chicane magnets is being discussed with the PANDA collaboration before the tendering process can be started. Interfacing with the architects of the FAIR buildings is an on-going process which needs continuous attention. For some small corrections change requests have been issued. After proper processing, FAIR accepted them. Contributions concerning sextupole magnets, steerer magnets and their power converters are expected from Romania. The technical links are well established. Work can start once the in-kind contract has been signed. Contributions for some diagnostics devices are expected from Slovenia. The technical links are being established. Work can start once the in-kind contract has been signed.

5 Day-one Experiment at HESR

The conceptual design of the luminosity monitor for the PANDA experiment is based on measuring the differential elastic Antiproton-Proton scattering rate by 4 planes of silicon pixel tracking detectors (HV-MAPS) in the forward area. The absolute precision to measure the integrated luminosity is limited by the lack of existing data on this system in the relevant momentum region, therefore a day-one experiment at HESR dedicated to antiproton-proton elastic scattering has been proposed. The goal of the experiment is to measure a wide range of 4-momentum transfer t ($0.0008 - 0.1 \text{ GeV}^2$) so that the contribution of the physical differential distribution to the absolute luminosity uncertainty is less than 1%. The polar angle of scattered antiprotons and the energy of recoil protons will be measured at forward angles by tracking detectors and by thick energy detectors near 90° , respectively. Figure 36 shows a sketch of the conceptual design of the day-one experiment at HESR. One of the recoil arms is being fabricated and will be commissioned with proton-proton elastic scattering at COSY in 2013.

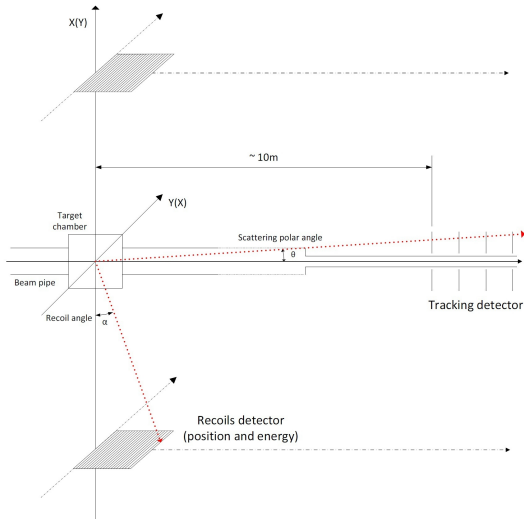


Fig. 36: Sketch of the day-one experiment at HESR.

In order to measure the energy as well as the polar angle of the recoil protons with kinetic energy in the range of 0.4–60 MeV, a dedicated detector system consisting of 2 silicon strip detectors and 2 germanium strip detectors with dimension of $7.64 \text{ cm} \times 5 \text{ cm} \times 1 \text{ mm}$ (thickness) and $8.04 \text{ cm} \times 5 \text{ cm} \times (5/11) \text{ mm}$ (thickness), respectively, has been proposed. All detectors have been fabricated as shown in Fig. 37. Functional tests of the detectors have been performed and further tests for final assembly are going on.

After detailed investigations, Mesytec electronics have been chosen for the readout of all detectors. The MPR16 and MSCF16 are 16 channel preamplifiers and shaping amplifiers, respectively. The 32 channels MADC32 is a typical peak sensing ADC for energy measurement. A CRYOMECH coldhead with 30 W cooling power has



Fig. 37: The fabricated Si with Aluminum holder (upper) and Ge with Copper frame (lower) detector of recoil arm.

been ordered as cooling device for the germanium detectors. Preliminary tests show that it would take about 25 minutes to reach 50 K without any load. The high precision Lakeshore temperature controller 336 has been tuned for cooling temperature control. By combining the coldhead and 336 controller, the cooling temperature for the germanium detector could be set to any desired value in a large range of reachable temperature. The remote control via internet for the 8 channels ISEG high voltage module integrated in an MPod crate has been realized by using the tcl-tk programming language based on Linux. The first 4 channels with 500 V output and the remaining 4 channels with maximum 2000 V output are dedicated to supply the silicon detector bias and the germanium detector bias, respectively. The DAQ system with a common ems framework for COSY experiments has been established for the day-one experiment commissioning at COSY.

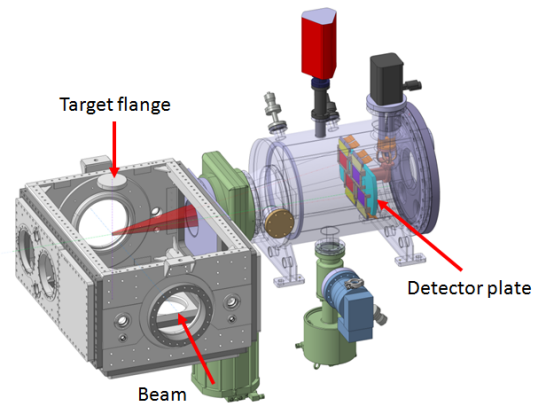


Fig. 38: Detector chamber (right) designed to match the existing ANKE target chamber (left).

In order to commission the newly built device at COSY, the existing cluster target at ANKE will be used. Due to the limited space, a new detector chamber will be added to the existing scattering chamber as shown in Fig. 38. Part of the detector chamber is being constructed and full chamber will be ready in early 2013.

6 The PANDA Experiment

6.1 Overview

The new Facility for Antiproton and Ion Research (FAIR) will be one of the largest accelerator facilities in the world giving access to a large variety of different experiments to gain new insights into the structure of matter and the evolution of the universe.

One main component of the FAIR complex is the HESR accelerator with the PANDA experiment. PANDA will utilize the excellent momentum resolution of the anti-proton beam provided by the HESR accelerator to do precision measurements in the charm energy sector. Many new states with open and hidden charm have been found in the last decade where the nature of these states is not clear. There are strong indications that at least some of these states could be exotic particles with more than three valence quarks. To reveal their true nature precision measurements of the width and the mass of these states are necessary which only can be done with the future PANDA experiment. In addition PANDA can search for states with higher angular momentum which are not easily accessible with existing experiments.

Crucial for the success of PANDA is its capability for precise tracking of charged particles. For this purpose a combination of different detector types is used. In the central part of PANDA, directly around the interaction point, a high precision silicon tracker called Micro Vertex Detector (MVD) is used which is surrounded by a large scale gaseous detector made out of thousands of small gas filled tubes called Straw Tube Tracker (STT).

Both detector components are under development in Jülich together with other groups inside the PANDA collaboration.

In contrary to other hadron physics experiments PANDA is not using a first level hardware trigger but reads out the complete detector data into a processing farm where the event selection is done. This concept has the advantage that much more complex selection criteria can be applied onto the data stream and the selection criteria can be adopted much easier to different physics channels of interest. In combination with the quasi continuous anti-proton beam this concept requires new reconstruction and event building algorithms and imposes high demands on the readout and processing hardware. To develop the required algorithms and to test the hardware architecture a new, time based simulation software was developed which allows the realistic reproduction of the data stream coming later from the experiment. This software framework is used to develop algorithms for online tracking and to port these algorithms to alternative hardware concepts like GPU processors.

6.2 Pre-assembly at FZJ

In order to significantly accelerate the construction, assembly and commissioning of the PANDA experiment

at FAIR, the PANDA collaboration has decided to pre-assemble major components of the detector at FZ-Jülich. This proposal has been agreed upon by the PANDA collaboration board and was also recommended by the FAIR Expert Committee for Experiments evaluating the technical design reports of FAIR. An endorsement for the PANDA pre-assembly at FZJ is also given in the interim report of the recent POF evaluation. The pre-assembly will enable a mechanical and functional integration of most components of the complex detector system, so that time consuming activities, like *e.g.* the field mapping of the superconducting solenoid, is possible before the final setup at FAIR, and is independent of the details of the civil construction time scale. In parallel, beam tests of individual detector components under realistic conditions are already in progress at COSY, and the PANDA cluster target is being constructed.

The following presents a representative list of a few detector components which are being planned to be part of the functional and mechanical integration in Jülich: The first detector surrounding the interaction region is a silicon pixel/strip Micro Vertex Detector (MVD) which will be able to reconstruct the vertices with a spatial resolution of approximately 50 micrometer. The central tracker surrounding the MVD consists of straw tube proportional chambers. The electromagnetic barrel calorimeter contains 11,360 anorganic PbWO crystals. The forward EMC end cap consists of 3,600 crystals which will be set up, tested, read out and pre-calibrated in Jülich. The most forward part of the PANDA detector will be a segmented shashlik calorimeter of 400 individual modules of Pb and scintillator material. Detailed measurements of spatial-, time-, and momentum- resolution of all detector components are indispensable. Furthermore, the reconstruction efficiencies of physics processes, the interplay of the complete detector system and the synchronized triggerless readout and data acquisition must be studied. The data acquisition/event filtering demonstrator currently being planned consists of a system of 26 ATCA-based compute nodes (5 FPGA Xilinx Virtex 5, 20GB DDR3 memory, 16 optical links SFP+, 6.5 Gb/s, bi-directional), a blade-server with storage-array and a small GPU-farm. For coupling of the components an ethernet switch will be used. One of the essential goals is to probe the event building of triggerless data streams of the individual subsystems and overlapping events. This gives the possibility to test and further develop in a realistic environment the online-algorithms (particle id, tracking, shower-recognition) to be used also later for operation at HESR in Darmstadt at highest event rates. With this approach PANDA will be able to start doing physics measurements as early as possible once the anti-proton beam is available at the HESR.

6.3 MVD

The purpose of the Micro Vertex Detector (MVD) of PANDA is the precise measurement of tracks from

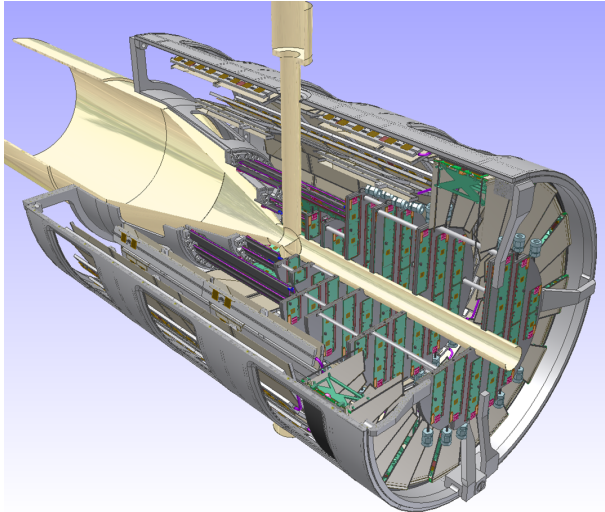


Fig. 39: CAD drawing of the Micro Vertex Detector(MVD).

charged particles close to the interaction point. With this data it is possible to identify short living particles which decay after a short flight path before they can be measured in a detector system and to determine the momentum of these particles with a very high resolution together with the central tracker. The MVD has four barrel layers with a radial distance from 4 up to 14 cm from the interaction point and six disk layers in the forward direction. Two different detector systems are used inside the MVD. The inner layers are equipped with silicon hybrid pixel detectors, which are able to cope with high track densities and large radiation damages while the outer layers use silicon strip detectors which have less radiation length by a comparable point resolution (Fig. 39).

The MVD faces the highest hit densities within \bar{P} ANDA due to the high interaction rate and the close position of the MVD to the interaction point. To cope with the high rates a new readout ASIC has to be developed which is done by the INFN Torino for the pixel part. At the moment the third prototype of the ASIC (ToPix3) is available which was tested end of 2012 in a COSY test beam. The focus of this test beam was to use the newly developed Jülich readout system to test the ToPix3 prototype with the highest rates the prototype can handle.

6.3.1 MVD rate studies with COSY

The \bar{P} ANDA experiment will deal with very high interaction rates up to $2 \cdot 10^7$ interactions/second. Since the MVD is the innermost detector it has to handle a high flux of particles. In the “hottest” areas of the MVD a pixel front end module has to handle an average particle rate of up to 2.9 Mcounts/s for a full size front end. For a peak rate even more than 4 Mcounts/s can be assumed. Due to the triggerless readout concept of \bar{P} ANDA the full data stream of the MVD has to be read out which is a novel and challenging feature for this kind of detector. To test the rate capability of the ToPix front end a dedicated test-

beam was performed at the COSY accelerator.

The last testbeam at the COSY accelerator was performed 2011 with the Torino readout system which is limited in readout capacitance. In this testbeam end of 2012 the ToPix was read out via the Juelich Digital Readout System which was developed at the IKP-1 and ZEA-2 (former ZEL). The system was designed for a high data rate handling of one or more ToPix modules. For the testbeam the recent front end prototype ToPix 3 was used, which has a reduced number of pixel cells of 640 compared to 12 760 of the final readout ASIC.

The intention of this testbeam was to do high intensity studies with the recent prototype. A single ToPix module was set directly into the proton beam (see Fig. 40) with an intensity up to 10^{10} protons per COSY extraction cycle (90 s).

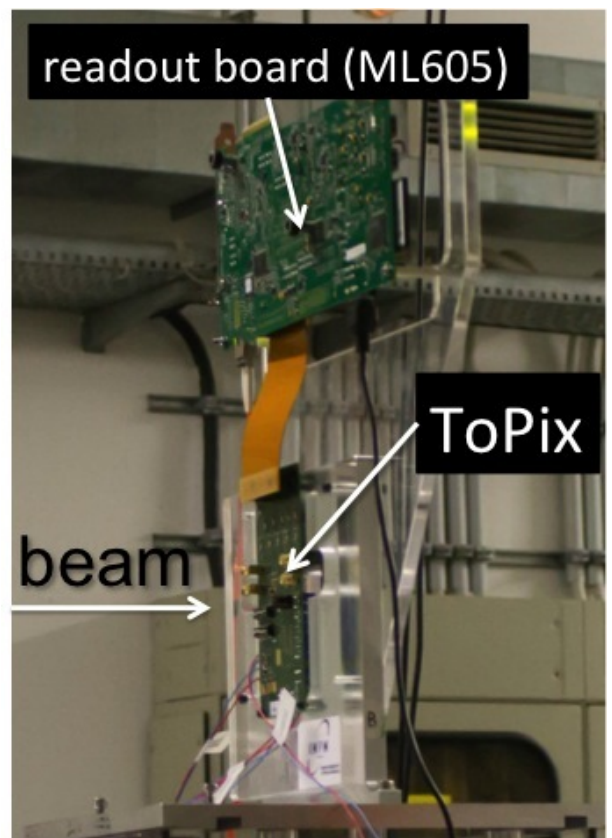


Fig. 40: Photograph of the testbeam setup of the ToPix 3 prototype. Beam is coming from the left side.

The testbeam was very successful. The hit rate could be increased to ~ 400 khits/sec for the whole module, which is twice the rate the front end would have to handle in \bar{P} ANDA according to its size and ~ 10 times more than what was achieved in the last test beam. The measurements have been done with a proton beam of 2.95 GeV/c at the Jessica area. Various tests were done with different front end settings and two modules. Measurements with different beam intensities will show the reliability of the ToPix at high rates. In total 150 GB of data have been recorded and are under study.

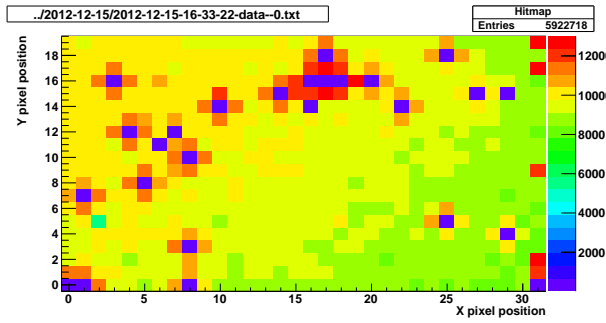


Fig. 41: Hit distribution of module 13. From lower right to upper left a beam structure is visible. The cross-like structures are related to bump-bonding issues.

As an example of the ongoing analysis Fig. 41 shows the hitmap of one of the two used modules. A beam structure is visible from right down to left up. The cross like structures are related to bump-bonding problems where a sensor cell is not connected to a readout cell. The functionality of the ASIC itself was tested with the internal injection circuit and is fully functional.

6.4 Time based simulation

The time based simulation framework is an extension of the existing Monte-Carlo simulation software FairRoot. It allows the simulation of pile-up effects inside the detectors, the mixture of different events and the randomization of the output data as it will happen later on in the real experiment.

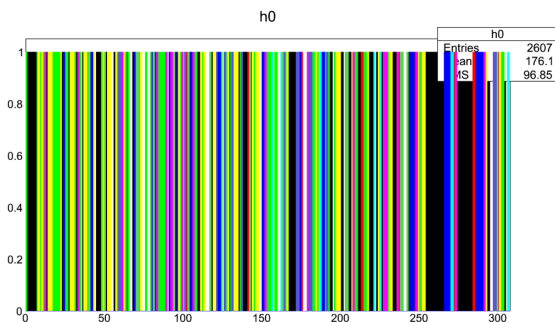


Fig. 42: Visualization of the randomized data of the MVD detector. Each color bar is a detector hit. Same color belongs to the same event. In a usual simulation hits with the same color would be adjacent to each other in the diagram.

Figure 42 shows the generated data stream of the Micro Vertex Detector after it has been simulated with the time based simulation framework. Each bar in the diagram corresponds to one detector hit where hits from the same event have the same color. If the old, event based simulation the hits with the same color would be next to each other and no mixture between events would occur. In the

new time based simulation the strict ordering by events is broken up and the events are mixed as it will be the case later on in the experiment.

6.5 Straw Tube Tracker

The Technical Design Report (TDR) of the PANDA Straw Tube Tracker (STT) was formally approved by FAIR in Jan 2013, following the unanimous recommendation of the Expert Committee Experiments (ECE) after a review meeting about the TDR in Nov 2012. The construction and installation of the PANDA-STT will be carried out in a joint project of institutions in Germany (FZ Jülich, Giessen Univ., GSI Darmstadt), Italy (LNF INFN Frascati, INFN and Univ. of Pavia, INFN and Univ. of Ferrara), Poland (IFJ PAN Krakow, Jag. Univ. Krakow, AGH Krakow), Romania (IFIN-HH Bucharest), and USA (North West. Univ. Evanston). The final commissioning of the assembled STT including the readout and data-acquisition system will be performed with a proton beam at the COSY accelerator in Jülich. After the completion of these tests the whole detection system will be shipped to the FAIR facility for the installation in the PANDA spectrometer at the HESR antiproton storage ring.

Overview

The STT as the central tracking detector in the PANDA target spectrometer features the spatial reconstruction of a charged particle track together with a measurement of the particle specific energy-loss (dE/dx) for an identification of the particle species. The helical trajectories of the charged particles in the solenoidal magnetic field are measured with a high spatial accuracy of about $150 \mu\text{m}$ transversal and 2–3 mm longitudinal to the beam, which yields together with the Micro-Vertex-Detector hits a high momentum resolution of about 1-2% in a broad momentum range from about a few 100 MeV/c up to 8 GeV/c at the nominal magnetic field strength of 2 Tesla. The identification and separation of protons, kaons, and pions in the low momentum region below about 1 GeV/c has to be done exclusively by the STT, based on the measured dE/dx information.

The high antiproton-proton annihilation of about $2 \times 10^7 \text{ s}^{-1}$ and the very rich spectrum of quite different reaction channels and topologies requires a continuous data-acquisition without the restriction to certain hardware trigger conditions. Very fast and efficient algorithms for the hit association of various sub detectors, the track and event reconstruction have to be processed in real-time (online) to recognize interesting reaction events and to start the storage of the event-assigned data to disk. A high number of FPGA-based compute nodes with large memory buffers that run at high clockspeeds are required for this online software triggering. The STT detector with its large geometrical acceptance and almost continuous tracking with up to 27 straw layers is the main part for the online charged particle tracking as input for the event recognition.

The IKP is involved in the PANDA-STT project with the mechanical construction, specific straw detector and readout setups, the (online) tracking and reconstruction, and commissioning tests of the PANDA-STT with proton or deuteron beams at COSY. Figure 43 shows the setup of a PANDA-STT prototype semi-barrel with a minimized mechanical frame structure. The self-supporting straw layer modules are attached to the frame only by two thermoplastic mounting brackets at both ends.

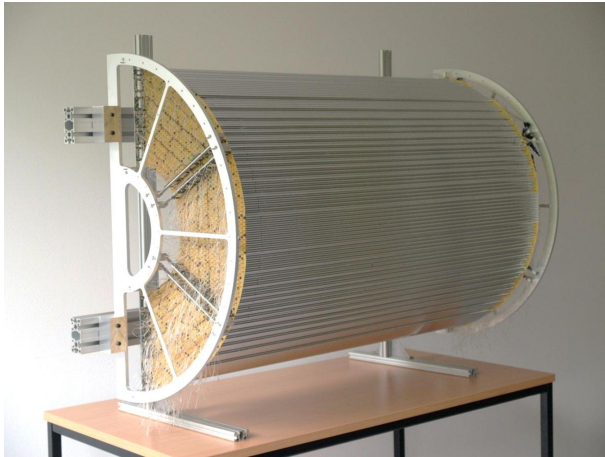


Fig. 43: Mechanical setup of an almost full-scale prototype of one semi-barrel of the PANDA-STT.

During the year dedicated assembly tools for the mechanical STT construction have been developed and set up and a first pilot straw mass production run with about 600 assembled straw tubes will be carefully checked to define the necessary material and production quality test procedures and selection criteria for the final PANDA straw productions. Several test measurements with two straw setups in a proton beam at the COSY Big-Karl area (see Fig. 44) have been performed in 2012. The straw detector operation and signal readout concepts of drift time and amplitude information were successfully tested at highest particle rates. The maximum proton beam intensities were up to several $10^6/\text{s}/\text{cm}^2$, exceeding the expected highest straw rates for the final PANDA-STT of about $10^6/\text{s}/\text{cm}^2$. The achieved spatial resolution was about $150\ \mu\text{m}$ and the energy-resolution (dE/dx) was better than 10 %, matching the requirements for the final PANDA-STT.

The next section describes the developments for the PANDA online tracking based on the STT hit information. A specific method, the so-called Triplet Finder, was invented for the charged particle tracking with the STT hits without requiring the knowledge of the exact event time. Since there are no dedicated event timing detectors in the PANDA setup, the event time has to be extracted from the continuous incoming data flow from various subdetectors during the online event reconstruction. The Triplet Finder method makes use of the equidistant cell geometry in the STT due to the close-packed straw layer geometry to combine three adjacent hit straws to a

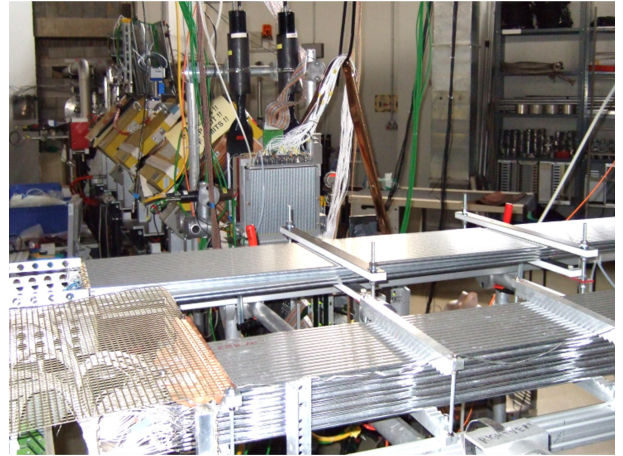


Fig. 44: Straw detectors in the COSY Big-Karl beam area. The proton beam is coming from the back.

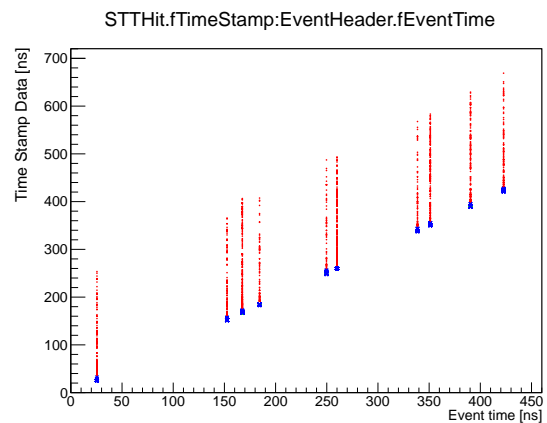


Fig. 45: Event mixing in the STT and MVD. The x -axis indicates the event start time and the y -axis indicates the recorded hit time with the drift time taken into account. Blue crosses indicate MVD hits, red dots indicate STT hits.

supercell (triplet hit) with an intrinsic higher average position accuracy than a single cell.

Online Tracking

One very interesting topic within the broad physics program of PANDA is the investigation of rare channels in antiproton-proton collisions. Due to the similar topologies of the interesting physics channels and the hadronic background, PANDA will implement a software trigger (also referred to as event filter) which allows to setup complex selection rules to achieve a three orders of magnitude background suppression.

The event filter decision will be based on information such as track multiplicities in an event, momentum information and particle identification information. Charged particle tracking is (among other data) required to determine this information.

An additional challenge is the very high interaction rate

of $2 \cdot 10^7$ annihilations per second. As a result, the hits of tracks from different events may overlap in time and have to be associated to their respective events (event building) prior to the filter decision. The resulting effect is illustrated in Fig. 45. While events occur at discrete times as shown on the x-axis, only the absolute hit time shown on the y-axis can be recorded. Due to the drift time of about 200 ns in the STT, hits from different events can be present in the detector within one time window (event mixing).

Due to the aforementioned operating conditions it is also hard to define simple criteria which could be used to execute the charged particle tracking for only a subset of hits. Instead, it is required to run the PANDA online tracking continuously in real time at the full PANDA interaction rate and attempt to reconstruct all tracks. This allows the tracking information to be used for both event deconvolution and the final filter decision.

Continuous Online Tracking

The operating mode of a continuous online tracking matches PANDA's continuous detector readout and the required high level input for the online event filter. There is no distinct bunch structure in the quasi-continuous beam, but the events can be organized in so-called bursts. One burst is equivalent to the events generated by one revolution (2000 ns) of the antiprotons stored in the HESR. An estimated gap of 400 ns between each burst allows the tracking algorithms to reset and realign to the incoming hit patterns. Another advantage of a continuous online tracking is that hits which have already been processed and assigned to a previously found track with a sufficiently high quality, may be skipped during processing of hits in later time windows. This can be used to obtain information about the event structure at an early stage before any event building has taken place.

Executing tracking algorithms in real time on all incoming hits requires a large amount of computing power. In PANDA, the computing power will be provided by a sufficient amount of FPGA-based computed nodes and eventually conventional PC farms utilizing (GP)GPU-computing. The burst structure also allows for a natural way of parallel processing by parallelizing the analysis of the individual bursts. This strategy of data parallelism scales very well with added nodes and does not impose any special constraints on the tracking algorithms.

PANDA's broad physics program results in a variety of different event topologies and tracks with very different properties (e.g. high momentum tracks ejected at shallow forward angles versus low momentum tracks ejected almost perpendicular to the beam pipe) to be reconstructed. Particles being ejected into different regions of the PANDA spectrometer also cause the tracks' hits to be distributed over several subdetectors which can be treated either in a global approach or individually separated by subdetector and then merged. Since a single algorithm can not show optimum performance for all pa-

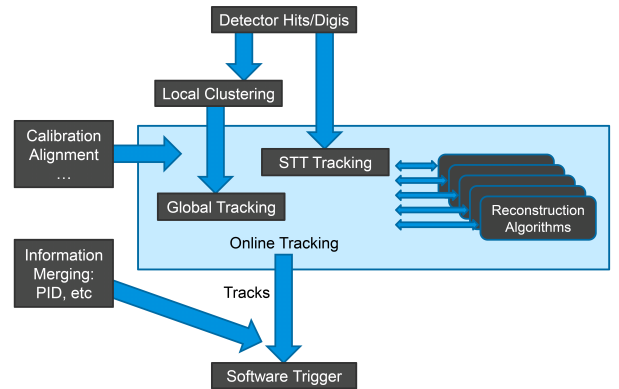


Fig. 46: Data flow through the online tracking framework.

parameter ranges, several tracking algorithms must be combined to achieve the highest reconstruction efficiency. In the following, a global framework to interface the different tracking algorithms and combine their results is described. Additional developments are the online tracking algorithm *Triplet Finder* and performance studies with Hough transform based track finding on GPUs.

Global Framework

The global strategy to combine the different tracking algorithms is to start with the identification of simple patterns. This subsequently reduces the hit sample to be processed by later stages which may in turn process more complex patterns and require more computational effort. Figure 46 illustrates the data flow to and from the global online tracking framework. After an eventual local clusterization stage (as for example done for the micro vertex detector), the track finding stage of the online tracking takes place with both local algorithms, dealing with individual subdetectors, and global algorithms combining information from several subdetectors. While in most cases it is useful to calculate three dimensional spatial coordinates for each hit, the straw tube tracker becomes part of the actual tracking procedure as full 3D information is obtained during track finding with the STT.

Triplet Finder

The Triplet Finder is a track reconstruction algorithm specifically designed for the PANDA-STT to reconstruct tracks of charged particles. It consists of two stages as illustrated in Fig. 47. Firstly, the individual Triplets are identified, then track circles are calculated which go through the origin and two Triplets.

The Triplet finding stage analyzes the pattern of three up to seven adjacent hit straw tubes and calculates the center of mass coordinates of such a pattern. Technically, they are n-lets but due to historical reasons all such patterns are called Triplets. Note, that due to the finite number of possible patterns the calculation of the center of mass can be implemented as a lookup table. The calculation

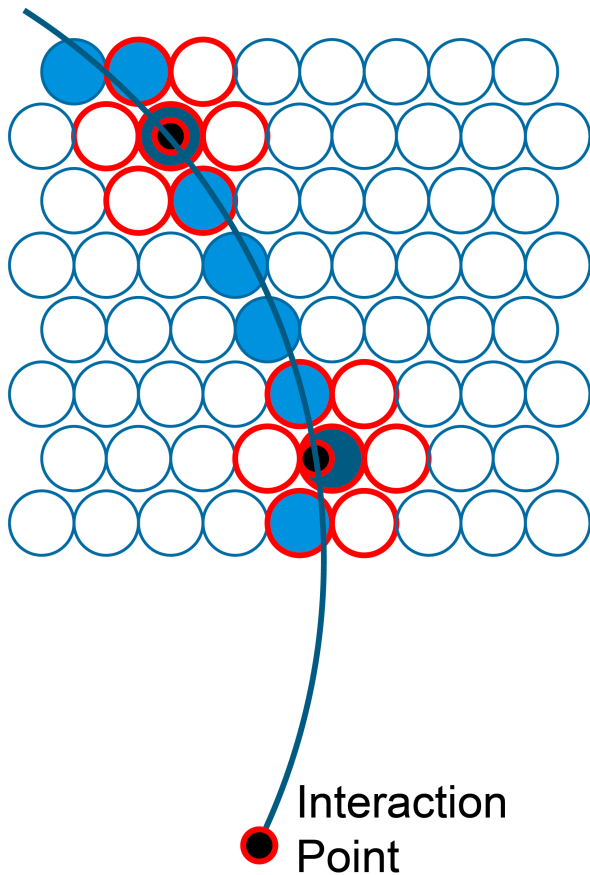
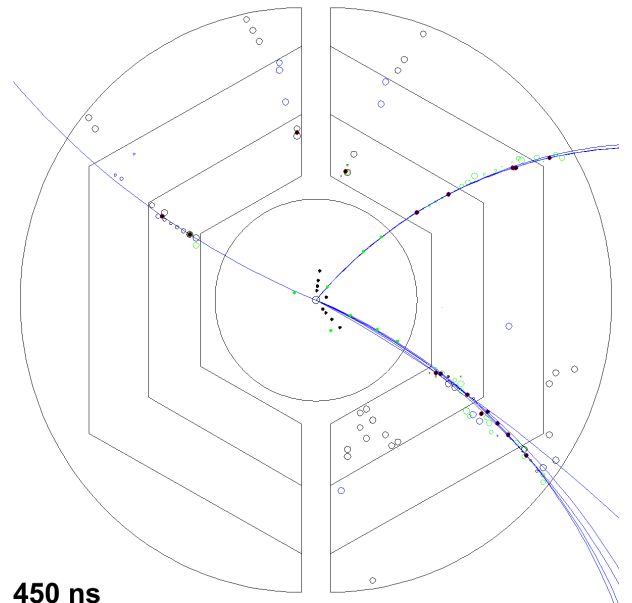


Fig. 47: Sketch (not to scale) of the Triplet finding and track calculation procedure. First, hit clusters are identified in the upper and lower portion of the STT and the center of mass of the hit cluster is calculated. The resulting center of mass points are called Triplets. Then, a circle is analytically calculated through the interaction point and two Triplets. Red outlines indicate the search area for Triplets, blue background indicates a straw hit.



450 ns
 Fig. 48: Snapshot at 450 ns running time. Shown are all detector hits and the found tracks calculated by the Triplet Finder.

of the track circle's parameters is then a simple analytical procedure. It is also possible to calculate the track circle through three arbitrary points. However one of the points being the origin serves as an additional simplification and a later processing of the remaining hits with three arbitrary points could be a useful extension of the Triplet Finder. In each case the purely analytic approach reduces the computational complexity of the algorithm.

The Triplet Finder for the STT exhibits several features beneficial in practice: Since only straw positions and the absolute hit times are required for the calculation, neither knowledge of the event start time nor any isochrone-drifttime calibration is required. Its simplicity and robustness makes the Triplet Finder a suitable candidate for a first level reconstruction which can be used to seed more precise algorithms which are executed later and may in turn require additional event features to be determined.

A proof of concept version of the Triplet Finder has already been implemented within PandaRoot and tested with DPM generated events at 15 GeV/c beam momentum at the nominal PANDA interaction rate. The simulation type was time ordered to include realistic event mixing due to the Poissonian distribution of the event rate. Fig. 48 shows the results with found tracks, associated hits and also early hits from a later event.

The visual inspection of tracks found with the Triplet Finder is already very promising. Therefore, the project will be continued for quantitative analysis of the reconstruction efficiency and implementation of the many possible optimizations which have been outlined in this section.

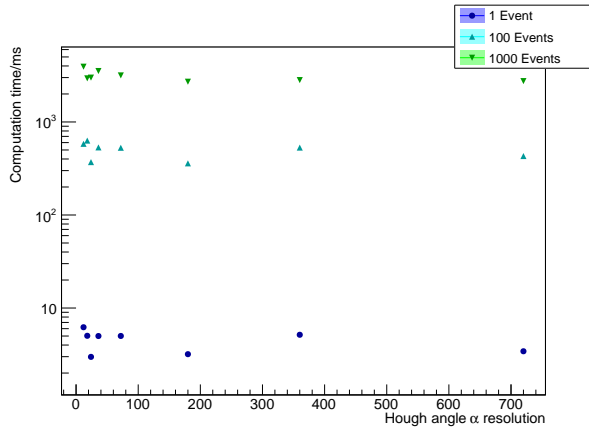


Fig. 49: Computation times in ms for different Hough Transforms (HT), including Conformal Mapping (CM). The x axis shows different HT resolutions, depending on the chosen HT angle parameter $\alpha \in [0^\circ, 360^\circ)$. For example the point at 720 represents one α value every 0.5° – a high resolution. Different event counts were used (1, 100, 1000).

GPU Computing

As part of our Online Tracking efforts we are investigating the feasibility of using GPUs (Graphics Processing Units) for track reconstruction. The first algorithm ported to the GPU is a Hough transform (HT) based track finder. It works as follows: Curved tracks are transformed into straight lines using a Conformal Mapping (CM). Next, the HT translates every hit point of these straight tracks into a line in the Hough space. Finally, the particle track is found as the peak in this space.

The implementation on the GPU allows a parallel execution of computations (*e.g.* several hits in CM, several parameters in HT), in contrast to a serial execution handling on a CPU.

In Fig. 49, a benchmark study of computation times of CM+HT is shown. Different event counts (1, 100, 1000) with hits of the PANDA STT were investigated. For each set of events, various HT resolutions were investigated in one single benchmark program. Generally, a higher resolution leads to more precise track parameters – up to the detector’s resolution.

It can be seen that for the investigated range of HT resolutions the computation time is roughly constant. A CM+HT net computation time (double precision) per event of < 4 ms was achieved in our preliminary simulations. The data transfer to the GPU has not been measured at this time.

In the future, we expect a reduction of the computation time due to hardware (more powerful GPUs) and software (plain CUDA implementation) optimizations.

7 Further Experimental Activities

7.1 Laser-induced Particle Acceleration

7.1.1 Polarization measurements with protons from foil targets

The field of laser-induced relativistic plasmas and, in particular, of laser-driven particle acceleration, has undergone dramatic progress in recent years. Despite this, it is a yet untouched issue how the particle spins are influenced by the huge magnetic fields inherently present in the plasmas. One may think of two potential mechanisms that cause a polarization of the particle beam: either due to a spin alignment or by spatial separation of different spin states through the field gradients. The second scenario relies on the same principle as the Stern-Gerlach experiment in which a beam of neutral Silver atoms is deflected in an inhomogeneous magnetic field depending on the spin state of the valence electron.

On the other hand, according to the “thesis of Bohr”, the spin states of free electrons, or any other charged particle, cannot be separated in a Stern-Gerlach like set-up. However, Garraway and Stenholm showed, that it is in principle possible to achieve spin separation even for charged particles by using a small diameter of the particle beam in the field region and a sufficiently long propagation time in an interaction free region afterwards — conditions that may be fulfilled in laser-plasma experiments. Thus, an observation of polarized beams from laser-induced plasmas could settle the long-standing discussion whether the Stern-Gerlach effect is measurable also for charged particles.

Laser-induced generation of polarized ion beams would also be of high importance for research with particle accelerators. In this context ${}^3\text{He}^{2+}$ ions have been widely discussed, since they can serve as effective polarized neutron beams. However, such beams currently are not available due to the lack of corresponding ion sources. Another question of outstanding importance is whether a pre-polarized target, like ${}^3\text{He}$ gas, retains its polarization during laser-heating. This is crucial for the feasibility of proposals aiming at an efficiency increase of fusion reactors by using polarized fuel since this efficiency strongly depends on the cross section of the fusion reactions. Calculations show that, *e.g.*, doubling the cross section leads to a 1500-fold increase of the energy yield; it is also known that via its spin dependence the cross sections of the ${}^3\text{He}(d,p){}^4\text{He}$ and ${}^3\text{H}(d,n){}^4\text{He}$ fusion reactions can be increased by a factor of ~ 1.5 .

Our first measurements were carried out at the Arcurus laser laboratory at the Heinrich-Heine University Düsseldorf, where a 100+200 TW Ti:Sa laser is currently in operation. Laser pulses with a typical duration of 25 fs can be produced at a rate of 10 Hz and focused on a target, where an intensity of several 10^{20} Wcm^{-2} is reached. Since few-MeV protons are most easily generated from thin foil targets, the laser was directed under an incident angle of 45° on a gold foil of $3 \mu\text{m}$ thickness and a lat-

eral size of a few mm. The energy that was delivered on the target amounts to $\sim 1.5 \text{ J}$, the intensity profile at the focal point was of Gaussian shape with a width of $5 \mu\text{m}$ (FWHM).

In order to measure the polarization of the proton bunches, a compact and easy-to-use polarimeter comprising a secondary scattering target has been developed, which makes use of the spin dependence of elastic proton scattering off nuclei. The polarimeter is located at a distance of a few cm behind the production target. Silicon is well suited as scattering target material at proton energies around 3 MeV since high precision data for both the analyzing power A_y and differential cross section $d\sigma/d\Omega$ of the $\text{Si}(p,p')\text{Si}$ reaction are available from measurements at the Cologne tandem accelerator. Our analysis of the scattering-angle dependence of the protons behind the Silicon target yields $d\sigma/d\Omega$ for the Laser-accelerated protons. The result is in excellent agreement with the tandem data which demonstrates the feasibility of a classical accelerator measurement with a Laser-driven particle source. From the azimuthal-angle dependence of the data — using the known values of A_y — the degree of polarization P of laser-accelerated protons could be determined for the first time.

For the two analyzed shots we find polarizations $P = 0.15 \pm 0.13(\text{stat}) \pm 0.08(\text{syst})$ and $P = 0.08 \pm 0.06(\text{stat}) \pm 0.08(\text{syst})$ for a proton kinetic energy of 3.2 MeV, *i.e.* no significant polarization build-up. This finding is supported by the results of simulations with EPOCH, a fully relativistic 2D particle-in-cell code. These were performed on the Juropa supercomputer of FZJ for a normally incident laser on a Au foil with a proton layer. The grid size was $n_x \times n_y = 6096 \times 4048$ and the number of simulated particles $n_{\text{Au}} = 4 \cdot 10^6$ and $n_p = 20 \cdot 10^6$.

The efficiency of the spin-flip scenario is governed by the Boltzmann factor

$$W(E) = \exp\left(-\frac{2\mu_p B}{k_B T}\right),$$

where μ_p is the proton magnetic moment, and the proton temperature T is derived here from the mean kinetic energy of the protons behind the target foil. Figure 50 shows the simulated time dependence of T as well as of the magnetic field strength B . It is seen that only at $t \sim 95 \text{ fs}$ do cold protons feel the influence of a strong magnetic field. This time, however, is much smaller than the typical time scale for a polarization build-up which is defined by their Larmor frequency. Thus, no significant proton polarization is to be expected since for all other times we find $2\mu_p B/k_B T \ll 1$. An efficient spin alignment would require cold targets, rapid decoupling of the accelerated protons from the heating plasma as well as large magnetic fields before the onset of heating.

In order to estimate the Stern-Gerlach deflection we then calculate the quantity

$$\alpha = \arctan \frac{\mu_p}{m_p v_x^2} \cdot \int \frac{\partial B}{\partial y} \cdot dx$$

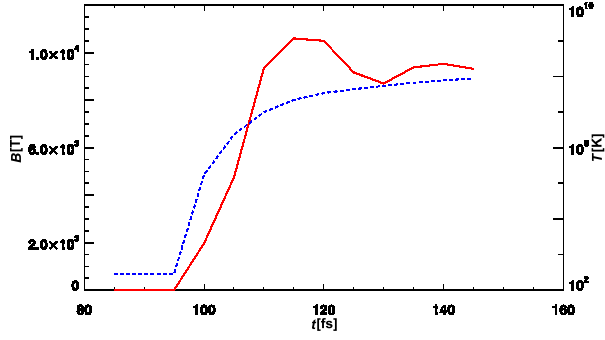


Fig. 50: Time evolution of the average proton temperature (blue dashed) and the maximum of the magnetic field strength (red solid) behind the target foil. The laser pulse hits the foil at $t \sim 90$ fs.

along the proton flight paths. α is an approximation for the deflection angle of a proton with magnetic moment μ_p , mass m_p and longitudinal velocity v_x which moves through a magnetic field with gradient $\partial B/\partial y$. As an example Figure 51 shows $\partial B/\partial y(x)$ at the center of the plasma where the gradients are largest. In general we find significant deflection angles only when the gradients are already sizeable at low proton velocities, *i.e.* at the onset of the acceleration through the electric fields. However, for all cases considered here α is below ~ 0.01 mrad, *i.e.* much smaller than the typical proton emission angles and experimental angular resolutions. Thus, also no emission regions with preferred spin alignments are to be expected.

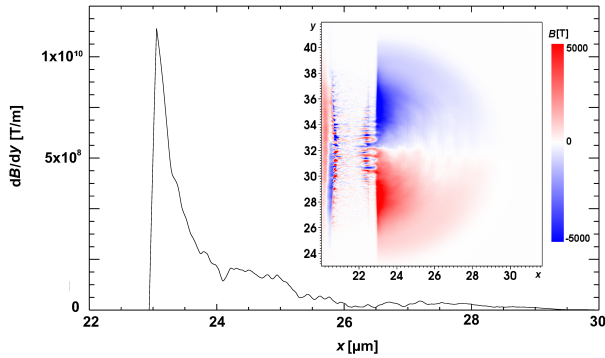


Fig. 51: Gradient of the magnetic field $\partial B/\partial y$ at $y = 32.5 \mu\text{m}$ behind the gold target foil (located at $x = 20.5 - 22.5 \mu\text{m}$) with a proton layer ($x = 22.5 - 23.0 \mu\text{m}$) at $t = 120$ fs. The insert shows the underlying magnetic field distribution $B_z(x, y)$.

As expected from the simulation calculations for the given target configuration, our data are consistent with an unpolarized beam $P = 0$. This finding can be interpreted such that the particle spins are not affected by the strong magnetic fields/gradients in relativistic plasma and thus seems promising for future applications using pre-polarized gas targets.

7.1.2 Measurements with gas targets

One of the major challenges on the way to a polarized ${}^3\text{He}^{2+}$ beam is that the ions have to be accelerated from a gaseous target (*i.e.* an underdense plasma) to kinetic energies of at least a few MeV. That has, so far, only been achieved in a single measurement at the VULCAN laser facility in 2006. A first experiment of that kind at Arc-turus, carried out in 2011 and using a standard gas-jet target of ~ 1.5 mm width, failed since there the pulse energies are much lower than at VULCAN. A second attempt in winter 2012/2013 with an improved set-up then resulted in the generation of ${}^4\text{He}$ ions with energies up to about 4 MeV, see Fig. 52.

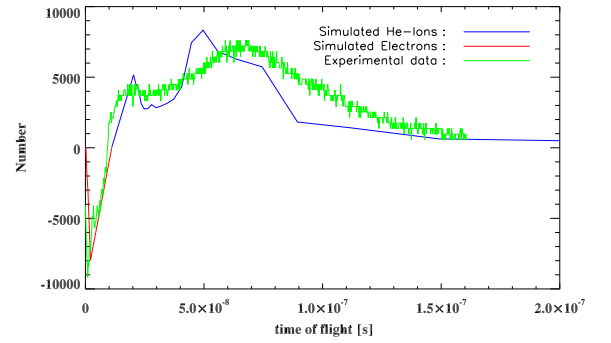


Fig. 52: Time-of-flight distribution of electrons and ${}^4\text{He}$ ions between the gas target and a Faraday cup 23 cm behind the target (green line). A PIC-code simulation under the same conditions (red line: electrons, blue line: helium ions) leads to similar results.

The most significant improvement was the use of a Laval nozzle produced at ZEA-1 of FZJ with a minimum diameter of only $167 \mu\text{m}$. Over a length of 2 mm the nozzle expands to the opening diameter of $500 \mu\text{m}$. Thus it was possible to provide a gas jet thinner than one mm. During the measurements the maximum achievable ion energy was optimized by a systematic tuning of parameters like the He backing pressure, the focus position in height and in laser direction as well as the laser-pulse length. A first rough data analysis reveals ${}^4\text{He}$ energies up to 4 MeV/nucleon, also in good agreement to PIC-code simulations with EPOCH on Juropa (see Fig. 52).

7.2 Nuclear Fusion with Polarized Particles

The idea to use nuclear polarized particles as fuel for future thermonuclear fusion reactors has been discussed since many years. For magnetic confinement as well as for inertial fusion it is shown that the total cross section can be increased by a significant factor. Especially for the most important fusion reactions, the $d + t \rightarrow {}^4\text{He} + n$ and the $d + {}^3\text{He} \rightarrow {}^4\text{He} + p$ reaction, a factor close to 1.5 is expected in the energy range below 100 keV. Main reaction channel in both cases is a s-wave dominated $J = 3/2^+$ resonance. Therefore, the fusion of the deuteron and the triton (${}^3\text{He}$) with anti-parallel combinations of the nuclear spins is very weak and 1/3 of the possible combinations of these fusion reactions are suppressed. With aligned spins of both reaction partners this suppression can be excluded. In addition, the polarization of the projectiles allows the control of the ejectile trajectories. Due to the dominating s-waves at low plasma energies the differential cross section in the center of mass system does not depend much on the scattering angle of the ejectiles. Only the transformation into the laboratory system produces an increased forward and backward cross section. This asymmetry can be increased or decreased with use of polarized fuel to simplify the energy extraction from the plasma to the reactor wall or to concentrate the neutron flux on defined wall areas.

In addition, the energy gain of a fusion reactor does not only depend linearly on the total cross section. M. Temporal et al. have shown that for a laser-induced inertial fusion reactor the energy gain can be increased by a factor 4 if polarized fuel will be used. Another option for polarized fuel would be to reduce the laser power by 25% and in parallel the energy gain can be still increased linearly. For a Tokamak reactor such calculations do not exist up to now. Nevertheless, more fusion reactions will lead to more heating of the plasma, e.g. by the thermalization of the higher density of α particles. Higher temperatures in the equilibrium will increase the total cross section again. But these calculations should be done for each magnetic confinement reactor separately.

Before polarized fuel can be considered to be used in future thermonuclear reactors of different types a long list of questions must be answered.

1. Fundamental Physics: What about the dd reactions?

For the reactions $d + d \rightarrow t + p$ and $d + d \rightarrow {}^3\text{He} + n$, which will happen concurrently, the situation is unknown. In Fig. 53 the predictions for the quintet-suppression factor, the ratio of the total cross sections $\sigma_{1,1}$ for parallel deuteron spins (quintet state) and the unpolarized total cross section σ_0 are shown. In the energy range of a Tokamak reactor (30–50 keV) predictions range from a suppression by a factor 10 up to an increase of a factor 2.5. These reactions are much more complicated to handle due to the strong influence of p- and d-waves. In a dedicated experiment in collab-

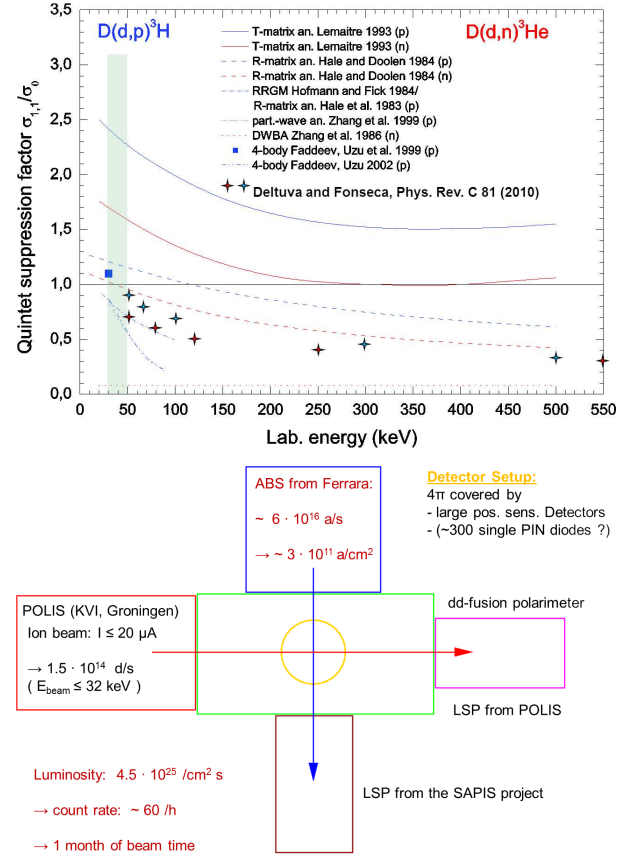


Fig. 53: Top: The different predictions for the ratio of the total cross section for parallel deuteron spins $\sigma_{1,1}$ and the unpolarized case σ_0 in the energy range up to 550 keV. Bottom: The principle of the double polarized dd measurements at energies below 100 keV at PNPI.

oration with the Petersburg Nuclear Physics Institute in Gatchina, Russia, and the University of Ferrara it is planned to measure the spin-correlation coefficients of the dd reactions at energies below 100 keV with crossed polarized deuterium and deuteron beams. The polarized deuteron source POLIS, a loan from the KVI in Groningen, the Netherlands, will start its operation beginning of 2013. The source for the polarized deuterium jet target is the contribution from the University of Ferrara and will be sent to Russia this year. FZJ will take care about the different polarimeters for the ion and the atomic beam. From these measurements the behaviour of the differential and the total cross section as functions of different polarization combinations of the deuterons can be deduced.

2. Can the polarization survive in the plasma?

Kulsrud et al. predicted in 1982 that the lifetime of polarized fuel in a Tokamak reactor should be long enough to influence the total cross section in a fusion plasma. But up to now this hypothesis was not verified in an experiment. For laser-induced fusion a measurement of the influence of the deuteron polarization in an HD-ice target on the cross section of the reactions $d(d,n)^3\text{He}$ and $d(p,\gamma)t$ is planned by a group from Orsay. In a collaboration of the University of Düsseldorf and the Institut für Kernphysik it is planned to produce a beam of polarized $^3\text{He}^{++}$ ions by ionizing polarized ^3He gas and to accelerate the ions to energies in the lower MeV range. If the polarization of the ^3He atoms will be preserved at least partially in the $^3\text{He}^{++}$ ions, this will be proof that the polarization survives in the laser-induced plasma.

3. How to get enough polarized fuel?

In order to use polarized particles to increase the energy gain of a fusion reactor enough polarized fuel must be provided before. This seems not to be a problem for ^3He and T, which both can be polarized by optical pumping. But polarized deuterium atoms are produced by atomic beam sources only and this will limit the production to $\sim 5 \times 10^{16}$ deuterium atoms per second. In addition, these atoms cannot be stored. Nevertheless, it was shown before that the polarization of protons and deuterons can partially survive in molecules, if polarized hydrogen and deuterium atoms recombine under special conditions. In a collaboration of the PNPI, the University of Cologne, and the Institute for Nuclear Physics at Forschungszentrum Jülich we built a dedicated experimental setup with a storage cell, with special coatings for the recombination process, in a superconducting coil (up to 1 T). The polarization of the molecules is measured with a Lambshift polarimeter. Fig. 54 shows a typical result for a gold surface in a magnetic field of 0.28 T for different temperatures. At least 50% of the

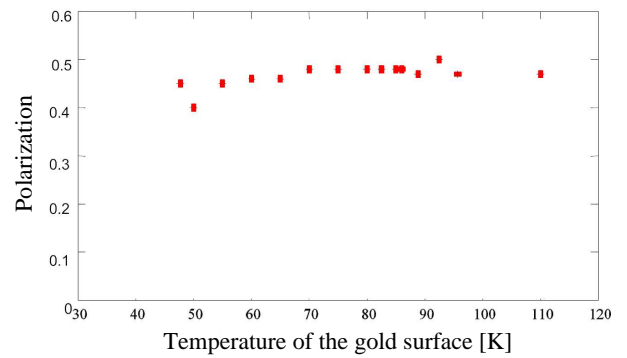


Fig. 54: Polarization of hydrogen molecules after the recombination of polarized hydrogen atoms at different temperatures on a gold surface at 0.28 T.

atomic polarization is conserved in the molecules, which can be collected and stored for a reasonable time.

7.3 Parity Violation in Hydrogen and Deuterium

The interaction of the magnetic moment of the electron with the nucleon spin is the reason for the variation of the binding energies of the different hyperfine substates of hydrogen and deuterium atoms. In addition, these energy levels depend on an external magnetic field which is shown in the Breit-Rabi diagram where the binding energy is plotted against the strength of the external magnetic field. For the first excited state of hydrogen and deuterium with $n = 2$ level crossings exist between the the β -substates ($J = -1/2$) of the $2S_{1/2}$ state and the $2P_{1/2}$ e-substates ($J = +1/2$) around 57 mT and of the β -substates and the f-substates ($J = -1/2$) at 120 mT (Fig. 55). Direct transitions between the states are forbidden at these crossing points by parity conservation of the electromagnetic interaction. However, the electroweak interaction of the standard model (SM) and its contribution to the binding force of the S-states leads to a small admixture of the parity-violating weak force. From this, all four polarized and unpolarized electron-nucleon and weak-neutral-current coupling constants C_{1p} , C_{2p} , C_{1n} and C_{2n} can be deduced, if such experiments are made for hydrogen and deuterium in parallel. When $C_{1D} = C_{1p} + C_{1n}$ and $C_{2D} = C_{2p} + C_{2n}$ are defined for deuterium, Table 2 shows which coupling constant can be deduced from which crossing point and the predictions from the standard model for the different parity mixing matrix elements (in terms of $i\overline{V}_w \approx 2\pi \times 0.013s^{-1}$)

Table 2: Different matrix elements and the corresponding electron-nucleon and weak-neutral-current coupling constants for the level crossings in the Breit-Rabi diagram of hydrogen and deuterium.

Matrix Element	Value	SM	Atom
$\langle e_2 V \beta_4 \rangle$	$-2C_{2p}$	-0.086	H
$\langle f_4 V \beta_4 \rangle$	$C_{1p} + 1.1C_{2p}$	0.083	H
$\langle f_3 V \beta_3 \rangle$	$C_{1p} - C_{2p}$	-0.007	H
$\langle e_2 V \beta_6 \rangle$	$-\sqrt{2}C_{2D}$	-0.010	D
$\langle e_3 V \beta_5 \rangle$	$-\sqrt{2}C_{2D}$	-0.010	D
$\langle f_6 V \beta_6 \rangle$	$C_{1D} + C_{2D}$	-0.452	D
$\langle f_5 V \beta_5 \rangle$	C_{1D}	-0.459	D
$\langle f_4 V \beta_4 \rangle$	$C_{1D} - C_{2D}$	-0.466	D

With the equation: $2C_{1p} = Q_W(p) \approx (1 - 4\sin^2\Theta_w)$ the weak charge of the proton $Q_W(p)$ and the weak mixing angle, i.e. the Weinberg angle $\sin^2\Theta_w$ are measured for very low momentum transfer and, therefore, the standard model can be tested.

The methods used to observe these transitions can be developed and optimized with the components of a Lamb-shift polarimeter (LSP) to increase the intensity. With a spinfilter a more direct technique is possible: With the components of a LSP a metastable deuterium beam in the hyperfine substate β_4 only can be produced. These atoms will be transmitted through a longitudinal homogeneous magnetic field, which can be continuously changed

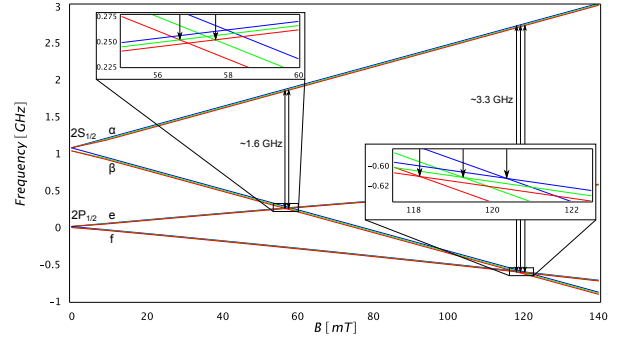


Fig. 55: Breit-Rabi diagram for deuterium with the crossing points of the β - and e-substates around 57 mT and of the β - and f-substates around 120 mT.

around 57 or about 120 mT. A cavity inside the magnetic field induces E1 transitions between the f_4 and the α_3 (~ 3.3 GHz) substates with sufficient power to produce oscillations between these states, very similar to the spinfilter itself. Without static electric fields inside (which are the main source for systematic uncertainties) transitions between the incoming atoms in the β_4 and f_4 substates can appear due to parity violation only. These atoms will be trapped in the oscillation between the f_4 and α_3 substates. Therefore, only transitions induced by parity violation can produce metastable hydrogen atoms in the α_3 substate and these atoms can be separated with another spinfilter. The residual metastable atoms are detected with an efficient quenching region afterwards.

If 10^{13} atoms/s in the β_4 substate reach the solenoid, about 10^4 atoms will be found in the oscillation between the α_3 and f_4 substates and about 100/s Lyman- α photons will be measured in a photomultiplier. This photomultiplier with a KBr photocathode and an MgF entrance window is optimized for Lyman- α photons (121 nm/10.2 eV) and has no dark current even without cooling and a tiny sensitive range between 115 and 135 nm. The sensitivity can be increased with a more efficient registration of single metastable hydrogen atoms. Another way to increase the signal is the use of a better hydrogen or deuterium source. In principle, the second spinfilter can be replaced by simple electric field plates at the end of the solenoid to quench all the beta-states into the ground state. The same setup can be used for the crossing points at 57 mT (RF: ~ 1.6 GHz) and for measurements with hydrogen.

A Councils

A.1 Hadron and Accelerator Physics Program Advisory Council

Prof. Mei Bai	Brookhaven National Laboratory, U.S.A.	
Prof. K.-T. Brinkmann	University Bonn	
Prof. M. Garçon	CEA-Saclay, FR	
Prof. A. Jankowiak	Helmholtz Zentrum Berlin	
Prof. K. Jungmann	KVI Groningen, NL	
Prof. K.-H. Kampert	University Wuppertal	
Prof. S. Paul	TU München	Chairperson
Prof. K. Peters	GSI Darmstadt	
Prof. D.-O. Riska	University Helsinki, FI	
Prof. C. Roberts	Argonne National Laboratory, U.S.A.	
Prof. S. Vigdor	Brookhaven National Laboratory, U.S.A.	

A.2 COSY Program Advisory Committee

Prof. M. Anselmino	L'Universita di Torino, IT	
Prof. D. Barber	DESY Hamburg	
Prof. E. Epelbaum	Universität Bochum	
Prof. M. Garçon	CEA-Saclay, F	Chairperson
Prof. N. Kaiser	TU München	
Prof. B. Kämpfer	FZ Dresden-Rossendorf	
Prof. O. Kester	GSI Darmstadt	
Prof. T. Kishimoto	RCNP Osaka, J	
Prof. A.K. Opper	George Washington University, USA	
Prof. P. Salabura	Jagellonian University Cracow, PL	
Prof. U. Thoma	Universität Bonn	
Prof. H. Weise	DESY, Hamburg	
Prof. H. Wilschut	KVI Groningen, NL	

B Publications

1. Experiment

1. **Trapped Antihydrogen in Its Ground State**
G. Gabrielse *et al.*
Phys. Rev. Lett. **108** 113002 (2012)
2. **$\pi^0\pi^0$ Production in Proton-Proton Collisions at $T_p=1.4$ GeV**
P. Adlarson *et al.* [WASA-at-COSY Collaboration],
Phys. Lett. B **706** 256 (2012) [arXiv:1107.0879 [hep-ex]]
3. **Exclusive Measurement of the $\eta \rightarrow \pi^+\pi^-\gamma$ Decay**
P. Adlarson *et al.* [WASA-at-COSY Collaboration],
Phys. Lett. B **707** 243 (2012) [arXiv:1107.5277 [nucl-ex]]
4. **Differential cross section and analysing power of the $pp \rightarrow pp_s\pi^0$ reaction at 353 MeV**
D. Tsirkov *et al.*,
Phys. Lett. B **712** 370 (2012) [arXiv:1112.3799 [nucl-ex]]
5. **Differential cross section and analysing power of the quasi-free $pn \rightarrow pp_s\pi^-$ reaction at 353 MeV**
S. Dymov *et al.*,
Phys. Lett. B **712** 375 (2012) [arXiv:1112.3808 [nucl-ex]]
6. **Efficient transfer of positrons from a buffer-gas-cooled accumulator into an orthogonally oriented superconducting solenoid for antihydrogen studies**
D. Comeau *et al.*,
New J. of Phys. **14** 45006 (2012)
7. **A semiconductor laser system for the production of antihydrogen**
A. Müllers *et al.*,
New J. of Phys. **14** 055009 (2012)
8. **Vector analyzing powers of deuteron-proton elastic scattering and breakup at 130 MeV**
L. Ciepal *et al.*,
Phys. Rev. C **85** 017001 (2012)
9. **Momentum dependence of the ϕ -meson nuclear transparency**
M. Hartmann *et al.*,
Phys. Rev. C **85** 035206 (2012) [arXiv:1201.3517 [nucl-ex]]
10. **Production of K^+K^- pairs in proton-proton collisions at 2.83 GeV**
Q. Ye *et al.*,
Phys. Rev. C **85** 035211 (2012) [arXiv:1202.5451 [nucl-ex]]
11. **Abashian-Booth-Crowe resonance structure in the double pionic fusion to ^4He**
P. Adlarson *et al.* [WASA-at-COSY Collaboration],
Phys. Rev. C **86** 032201 (2012) [arXiv:1206.6337 [nucl-ex]]
12. **New determination of the mass of the η meson at COSY-ANKE**
P. Goslowski *et al.*,
Phys. Rev. D **85** 112011 (2012) [arXiv:1204.3520 [nucl-ex]]
13. **Formation of the $S = -1$ resonance $X(2265)$ in the reaction $pp \rightarrow X + K^+$ at 2.50 and 2.85 GeV**
P. Kienle *et al.*,
Eur. Phys. J. A **48** 183 (2012)
14. **The $pp \rightarrow nK^+\Sigma^+$ reaction at 2.95 GeV/c**
M. Abdel-Bary *et al.* [COSY-TOF Collaboration],
Eur. Phys. J. A **48** 37 (2012)
15. **The $pK^0\Sigma^+$ final state in proton-proton collisions**
M. Abdel-Bary *et al.* [COSY-TOF Collaboration],
Eur. Phys. J. A **48** 23 (2012)

16. **Luminosity determination for the pd reaction at 2.14 GeV with WASA-at-COSY**
C. Zheng *et al.*,
Chin. Phys. C **36** 605 (2012) [arXiv:1109.5911 [nucl-ex]]
17. **Width of the ϕ meson in nuclear matter**
M. Hartmann *et al.*,
Phys. Atom. Nucl. **75** 63 (2012), Yad. Fiz. **75** 100 (2012)
18. **Determination of the $D_{s0}^*(2317)$ width with the PANDA detector**
M.C. Mertens
Hyperfine Interactions **209** 111 (2012)
19. **Prospects for antiproton physics, my perspective**
W. Oelert
Hyperfine Interactions **213** 237 (2012)
20. **AD performance and its extension towards ELENA**
W. Oelert, T. Eriksson, P. Belochitskii and G. Tranquille,
Hyperfine interactions **213** 227 (2012)
21. **About an analytical application of the spherical symmetric diffusion equation**
J. Fiedler and F. Goldenbaum,
Zeitschrift für angewandte Mathematik und Physik **63** 975 (2012)
22. **Pionic deuterium**
D. Gotta,
Europhys. News **43** 28 (2012)
23. **Meeting Report on the 12th International Workshop on Meson Production, Properties and Interaction (MESON2012)**
C. Guaraldo, S. Kistryn, H. Ströher,
Nucl. Phys. News **22** 36 (2012)

2. Theory

24. **Signatures of three-nucleon interactions in few-nucleon systems**
N. Kalantar-Nayestanaki, E. Epelbaum, J.G. Messchendorp, A. Nogga,
Rep. Prog. Phys. **75** 016301 (2012) [arXiv:1108.1227 [nucl-th]]
25. **Chiral dynamics of few- and many-nucleon systems**
E. Epelbaum, U.-G. Meißner,
Ann. Rev. Nucl. Part. Sci. **62** 159 (2012) [arXiv:1201.2136 [nucl-th]]
26. **Examining Coupled-Channel Effects in Radiative Charmonium Transitions**
F.K. Guo, U.-G. Meißner,
Phys. Rev. Lett. **108** 112002 (2012) [arXiv:1111.1151 [hep-ph]]
27. **Light quark mass dependence in heavy quarkonium physics**
F.K. Guo, U.-G. Meißner,
Phys. Rev. Lett. **109** 062001 (2012) [arXiv:1203.1116 [hep-ph]]
28. **Self-Consistent Calculations of the Electric Giant Dipole Resonances in Light and Heavy Nuclei**
N. Lyutorovich *et al.*,
Phys. Rev. Lett. **109** 092502 (2012) [arXiv:1207.0664 [nucl-th]]
29. **Structure and Rotations of the Hoyle State**
E. Epelbaum, H. Krebs, T.A. Lähde, D. Lee, U.-G. Meißner,
Phys. Rev. Lett. **109** 252501 (2012) [arXiv:1208.1328 [nucl-th]]
30. **Finite volume effects in pion-kaon scattering and reconstruction of the $\kappa(800)$ resonance**
M. Döring, U.-G. Meißner,
JHEP **1201** 009 (2012) [arXiv:1111.0616 [hep-lat]]
31. **Roy-Steiner equations for pion-nucleon scattering**
C. Ditsche, M. Hoferichter, B. Kubis, U.-G. Meißner,
JHEP **1206** 043 (2012) [arXiv:1203.4758 [hep-ph]]
32. **Dispersive analysis of the scalar form factor of the nucleon**
M. Hoferichter, C. Ditsche, B. Kubis, U.-G. Meißner,
JHEP **1206** 063 (2012) [arXiv:1204.6251 [hep-ph]]
33. **Matrix elements of unstable states**
V. Bernard, D. Hoja, U.-G. Meißner, A. Rusetsky,
JHEP **1209** 023 (2012) [arXiv:1205.4642 [hep-lat]]
34. **Baryon electric dipole moments from strong CP violation**
F.K. Guo, U.-G. Meißner,
JHEP **1212** 097 (2012) [arXiv:1210.5887 [hep-ph]]
35. **Model-independent approach to $\eta \rightarrow \pi^+\pi^-\gamma$ and $\eta' \rightarrow \pi^+\pi^-\gamma$**
F. Stollenwerk, C. Hanhart, A. Kupsc, U.-G. Meißner, A. Wirzba,
Phys. Lett. B **707** 184 (2012)
36. **A new parameterization for the pion vector form factor**
C. Hanhart *et al.*,
Phys. Lett. B **715** 170 (2012) [arXiv:1203.6839 [hep-ph]]
37. **Scattering lengths of strangeness $S=-2$ baryon-baryon interactions**
A. Gasparyan, J. Haidenbauer, C. Hanhart,
Phys. Rev. C **85** 015204 (2012) [arXiv:1111.0513 [nucl-th]]
38. **Pion production in nucleon-nucleon collisions in chiral effective field theory: Next-to-next-to-leading order contributions**
A. Filin *et al.*,
Phys. Rev. C **85** 054001 (2012) [arXiv:1201.4331 [nucl-th]]

39. **Pion photoproduction in a dynamical coupled-channels model**
F. Huang *et al.*,
Phys. Rev. C **85** 054003 (2012) [arXiv:1110.3833 [nucl-th]]
40. **Self-consistent calculations of quadrupole moments of the first 2^+ states in Sn and Pb isotopes**
D. Voitenkov, S. Kamedzhiev, S. Krewald, E. Saperstein, S. Tolokonnikov,
Phys. Rev. C **85** 054319 (2012) [arXiv:1112.6004 [nucl-th]]
41. **Precise calculation of the two-step process for $K^-d \rightarrow \pi\Sigma N$ in the $\Lambda(1405)$ resonance region**
K. Miyagawa, J. Haidenbauer,
Phys. Rev. C **85** 065201 (2012) [arXiv:1202.4272 [nucl-th]]
42. **Benchmark calculations for elastic fermion-dimer scattering**
S. Bour, H.-W. Hammer, D. Lee, U.-G. Meißner,
Phys. Rev. C **86** 034003 (2012) [arXiv:1206.1765 [nucl-th]]
43. **Remarks on the quantum numbers of X(3872) from the invariant mass distributions of the $\rho J/\psi$ and $\omega J/\psi$ final states**
C. Hanhart, Yu. Kalashnikova, A. Kudryavtsev, A. Nefediev,
Phys. Rev. D **85** 011501 (2012) [arXiv:1111.6241 [hep-ph]]
44. **Anomalous decays of η' and η into four pions**
F.K. Guo, B. Kubis, A. Wirzba,
Phys. Rev. D **85** 014014 (2012) [arXiv:1111.5949 [hep-ph]]
45. **Review of Particle Physics (RPP)**
J. Beringer *et al.* [Particle Data Group],
Phys. Rev. D **86** 010001 (2012)
46. **The proton-antiproton mass threshold structure in $\psi(3686)$ radiative decay revisited**
J. Haidenbauer, U.-G. Meißner,
Phys. Rev. D **86** 077503 (2012) [arXiv:1208.3343 [hep-ph]]
47. **Where is the $\chi_{c0}(2P)$?**
F.K. Guo, U.-G. Meißner,
Phys. Rev. D **86** 091501 (2012) [arXiv:1208.1134 [hep-ph]]
48. **Scattering phases for meson and baryon resonances on general moving-frame lattices**
M. Göckeler *et al.*,
Phys. Rev. D **86** 094513 (2012) [arXiv:1206.4141 [hep-lat]]
49. **The Multiple-scattering series in pion-deuteron scattering and the nucleon-nucleon potential: Perspectives from effective field theory**
V. Baru *et al.*,
Eur. Phys. J. A **48** 69 (2012) [arXiv:1202.0208 [nucl-th]]
50. **Quadrupole moments of spherical semi-magic nuclei within the self-consistent Theory of Finite Fermi Systems**
S.V. Tolokonnikov, S. Kamedzhiev, S. Krewald, E.E. Saperstein, D. Voitenkov,
Eur. Phys. J. A **48** 70 (2012) [arXiv:1111.3117 [nucl-th]]
51. **Scalar mesons moving in a finite volume and the role of partial wave mixing**
M. Döring, U.-G. Meißner, E. Oset, A. Rusetsky,
Eur. Phys. J. A **48** 114 (2012) [arXiv:1205.4838 [hep-lat]]
52. **The size of the proton — Closing in on the radius puzzle**
I.T. Lorenz, H.-W. Hammer, U.-G. Meißner,
Eur. Phys. J. A **48** 151 (2012) [arXiv:1205.6628 [hep-ph]]
53. **Exotic bound states of two baryons in light of chiral effective field theory**
J. Haidenbauer, U.-G. Meißner,
Nucl. Phys. A **881** 44 (2012) [arXiv:1111.4069 [nucl-th]]

54. **A Three-Dimensional Treatment of the Three-Nucleon Bound State**
J. Gólak *et al.*,
Few Body Syst. **53** 20 (2012) [arXiv:1206.3192 [nucl-th]]
55. **Different Methods for the Two-Nucleon T-Matrix in the Operator Form**
J. Gólak *et al.*,
Few Body Syst. **53** 237 (2012) [arXiv:1206.3155 [nucl-th]]

3. Accelerator (including conference proceedings)

56. **Polarization of a stored beam by spin-filtering**
W. Augustyniak *et al.*,
Phys. Lett. B **718** 64 (2012)
57. **Synchrotron oscillation effects on an rf-solenoid spin resonance**
P. Benati *et al.*,
Phys. Rev. ST — Accelerators and Beams **15** 124202 (2012)
58. **Polarization of laser-accelerated ions**
A. Holler *et al.*
Proc. of the International School of Physics “Enrico Fermi”, Course CLXXIX “Laser-Plasma Acceleration”, ISBN 978-1-61499-129-8, pp. 205–212; Varenna, Italy; 20.–25.06.2011
59. **Polarized Electron-Nucleon Collider ENC at FAIR**
A. Lehrach
ICFA Beam Dynamics News Letters **58**; Melbourne, Australia; 07.08.2012; pp. 29–35
60. **Project Overview and Computational Needs to Measure Electric Dipole Moments at Storage Rings**
A. Lehrach
Proc. 11th International Computational Accelerator Physics Conference (ICAP2012); ISBN 978-3-95450-116-8; Rostock, Germany; 19.–24.08.2012
61. **Storage Ring Electric Dipole Moment Methods: The road to the next sensitivity level of hadronic EDMs**
A. Lehrach *et al.*
Proc. of Open Symposium — European Strategy Preparatory Group; Cracow, Poland; 10.–12.09.2012
62. **Alternating spin aberration electrostatic lattice for EDM ring**
R. Maier, Yu. Senichev, D. Zyuzin, M. Berz
Proc. of International Particle Accelerator Conference (IPAC2012); New Orleans, U.S.A.; 20.–25.05.2012
Conf. Proc. C **1205201** 1332 (2012)
63. **Comparison of different numerical modeling methods for beam dynamics in electrostatic rings**
R. Maier, Yu. Senichev, D. Zyuzin, M. Berz
Proc. of International Particle Accelerator Conference (IPAC2012); New Orleans, U.S.A.; 20.–25.05.2012
Conf. Proc. C **1205201** 1332 (2012)
64. **Storage Ring EDM Simulations: Methods and Results**
Yu. Senichev *et al.*
Proc. 11th International Computational Accelerator Physics Conference (ICAP2012); ISBN 978-3-95450-116-8; Rostock, Germany; 19.–24.08.2012
65. **RF and Stochastic Cooling System of the HESR**
R. Stassen *et al.*
Proc. of International Particle Accelerator Conference (IPAC2012); New Orleans, U.S.A.; 20.–25.05.2012
Conf. Proc. C **1205201** 385 (2012)
66. **Operation of the HESR Storage Ring of the Fair Project with ions and rare isotopes**
M. Steck *et al.*
Proc. of International Particle Accelerator Conference (IPAC2012); New Orleans, U.S.A.; 20.–25.05.2012
Conf. Proc. C **1205201** 3722 (2012)
67. **Stochastic Cooling Developments for HESR at FAIR**
H. Stockhorst *et al.*
Proc. of International Particle Accelerator Conference (IPAC2012); New Orleans, U.S.A.; 20.–25.05.2012
Conf. Proc. C **1205201** 388 (2012)

C Talks and Colloquia

1. H. Bhatt
Physics Analysis and Simulation of Dilepton and Multi-Pion Final States from WASA to PANDA
30th CANU and 7th COSY-FFE Workshop
Physikzentrum Bad Honnef, Germany, 17.–18.12.2012
2. M. Büscher
News from the Pellet Target
XLI PANDA collaboration meeting
Northwestern University, Evanston IL, USA, 25.-29.06.2012
3. M. Büscher
Laser-induced particle acceleration — An introduction
Hadron Physics Summer School 2012
Bad Honnef, Germany, 30.08.2012
4. M. Büscher
Pellet Target
XLIII PANDA Collaboration Meeting
GSI Darmstadt, Germany, 10.–14.12.2012
5. D. Coderre
Measurements of Charged η Decays in $pd \rightarrow {}^3\text{He}\eta$ with WASA-at-COSY
30th CANU and 7th COSY-FFE Workshop
Physikzentrum Bad Honnef, Germany, 17.–18.12.2012
6. R.W. Engels
The Spinfilter of the BOB Experiment and for what it can be used
Status Meeting zum DFG Schwerpunkt 1491
Abtei Frauenwörth, Germany, 13.–16.03.2012
7. R.W. Engels
Polarimeters for the Polarized Fusion and other Projects
Workshop on Existing and Future Projects between PNPI (Gatchina) and FZJ
Gatchina, Russia, 24.–28.06.2012
8. R.W. Engels
Polarized Fusion
XXth International Symposium on Spin Physics (SPIN2012)
JINR Dubna, Russia, 17.–22.09.2012
9. R.W. Engels
Workshop Summary
XXth International Symposium on Spin Physics (SPIN2012)
JINR Dubna, Russia, 17.–22.09.2012
10. I. Engin
High-intensity Lasers for particle physics
Fifth Caucasian-German School and Workshop on Hadron Physics (Basic Science)
Tbilisi, Georgia, 06.–10.08.2012
11. P. Fedorets
News from the Pellet Target
XL PANDA Collaboration Meeting
GSI Darmstadt, Germany, 05.–09.03.2012
12. P. Fedorets
News from the Pellet Target
XLII PANDA Collaboration Meeting
Paris, France 10.–14.09.2012

13. M. Gaißer
 Optimization of Atomic Beam Sources for Polarization Experiments
 Fifth Caucasian-German School and Workshop on Hadron Physics (Basic Science)
 Tbilisi, Georgia, 06.–10.08.2012

14. F. Goldenbaum
 Review on existing data / databases and facilities
 Workshop on Nuclear physics for galactic cosmic rays in the AMS-02 era
 LPSC Grenoble, France, 03.–04.12.2012

15. D. Gotta
 Exotic Atoms
 Fifth Caucasian-German School and Workshop on Hadron Physics (Basic Science)
 Tbilisi, Georgia, 06.–10.08.2012

16. D. Gotta
 Detectors
 Fifth Caucasian-German School and Workshop on Hadron Physics (Basic Science)
 Tbilisi, Georgia, 06.–10.08.2012

17. D. Gotta
 Muonic Hydrogen
 XXth International Symposium on Spin Physics (SPIN2012)
 JINR Dubna, Russia, 17.–22.09.2012

18. D. Grzonka
 Possibilities of Foundational Tests at the Facility FLAIR: Status & Future
 Erwin-Schrödinger-Institute Vienna, Austria, 29.–30.11.2012

19. J. Haidenbauer
 Near threshold antiproton-proton enhancement in J/ψ decays
 Workshop: From nucleon structure to nuclear structure and compact astrophysical objects
 KITPC Beijing, China, 02.–06.07.2012

20. J. Haidenbauer
 Hyperon-nucleon interaction in chiral EFT
 7th International Workshop on Chiral Dynamics
 JLAB Newport News VA, U.S.A., 06.–10.08.2012

21. J. Haidenbauer
 Results for YN at NLO
 Micro-Workshop CRC 100
 Munich, Germany, 25.–26.10.2012

22. J. Haidenbauer
 Baryon-baryon interactions from chiral effective field theory
 11th International Conference on Hypernuclear and Strange Particle Physics (HYP2012)
 Barcelona, Spain, 01.–05.10.2012

23. C. Hanhart
 Perspectives in Hadron Physics
 Madrid, Spain, 26.03.2012

24. C. Hanhart
 How to reveal the mysteries of strong QCD
 Dublin, Ireland, 08.05.2012

25. C. Hanhart
 A new parametrization of the pion vector form factor
 Workshop on transition formfactors
 Cracow, Poland, 30.–31.05.2012

26. C. Hanhart
Recent insights into quarkonium properties
Workshop: From nucleon structure to nuclear structure and compact astrophysical objects
KITPC Beijing, China, 02.–06.07.2012
27. M. Hartmann
New results on $pp \rightarrow pp\phi/K^+K^-$ pair production and the momentum dependence of ϕ -meson nuclear transparency
Resonance Workshop
Austin TX, U.S.A., 05.–07.03.2012
28. F. Hauenstein
Status of the analysis of the $pp \rightarrow pK^+\Lambda$ reaction at $p = 2.7$ GeV/C with COSY-TOF
30th CANU and 7th COSY-FFE Workshop
Physikzentrum Bad Honnef, Germany, 17.–18.12.2012
29. A. Holler
A Method to Measure the Polarization of Laser-Accelerated Protons
2nd European Nuclear Physics Conference
Bukarest, Romania, 17.–21.09.2012
30. Q. Hu
Preparations to commission the HESR-Day one experiment at COSY
30th CANU and 7th COSY-FFE Workshop
Physikzentrum Bad Honnef, Germany, 17.–18.12.2012
31. F.A. Khan
 ω Meson Decays with WASA-at-COSY
30th CANU and 7th COSY-FFE Workshop
Physikzentrum Bad Honnef, Germany, 17.–18.12.2012
32. P. Klaja
Status of the $pp \rightarrow nK^+\Sigma^+$ reaction analysis at COSY-TOF
30th CANU and 7th COSY-FFE Workshop
Physikzentrum Bad Honnef, Germany, 17.–18.12.2012
33. S. Krewald
Effective Field Theory Approach to Nuclear Matter
Los Alamos NM, U.S.A., 09.08.2012
34. S. Krewald
Coupled Channel Dynamics in Lambda and Sigma Production
EmNN 2012 Workshop “Nucleon Resonance Structure in Exclusive Electroproduction at High Photon Virtualities”
Columbia SC, U.S.A., 11.-16.08.2012
35. S. Krewald
Giant Dipole Resonance in light and heavy nuclei beyond selfconsistent mean field theory
Annual Fall Meeting of the Division of Nuclear Physics
Newport Beach CA, USA, 24.–27.10.2012
36. P. Kulesa
Overview of PANDA STT readout activities
30th CANU and 7th COSY-FFE Workshop
Physikzentrum Bad Honnef, Germany, 17.–18.12.2012
37. A. Lehrach
Beam physics for the HESR
Beam physics for FAIR 2012
GSI Darmstadt, Germany, 10.–11.05.2012
38. A. Lehrach
Accelerator Related Issues for Storage Ring EDM Searches
Kernphysikalisches Kolloquium des Helmholtz-Instituts für Strahlen- und Kernphysik
Universität Bonn, Germany, 12.07.2012

39. A. Lehrach
Computational needs for new storage rings to measure electric dipole moments
11th Int. Computational Accelerator Physics Conference
Rostock, Germany, 19.–24.08.2012
40. A. Lehrach
Search on EDMs in Storage Rings
ECT* Workshop “EDM Searches at Storage Rings”
Trento, Italy, 01.–05.10.2012
41. A. Lehrach
Perspectives for EDM search in storage rings
ECT* Workshop “EDM Searches at Storage Rings”
Trento, Italy, 01.–05.10.2012
42. U.-G. Meißner
Nuclear Physics from Lattice Simulations
NIC Symposium 2012
Forschungszentrum Jülich, Germany, 07.–08.02.2012
43. U.-G. Meißner
Nuclear Physics from Lattice Simulations
Workshop on Nuclear Ground-State Properties of the Lightest Nuclei: Status and Perspectives
Physikzentrum Bad Honnef, Germany, 19.–21.03.2012
44. U.-G. Meißner
Roy-Steiner equations for pion-nucleon scattering
VIth International Conference on Quarks and Nuclear Physics (QNP2012)
Palaiseau, France, 16.–20.04.2012
45. U.-G. Meißner
Hadron resonances in a finite volume
VIth International Conference on Quarks and Nuclear Physics (QNP2012)
Palaiseau, France, 16.–20.04.2012
46. U.-G. Meißner
Hadron-hadron scattering: Lessons from chiral symmetry
12th International Workshop on Meson Production, Properties and Interaction (MESON 2012)
Cracow, Poland, 31.05.–05.06.2012
47. U.-G. Meißner
Symmetries and the emergence of structure in QCD — Introduction to the CRC 110
Workshop: From nucleon structure to nuclear structure and compact astrophysical objects
KITPC Beijing, China, 02.–06.07.2012
48. U.-G. Meißner
Nuclear lattice simulations
Workshop: From nucleon structure to nuclear structure and compact astrophysical objects
KITPC Beijing, China, 02.–06.07.2012
49. U.-G. Meißner
Effective Field Theories
School on High Energy Physics (TAE 2012)
Universidad Complutense, Madrid, Spain, 16.–27-07.2012
50. U.-G. Meißner
A walk through the world of chiral dynamics
7th International Workshop on Chiral Dynamics
JLAB Newport News VA, U.S.A., 06.–10.08.2012
51. U.-G. Meißner
Theory of baryon EDMs — new insights
ECT* Workshop “EDM Searches at Storage Rings”
Trento, Italy, 01.–05.10.2012

52. U.-G. Meißner
Testing the anthropic principle with lattice simulations
Workshop on Light nuclei from first principles
INT Seattle WA, U.S.A., 10.10.2012
53. U.-G. Meißner
Symmetries and the emergence of structure in QCD
30th CANU and 7th COSY-FFE Workshop
Physikzentrum Bad Honnef, Germany, 17.–18.12.2012
54. A. Nass
Instrumentation for PAX Experiment at COSY
Fifth Caucasian-German School and Workshop on Hadron Physics (Basic Science)
Tbilisi, Georgia, 06.–10.08.2012
55. A. Nass
Spin Filtering at COSY and Perspectives for PAX
XXth International Symposium on Spin Physics (SPIN2012) JNR Dubna, Russia, 17.–22.09.2012
56. A. Nogga
Light hypernuclei based on chiral and phenomenological interactions
XI International Conference on “Hypernuclear and Strange Particle Physics”
Barcelona, Spain, 02.10.2012
57. A. Nogga
Light hypernuclei: a challenge for hyperon-nucleon forces
Workshop: From nucleon structure to nuclear structure and compact astrophysical objects
KITPC Beijing, China, 02.–06.07.2012
58. A. Nogga
Light hypernuclei
CRC 110 Micro-Workshop on “Strangeness and Nuclear Physics”
Munich, Germany, 26.10.2012
59. W. Oelert
ELENA — an upgrade to the CERN Antiproton Decelerator
Plenary talk at the DPG-Frühjahrstagung
Mainz, Germany, 19.–23.03.2012
60. D. Rönchen
Coupled-channel dynamics in pion- and photon-induced reaction — the Jülich model
Institutsseminar Kernphysik, Institut für Kernphysik
Mainz, Germany, 03.12.2012
61. D. Rönchen
Pion- and photon-induced hadronic reactions in a combined coupled-channel analysis
Bled Mini-Workshop “Hadronic Resonances”
Bled, Slovenia, 01.–08.07.2012
62. S. Schadmand
Rare Meson Decays and Transition Form Factors
6th International Conference on Quarks and Nuclear Physics
Palaiseau, France, 16.–20.04.2012
63. S. Schadmand
Experimental Determination of Light Meson Transition Form Factors
Light Meson Decays Workshop
JLB Newport News VA, U.S.A., 05.08.2012
64. Y. Senichev
Electrostatic lattice for EDM storage ring with alternating spin aberration
EDM Workshop
Gatchina, Russia, 23.–28.06.2012

65. Y. Senichev
Storage Ring EDM Simulations: Methods and Results
11th Int. Computational Accelerator Physics Conference
Rostock, Germany, 19.–24.08.2012
66. A. Senichev
Electrostatic lattice with alternating spin aberration
ECT* Workshop “EDM Searches at Storage Rings”
Trento, Italy, 01.–05.10.2012
67. H. Stockhorst
HESR Stochastic Cooling of Heavy Ions
Meeting on Beam Cooling Issues for Antiproton and Ion Beams in CR-HESR
GSI Darmstadt, Germany, 26.–30.01.2012
68. H. Stockhorst
Stochastic Cooling of a Polarized Proton Beam at COSY
ECT* Workshop “EDM Searches at Storage Rings”
Trento, Italy, 01.–05.10.2012
69. H. Stockhorst
Simulation of Capture, Preparation and Acceleration of a Bare Uranium Beam to 2 GeV/u for Internal Target
Experiments with Stochastic Cooling in the HESR
9th International Topical SPARC Workshop
Vienna, Austria, 26.–28.11.2012
70. H. Ströher
The Next Step: Polarized Antiprotons for FAIR/HESR
Int. Workshop on non-perturbative Phenomena in Hadron and Particle Physics
Sao Paulo, Brazil, 30.04.–05.05.2012
71. H. Ströher
Grand Challenges in Basic Sciences: How to Understand our World, and Georgia’s (possible) Role in this Quest
Int. Sc. Conf. dedicated to the 90th Anniversary of Georgian Technical University
Tbilisi, Georgia, 19.–21.09.2012
72. H. Ströher
Opening Remarks
ECT* Workshop “EDM Searches at Storage Rings”
Trento, Italy, 01.–05.10.2012
73. H. Ströher
From Hadron Physics to the Precision Frontier
Fifth Caucasian-German School and Workshop on Hadron Physics (Basic Science) Tbilisi, Georgia, 06.–10.08.2012
74. H. Ströher
Summary and Outlook
ECT* Workshop “EDM Searches at Storage Rings”
Trento, Italy, 01.–05.10.2012
75. H. Ströher
The Joint Times with Herbert Löhner in TAPS and COSY
Symposium to honor Muhsin Harakeh and Herbert Löhner
Groningen, The Netherlands, 30.11.2012
76. A. Wirzba
Permanent EDMs, hadrons and low-energy effective field theory
Seminar: Precision Experiments in Storage Rings RWTH Aachen und IKP
Forschungszentrum Jülich, Germany, 10.05.2012
77. A. Wirzba
Electric Dipole Moments
Hadron Physics Summerschool 2012
Bad Honnef, Germany, 27.–31.08.2012 - 08/31/2012

78. A. Wirzba
Theory Outlook
ECT* Workshop “EDM Searches at Storage Rings”
Trento, Italy, 01.–05.10.2012
79. A. Wirzba
The four-pion decays of η' and η
12th International Workshop on Meson Production, Properties and Interaction (MESON 2012)
Cracow, Poland, 31.05.–05.06.2012
80. A. Wirzba
 $\eta, \eta' \rightarrow \pi^+, \pi^- \gamma$: a model-independent approach
Workshop on transition formfactors
Cracow, Poland, 30.–31.05.2012
81. Q.J. Ye
New trends in the low-energy QCD in the strangeness sector: experimental and theoretical aspects
ECT* Trento, Italy, 15.–19.10.2012

D Diploma and Ph.D. Theses

1. Bachelor, Master, Diploma

1. J. Elis,
Vermessung der Eigenschaften von Strahlen gefrorener Mikro-Kügelchen mit einem Zeilenkamera-System Bachelorarbeit, FH Aachen, Campus Jülich
2. V. Gupta,
Modification of the Pumping System of the Atomic Beam Source at the ANKE facility in COSY-Jülich, Diplomarbeit, FH Aachen, Campus Jülich
3. J. Lumbeck,
Persistente Speicherung von geometrischen Objekten aus Google Earth, Bachelorarbeit, FH Aachen, Campus Jülich

2. Ph.D.

4. E. Borodina,
Online system for data monitoring, visualisation and control at the COSY-TOF experiment,
Moscow State Institute of Electronics and Mathematics (Technical University), Russia
5. D. Coderre,
The Branching Ratio and CP-Violating Asymmetry of $\eta \rightarrow \pi^+ \pi^- e^+ e^-$,
Ruhr-Universität Bochum
6. R. Dzhygadlo,
Differential Cross Section distributions and Polarization Observables in the reaction $\bar{p}p \rightarrow pK^0\Sigma^+$ at $p_p = 2.95$ GeV/c,
Rheinische Friedrich-Wilhelms-Universität Bonn
7. M. Hodana,
Study of the $\eta \rightarrow e^+ e^- \gamma$ decay using WASA-at-COSY detector system,
Jagiellonian University Cracow, Poland
8. T. Randriamalala,
Conceptual Design of the PANDA Luminosity Monitor and Reconstruction Strategy to Measure the width of the $X(3872)$ State,
Ruhr-Universität Bochum
9. M. Röder,
Final State Interactions and Polarization Variables in the reaction $pp \rightarrow pK^+\Lambda$ Close to Threshold,
Ruhr-Universität Bochum
10. C. Weidemann
Preparations for the Spin-Filtering Experiments at COSY/Jülich,
Universität zu Köln
11. P. Wurm
Measurement of the $\eta \rightarrow e^+ e^- e^+ e^-$ double Dalitz decay and the search for new physics beyond the Standard Model in $\eta \rightarrow e^+ e^-$ with WASA-at-COSY,
Universität zu Köln

E Awards & Offers for Professorships

C. Hanhart: Member of the Particle Data Group

S. Krewald: Editorial Board of Physical Review C for the period 2011 – 2013

J. Ritman: Elected as spokesperson of the PANDA collaboration from January 1, 2013

F Funded Projects

Project	Responsible	Partner Institute	Funded by
Virtual Institute Spin and Strong QCD	U.-G. Meißner	GSI, Univ.'s Bern, Bonn, Ferrara, Cracow, Torino	HGF
Nuclear Astrophysics Virtual Institute (NAVI)	U.-G. Meißner	GSI, TU Darmstadt, Univ. Basel	HGF
Helm.-Russia Joint Research Group (HESR)	J. Dietrich	TU Dortmund; BINP Novosibirsk, JINR Dubna (Russia)	HGF
HGF-CSC fellowship program	R. Maier		HGF, CSC
Project FAIR	R. Toelle	GSI	EU/FP7
HadronPhysics 3 (RTD)	M. Büscher		EU/FP7
HadronPhysics 3 (RTD)	D. Goldenbaum		EU/FP7
HadronPhysics 3 (RTD)	F. Rathmann		EU/FP7
HadronPhysics 3 (Support)	D. Grzonka		EU/FP7
HadronPhysics 3 (Coordination)	D. Grzonka		EU/FP7
HadronPhysics 3 (Coordination)		U.-G. Meißner	EU/FP7
HadronPhysics 3 (Coordination)	A. Lehrach		EU/FP7
POLPBAR ERC Advanced Grant	H. Ströher		EU/FP7
SFB/TRR 110	U.-G. Meißner	Univ. Bonn, München, Beijing, IHEP Beijing	DFG
Meson-Baryon Dynamics	S. Krewald	Univ. Tashkent (Uzbekistan)	DAAD
Broken Symmetries	H. Machner	Univ. Helsinki (Finland)	DAAD
Deexcitation mechanisms and reaction kinetics in exotic atoms	D. Gotta		BMBF/WTZ
Spin Physics from COSY to FAIR	H. Ströher		BMBF/WTZ
Bilat. Zusammenarbeit mit Georgien	H. Ströher		BMBF/WTZ
Polarisationseffekte in der $\bar{p}d$ Streuung	J. Haidenbauer		BMBF/WTZ
IFMIF-EVEDA	E. Zaplatin		CEA Saclay
HESR/P1SR	R. Toelle		BMBF
HESR-Magnete	U. Bechstedt		BMBF
HESR-Netzgeräte	M. Retzlaff		BMBF
HESR-Hochfrequenz	R. Stassen		BMBF
HESR-Injektion	R. Toelle		BMBF
HESR-Strahldiagnose	V. Kamerzhiev		BMBF
HESR-Vakuum	F. Esser		BMBF
HESR-Stoch. Kühlung	R. Stassen		BMBF
HESR-PANDA Integration	D. Prasuhn		BMBF

G JCHP-FFE Projects

Project	Institute	Responsible
PD Dr. A. Khoukaz	Westfälische Wilhelms-Universität Münster	Mesonenproduktion in Nukleon-Nukleon- und Nukleon-Kern-Stößen an COSY
Prof. Dr. K. Nakayama	University of Georgia	Unified analysis of meson production in hadron- and photon-induced reactions in the resonance energy region
Prof. Dr. A. Vasilyev	PNPI Gatchina	Development, commissioning and operation of components for the COSY Experiments WASA and ANKE and spin-filtering studies at COSY as preparation for PAX at FAIR
Prof. Dr. V. Koptev	PNPI Gatchina	ANKE
Prof. Dr. B. Kämpfer	Forschungszentrum Dresden-Rossendorf	Weiterentwicklung des STT Software Pakets von ANKE zum Einsatz in zukünftigen Experimenten
Prof. Dr. M. Nioradze	Tbilisi State University	NN-elastic scattering studies at COSY
Prof. Dr. U. Thoma	HISKP Universität Bonn	Partialwellenanalyse von Daten aus proton-induzierten Reaktionen
Prof. Dr. H. Clement	Universität Tübingen	Experimente an COSY-TOF
Prof. Dr. O. Willi	Universität Düsseldorf	Measurements of the degree of polarization of laser accelerated protons
Prof. Dr. Y. Kiselev	ITEP Moscow	Phi meson production in pN and pA Reactions
PD Dr. A. Rusetsky	HISKP Universität Bonn	Inelastic baryon resonances from lattice QCD
PD M. Jezabek	Polish Academy of Sciences	Development of the signal processing method for high performance PANDA STT
Dr. H. Calen	Uppsala University	A pellet tracking system for PANDA and for WASA
Prof. D. U. Wiedner	Ruhr-Universität Bochum	Entwicklung eines innovativen, kompakten Monitorsystems für einen elektromagnetischen Kristallkalorimeter und Entwicklung von Software-Werkzeugen zur Teilchenidentifikation mit elektromagnetischen Kristallkalorimetern
Prof. Dr. T. Weis	TU Dortmund	Development of a Fast Orbit Feedback System for the HESR and Beam Tests at COSY
Prof. Dr. U. Wiedner	Ruhr-Universität Bochum	Measurement of $\eta \rightarrow \pi^+ \pi^- e^+ e^-$ with WASA-at-COSY
Prof. H. Gao	Duke University, USA	Investigation of K-p & K+K- final state interaction and a deeply bound K-pp state from proton proton reactions
Prof. Dr. P. Moskal	Jagellonian University Krakow	η meson production with polarized proton beam
Prof. A. Roy	Indian Institute of Technology Indore, India	Meson Decays with WASA-at-COSY
Prof. Dr. A. Magiera	Jagellonian University Krakow	Investigations of Charge Symmetry Breaking in the $dd \rightarrow {}^4\text{He} \pi^0$

Prof. T. Johansson	Uppsala University	Study of the $\omega \rightarrow \pi^+\pi^-\pi^0$ Dalitz plot distribution with WASA
Prof. A. Roy	Indian Institute of Technology Indore, India	ω Meson Decays with WASA-at-COSY
PD Dr. D. Eversheim	HISKP Universität Bonn	Time Reversal Invariance Test at COSY (TRIC)
Prof. N. Nikolaev	L.D. Landau Institute Moscow, Russia	Numerical simulations of spin dynamics for JEDI experiments, searching for permanent Electric Dipole Moments of deuterons and protons at COSY
Prof. Dr. E. Steffens	Universität Erlangen-Nürnberg	Spin-Experiment an ANKE
Prof. Dr. H. Clement	Universität Tübingen	Installation of a DIRC-Prototyp Detector for PANDA and Experiments with WASA-at-COSY
Prof. Dr. W. Eyrich	Universität Erlangen-Nürnberg	Experimente an TOF und WASA an COSY
Prof. A. Gerasimov	ITEP Moscow	Development of a Frozen-Pellet Target
Prof. Dr. W. Kühn	Universität Giessen	Realtime Tracking for the PANDA Target Spectrometer
Prof. Dr. M. Düren	Justus-Liebig-Universität Gießen	Development of a DIRC Cherenkov detector for WASA at COSY
Dr. P. Lenisa	Università degli Studi di Ferrara, Italy	Spin-filtering studies in storage rings
Prof. Dr. A. Kulikov	JINR Dubna, Russia	Experiments with ANKE, WASA and PAX at FAIR
Prof. Dr. K. Brinkmann	HISKP Universität Bonn	Prototyping for PANDA at COSY
Prof. J. Wang	Chinese Academy of Sciences, Lanzhou, China	Commissioning of the HESR day one experiment at COSY
Prof. Dr. A. Schäfer	Universität Regensburg	Mesonen Distributions-Amplituden
Prof. Dr. U. Wiedner	Ruhr-Universität Bochum	Development for the forward endcap of the PANDA EMC and buildup of the final endcap within PANDA in Jülich
Prof. Dr. U. Wiedner	Ruhr-Universität Bochum	Development of the Cryogenic Supply System for tests of the PANDA Target Spectrometer Solenoid
Prof. O. Bezshyyko	University of Kyiv, Ukraine	Development of a detector readout with real-time tracking for the PANDA STT
Prof. R. Varma	Indian Institute of Technology Indore, India	Physics Analysis and Simulation of Dilepton and Multi-Pion Final States from WASA to PANDA
Prof. Dr. K. Brinkmann	Justus-Liebig-Universität Gießen	Development and Validation of a Free-Running Silicon-Strip Front-End ASIC for the PANDA MVD

H Conferences (co-)organized by the IKP

H.1 Workshop on Meson Transition Form Factors

The workshop was the main activity of the European Network MesonNet, <https://sites.google.com/site/mesonnet/work/>, a network within the project ‘Study of Strongly Interacting Matter’ (Hadron Physics3), an Integrating Activity within the Seventh Framework Program of EU. The meeting took place on May 29-30, 2012 in Cracow, Poland, immediately before (and co-located with) the biennial conference MESON 2012.

The goal of the workshop was to discuss results and plans for experimental and theoretical studies of meson transition form factors. These are of interest because of a possible relation of such form factors to the models used for the calculations of the hadronic light-by-light contribution to muon $g-2$ as well as for various theoretical models describing low-energy meson physics.



Fig. 56: Participants of the MesonNet workshop at the Jagiellonian University in Cracow.

Experimentalists and theorists had been invited to present and discuss the workshop topics

- radiative, Dalitz and conversion decays of vector and pseudoscalar mesons
- two-photon production of resonances
- rare leptonic decays of mesons
- Primakoff effect
- other closely related topics

52 participants yielded lively and fruitful discussions around 32 presentations. The organizers E. Czerwinski, S. Eidelman, C. Hanhart, A. Kupsc, S. Leupold, P. Moskal, and S. Schadmand, have published the mini-proceedings at arXiv:1207.6556 [hep-ph].

H.2 MESON 2012

The 12th International Workshop on Meson Production, Properties and Interaction (MESON 2012) took place in Cracow, Poland, from May 31 to June 5 2012, with the participation of nearly 200 experimental and theoretical physicists from 20 countries.

The MESON conferences aim to provide an overview of the present status of meson physics in various hadronic and electromagnetic reactions, including structure and interaction of hadrons, fundamental symmetries, and exotic systems, in both experimental and theoretical aspects. In particular, the conference program covered the broad spectrum of experiments using the major accelerators in the field: hadron machines, electron facilities and electron-positron colliders.

A wide spectrum of problems in the light meson sector was presented, including preliminary results on tests of fundamental symmetries and the search for phenomena beyond the Standard Model. Heavier mesons were also extensively discussed, as well as kaon physics: deeply bound kaonic nuclear states and kaonic atoms.

Future facilities, ongoing and planned facility upgrades, and many experimental programs on existing installations were presented. Great attention was addressed to the status and perspectives of theoretical research on mesons, including QCD inspired models, like effective field theory or lattice QCD.

In total, there were 40 plenary talks and 64 parallel session talks, plus 47 posters.

H.3 5th Georgian-German School and Workshop in Basic Science

Within the Georgian-German Science Bridge, the FZJ together with its Georgian partner institutions, the Ivane Javakhishvili Tbilisi State University (TSU) and the Georgian Technical University (GTU), intend to enforce the scientific and technological cooperation between the two countries. Within this framework the bi-annual Georgian-German School and Workshop in Basic Science (GGSWBS) is organized in Georgia. The 5th such workshop took place in Tbilisi during August 6–10, and the summer school was held at Batumi State University (BSU) from August 13–17 (<http://collaborations.fz-juelich.de/ikp/cgswbp/cgswbp12/index.shtml>).

The program of workshop and school comprised:

- Existing and future physics projects at large-scale facilities
- Search for electric dipole moments at storage rings
- Solid state physics
- Bio- and geoscience
- Material science
- Engineering science



Fig. 57: Summer school participants at BSU.

- Neuro-science and medicine
- Information technology and computing
- Introductory courses for Bachelor, Master and PhD students

For the up-coming gathering in October 2013 it is planned to have a dedicated lecturing courses for the Bachelor and Master students in nuclear and medical physics (<http://studmedia.ge/autumn-lectures>).

H.4 ECT* Workshop “EDM Searches at Storage Rings”

The aim of the workshop on October 1–5, 2012, was to highlight the physics potential of the search for permanent electric dipole moments (EDM) for the discovery/establishment of new physics (*i.e.* physics beyond the Standard Model (BSM) of Elementary Particle Physics) and to present (and discuss) the different approaches to search for EDMs in leptons, hadrons and more complex systems (*e.g.* nuclei, atoms and molecules). Emphasis was given to the presentation and discussion of a new experimental proposal/approach to use polarized charged particles in storage rings. Technological and metrological challenges were described and scrutinized. In addition the theoretical background and methods in order to calculate EDMs and to identify the CP-violating sources were presented and discussed.

In 49 talks (10 theory, 15 experiment, and 24 accelerator/metrology) as well as 2 outlook presentations, the above mentioned objectives of the meeting were all covered. The achievements can be summarized as follows:

- The physics case (baryogenesis, CP violation beyond CKM, new physics BSM) is most compelling: discovery of a finite EDM for any fundamental particle would be a major milestone and the smoking gun for physics beyond the Standard Model.



Fig. 58: Participants of the ECT* workshop at the Villa Tambosi in Trento.

- EDMs must exist, but the question is whether they can be observed — in case of an EDM discovery, a series of observations (*e.g.* for neutron, proton and the deuteron) will be necessary to disentangle the source.
- Current EDM upper limits for electron, muon and neutron are impressive and new projects are underway to improve these limits by at least an order-of-magnitude during the next decade.
- Although technological and metrological challenges for storage ring EDM measurements (srEDM) are severe, the current proposals — an all-electric srEDM ring for proton (pursued by BNL, US-srEDM collaboration) and an all-in-one combined E/B srEDM ring (Jülich, JEDI-collaboration) — exploiting counter-rotating beams seem the right track to tackle these problems. It seems obvious, however, that the final sensitivity goal of 10^{-29} e cm (or even beyond) can/will not be achieved in one gigantic leap: JEDI therefore proposes to use the conventional COSY storage ring for a precursor EDM-experiment with the aim to obtain a proof-of-principle as well as first directly measured EDM-limits for proton and deuteron.

H.5 Farewell to Walter Oelert

On November 16 a symposium took place on the occasion of Prof. Walter Oelert’s farewell. An overview of his activities at FZJ and CERN was given by the former head of IKP-1, Prof. Kilian. Results from the COSY-11 experiment were presented by Prof. Wolke from Uppsala, and Prof. Moskal from Kracow. The physics of antimatter, especially antihydrogen, was introduced in talks by Prof. Walz from the University of Mainz and by Prof. Hayano from Tokyo University. Besides COSY-11 that was the main topic of Prof. Oelert’s research activities since 1995

when he created the first antihydrogen atoms at CERN. The future of CERN's low energy antiproton decelerator AD, an upgrade by a further deceleration ring ELENA, was described by Dr. Maury from CERN. Prof. Oelert was strongly involved in the realization of ELENA and he will continue his activities at CERN with the affiliation to the University of Mainz.

I Teaching Positions

Institute	Name	University
IKP-1	PD Dr. A. Gillitzer	Bonn
	PD Dr. F. Goldenbaum	Wuppertal
	Prof. Dr. J. Ritman	Bochum
	PD Dr. S. Schadmand	Köln
	Dr. T. Stockmanns	Bochum
IKP-2	PD Dr. M. Büscher	Köln
	Prof. Dr. D. Gotta	Köln
	PD Dr. F. Rathmann	Erlangen-Nürnberg
	Prof. Dr. H. Ströher	Köln
IKP-3/IAS-4	Univ. Doz. Dr. J. Haidenbauer	Graz
	PD Dr. C. Hanhart	Bonn
	Prof. Dr. S. Krewald	Bonn
	Prof. Dr. U.-G. Meißner	Bonn
	Prof. Dr. N.N. Nikolaev	Moscow
	Dr. A. Nogga	Bonn
IKP-4	PD Dr. A. Wirzba	Bonn
	Prof. Dr. Dr. h.c. J. Dietrich	Dortmund
	PD Dr. A. Lehrach	Bonn
	Prof. Dr. R. Maier	Bonn

J Personnel

J.1 Scientific Staff

Msc. Z. Bagdasarian (IKP-2) (since 19 November 2012)
Dr. U. Bechstedt (IKP-4)
Dr. K. Bongardt (IKP-4)
DI N. Bongers (IKP-4)
DI R. Brings (IKP-4)
Y. Bsaisou (IKP-3)
PD Dr. M. Büscher (IKP-2)
M. Cleven (IKP-3)
DI F.U. Dahmen (IKP-4)
DP D. Deermann (IKP-1) (since 4 August 2011)
Prof. Dr.Dr.h.c. J. Dietrich (IKP-4) (until 29 February 2012)
DI N. Dolfus (IKP-TA) (until 31 August 2012)
Dr. R. Dzhygadlo (IKP-1)
Dr. R. Engels (IKP-2)
DP I. Engin (IKP-2) (since 01 March 2012)
DP S. Esch (IKP-1)
DI F.-J. Etzkorn (IKP-4)
Dr. O. Felden (IKP-TA)
DP M. Gaißer (IKP-2)
Dr. W. Gast (IKP-1)
Dr. R. Gebel (IKP-4)
PD Dr. A. Gillitzer (IKP-1)
A. Goerres (IKP-1) (since 01 February 2012)
PD Dr. F. Goldenbaum (IKP-1)
Prof. Dr. D. Gotta (IKP-2)
Dr. F. Grümmer (IAS-4)
Dr. D. Grzonka (IKP-1)
DI W. Günther (IKP-4)
Univ. Doz. Dr. J. Haidenbauer (IAS-4)
PD Dr. C. Hanhart (IAS-4)
Dr. M. Hartmann (IKP-2)
Dr. V. Hejny (IKP-2)
DI K. Henn (IKP-4)
DP A. Herten (IKP-1)
DP A. Holler (IKP-4)
MSc M. Jabua (IKP-2) (since 19 November 2012)
Dr. V. Kamerdjiev (IKP-4)
Dr. A. Kacharava (IKP-2)
DP St. Kölling (IKP-3) (until 30 April 2011)
Prof. Dr. S. Krewald (IAS-4)
PD Dr. A. Lehrach (IKP-4)
DP D. Lersch (IKP-1) (since 1 March 2011)
DP S. Liebig (IKP-3)
Dr. B. Lorentz (IKP-4)
Dr. L. Mao (IKP-4)
Prof. Dr. R. Maier (IKP-4)
Prof. Dr. U.-G. Meißner (IKP-3/IAS-4)
DP M. Mertens (IKP-1)
Dr. S. Merzliakov (IKP-2)
DP S. Mikirtychiants (IKP-2)
Dr. A. Naß (IKP-2)
Prof. Dr. N.N. Nikolaev (IKP-3) (until 30 June 2012)
Dr. A. Nogga (IAS-4)
Prof. Dr. W. Oelert (IKP-1) (until 31 December 2012)
DP D. Oellers (IKP-2)
Dr. H. Ohm (IKP-2)
DI N. Paul (IKP-1)
Dr. D. Prasuhn (IKP-4)
DP T. Randriamalala (IKP-1) (since 1 August 2011)
PD Dr. F. Rathmann (IKP-2)
DP M. Retzlaff (IKP-4)
DI A. Richert (IKP-4)
Prof. Dr. J. Ritman (IKP-1)
Dr. E. Roderburg (IKP-1)
DP M. Röder (IKP-1)
DP D. Rönchen (IKP-3) (since 01 July 2012)
DP M. Rosenthal (IKP-4) (since 01 November 2012)
DI J. Sarkadi (IKP-TA) (until 31 October 2012)
PD Dr. S. Schadmand (IKP-1)
Dr. R. Schleichert (IKP-2)
DI G. Schug (IKP-4)
Dr. Th. Sefzick (IKP-TA)
Prof. Dr. Y. Senichev (IKP-4)
Dr. V. Serdyuk (IKP-1) (since 01 January 2012)

DI M. Simon (IKP-4)
Dr. R. Stassen (IKP-4)
Dr. H. Stockhorst (IKP-4)
Dr. T. Stockmanns (IKP-1)
Prof. Dr.Dr.h.c. H. Ströher (IKP-2)
Dr. R. Tölle (IKP-4)
DI T. Vashegyi (IKP-4)
Dr. Q. Wang (IAS-4) (since 20 August 2012)
DP P. Weiß (IKP-2) (since 10 September 2012)
Dr. P. Wintz (IKP-1)
PD Dr. A. Wirzba (IAS-4)
DI J.-D. Witt (IKP-4)
DP P. Wurm (IKP-2)
Dr. H. Xu (IKP-1)
Dr. E. Zaplatin (IKP-4)
DP D. Zyuzin (IKP-4)

J.2 Technical and Administrative Staff

C. Berchem (IKP-TA)
M. Böhnke (IKP-4)
P. Brittner (IKP-4)
J. But (IKP-TA)
W. Classen (IKP-4)
M. Comuth-Werner (IKP-TA)
B. Dahmen (IKP-4)
C. Deliege (IKP-4)
G. D'Orsaneo (IKP-2)
R. Dossall (IKP-1)
C. Ehrlich (IKP-4) (since 01 July 2012)
P. Erben (IKP-2)
B. Erkes (IKP-4)
K. Esser (IKP-TA)
H.-W. Firmenich (IKP-TA)
J. Göbbels (IKP-TA)
R. Gorski (IKP-2) (since 01 August 2012)
P. Greven (IKP-2) (since 15 March 2012)
V. Gupta (IKP-2) (until 31 January 2012)
R. Hecker (IKP-4)
E. Heßler (IKP-TA)
M. Holona (IKP-TA)
W. Hu (IKP-4) (since 01 December 2012)
A. Kelleners (IKP-TA) (since 01 June 2012)
A. Kieven (IKP-4)
S. Kistemann (IKP-TA) (since 01 November 2012)
M. Kremer (IKP-TA)
G. Krol (IKP-4)
V. Kau (IKP-TA)
G. Kukhalashvili (IKP-4) (since 19 November 2012)
M. Küven (IKP-4)
K.-G. Langenberg (IKP-4)
J. Lumbeck (IKP-4) (since 29 August 2012)
L. Magallanes-Hernandez (IKP-4) (until 30 September 2012)
H. Metz-Nellen (IKP-TA) (until 31 August 2012)
S. Mey (IKP-4) (since 01 December 2012)
S. Müller (IKP-TA)
R. Nellen (IKP-TA)
C. Oslender (IKP-TA)
T. Preuhs (IKP-1) (since 13 August 2012)
H. Pütz (IKP-4)
K. Reimers (IKP-4)
G. Roes (IKP-TA)
N. Rotert (IKP-4)
D. Ruhrig (IKP-4)
F. Scheiba (IKP-4)
H. Schiffer (IKP-TA)
J. Schmitz (IKP-4)
M. Schmühl (IKP-4)
F. Schultheiß (IKP-TA) (until 31 December 2012)
D. Spölgel (IKP-2)
G. Sterzenbach (IKP-1)
M. Theisen (IKP-2) (since 16 July 2012)
J. Strehl (IKP-TA)
J. Uehlemann (IKP-1)
H. Zens (IKP-4)

IKP-1 = Experimental Hadron Structure
IKP-2 = Experimental Hadron Dynamics
IKP-3 = Theory of the Strong Interactions
IKP-4 = Large-Scale Nuclear Physics Equipment
IKP-TA = Technical Services and Administration
IAS-4 = Theory of the Strong Interactions

K Further Contributions

(articles available on-line: <http://donald.cc.kfa-juelich.de/wochenplan/publications/AR2012/articles/>)

1. Experimental Hadron Physics
 - 1.1 Measurements of $A_{x,x}$ and $A_{y,y}$ in the $np \rightarrow d\pi^0$ reaction at 353 MeV
 - 1.2 Luminosity Determination for the Quasi-free $pn \rightarrow pn\eta'$ Reaction
 - 1.3 Analysis of $\eta \rightarrow \pi^+\pi^-\gamma$ with WASA-at-COSY
 - 1.4 Search for $({}^4\text{He}-\eta)_{\text{bound}}$ with WASA-at-COSY
 - 1.5 Calibration of the COSY-TOF Straw Tube Tracker
 - 1.6 Analysis of the $pp \rightarrow nK^+\sigma^+$ Reaction from COSY-TOF Data
 - 1.7 Analysis of a Feasibility Study of the Reaction $pn \rightarrow pK^0\Lambda$
 - 1.8 Transverse Spin Filtering at COSY — Final Results
 - 1.9 Polarization in proton deuteron breakup at 50 MeV
 - 1.10 Measurement of the nuclear polarization in H_2 and D_2 molecules after recombination of polarized hydrogen or deuterium atoms
 - 1.11 Energy Calibration For The WASA-at-COSY Forward Detector
2. Theoretical Physics (see Sect. B for links to published papers)
3. Accelerator Division
 - 3.1 Radiation Protection
 - 3.2 Calculation of electron motion in the toroid of the 2 MeV cooler at COSY
4. Preparations for FAIR
 - 4.1 Design Simulations for Pellet Tracking Systems
 - 4.2 Development of a Readout and Test System for the Forward Strip Part of the Micro Vertex Detector of PANDA
 - 4.3 Development of Front End Electronics for the PANDA Straw Tube Tracker (STT)
 - 4.4 Upgrade of the Jülich Digital Readout System for the PANDA-MVD
 - 4.5 Implementing an Ethernet Communication Module Based on the UDP Standard into the Jülich Digital Readout System
 - 4.6 Implementations of Hough Transformations on GPUs for PANDA
 - 4.7 Si Detector Test for the HESR Day-One Experiment
 - 4.8 Towards the Data Transmission from PandaRoot to the Compute Node
 - 4.9 Time Resolution of a Flash-ADC System for the PANDA STT